UNIVERSITEIT VAN PRETORIA
UNIVERSITY OF PRETORIA
YUNIBESITHI YA PRETORIA

ROCK BOLT CONDITION MONITORING USING ULTRASONIC GUIDED WAVES

By

BJ BUYS

Submitted in fulfilment of part of the requirements for the degree of
Master of Engineering in the Faculty of Engineering, Built Environment and Information Technology
of the
University of Pretoria

Supervisors: Professor P. S. Heyns, Dr. P. Loveday

October 2008

ABSTRACT

Rock Bolt Condition Monitoring using Ultrasonic Guided Waves

by

Barend Jakobus Buys

Supervisors: Professor P.S. Heyns, Dr. P Loveday

Department of Mechanical and Aeronautical Engineering

Degree: M Eng

The resin anchored rock bolt is used extensively in the mining industry to stabilize the roof and prevent it from collapsing. However, there are different defects associated with a resin anchored rock bolt. Examples are partially encapsulated bolts, over-spinned bolts and corroded bolts. These defects reduce the integrity of the roof, and thereby have an effect on the safety and productivity of the mines.

The integrity of the rock bolts is a critical issue for the mining industry because of its influence on the safety of mining operations. Different research groups around the world have addressed the problem of determining rock bolt integrity. The most promising technique found in the literature study was based on guided ultrasonic waves (Beard and Lowe, 2003).

This study extended the previous work by Beard and Lowe (2003) using guided ultrasonic waves, to investigate damage in more realistic embedded bolts which deviate from pure cylinders. The fundamental L(0,1) mode in its lower frequency range, as suggested by Beard and Lowe was utilized. This was done through the use of finite element model simulations of various defect scenarios, which were compared to experimental measurements on bolts. Defects like loss of resin

encapsulation, voids and local corrosion cracks were addressed. The time traces of the different finite element defect scenarios could be directly compared to experimental time traces which distinguish this study from the analytical approach.

Some finite element modelling issues were investigated and it was found that the time step is critical if an implicit solver is used, whereas for an explicit solver the element size is critical if accurate answers are needed. Furthermore it was also apparent that the boundary of the mortar has an influence on the results. The method used in the study was to move the boundaries far enough to prevent interference. This however increases the model size and thereby the computer resources required.

Axisymmetric defects were modelled using axisymmetric finite elements to reduce the problem size. These models gave results comparable to the measured bolts. Three-dimensional finite element models seemed to be promising for simulating non-axisymmetric defects. It was found that it is not possible to solve large three-dimensional models without energy absorbing boundaries.

Axisymmetrical and three dimensional finite element models of a partially encapsulated bolt and a bolt with a local corrosion crack were built. It was possible to detect simulated local corrosion cracks with the finite element models. Clear reflections for the crack in the bolt could be seen. If the bolt, resin and rock are cracked, different reflections will be detected. These different reflections complicated the interpretation of the results.

Once the integrity of models such as these has been established, the models could in principle be used to train neural networks for use in commercial equipment. The present study was limited to lower frequencies because of computer resource limitations. Basic principles and modelling issues could however be addressed and it may be expected that these principles could soon be extended to higher frequencies with a new generation of computers.

KEYWORDS: rock bolt, embedded bolt, non-destructive testing, ultrasonic, guided waves, wave propagation, finite element modelling.

ACKNOWLEDGEMENTS

I would like to thank the following people:

- Professor Stephan Heyns for his excellent guidance with the project.
- Dr. Phillip Loveday for his expert help and guidance with the project.
- All the staff of the Sasol Laborotory for Structural Mechanics at the University of Pretoria, expecially Frans Windell, Danie Drent and Jimmy Mokhafela.
- I also gratefully acknowledge the financial support of the Mine Health and Safety Council in the execution of this research.

I would like to thank my parents, brother, sisters and Elani for all their love and support.

Finally to the Lord who graced me with the talents and oppurtunities. To Him all the glory.

Rom 11:36

“For of Him and through Him and to Him are all things, to whom be glory forever. Amen”

TABLE OF CONTENTS

INTRODUCTION AND LITERATURE SURVEY 1

1.1. INTRODUCTION 1
1.2 BACKGROUND TO ROOF SUPPORT AND ROCK BOLT TYPES 5
1.3 FAILURE MECHANISMS OF RESIN ANCHORED BOLTS 8
1.3.1 Anchorage failure 9
1.4 THE HISTORY OF ROCK BOLT CONDITION MONITORING 11
1.5 REVIEW OF DESTRUCTIVE ROCK BOLT TESTING 12
1.5.1 Pull-out test 12
1.6 REVIEW OF NON-DESTRUCTIVE ROCK BOLT TESTING 13
1.6.1 Boltometer 13
1.6.2 JK rockbolt tester 15
1.6.3 GRANIT 15
1.6.4 Ultrasonic Guide Wave Testing 16
1.7 PHYSICS OF ULTRASONIC GUIDED WAVES 18
1.8 MODELLING OF ULTRASONIC WAVES 21
1.8.1 Dispersion curves 21
1.9 THE FINITE ELEMENT METHOD 24
1.9.1 Implicit Integration 25
1.9.2 Explicit Integration 27
1.10 SUMMARY OF THE LITERATURE STUDY 29
1.11 SCOPE 30

MODELLING ISSUES 31

2.1 INTRODUCTION 31
2.2 THE INFLUENCE OF MESH DENSITY AND TIME STEP SIZE 32
2.2.1 Axisymmetric model 32
2.2.2 Three Dimensional model – Implicit Solver (MSC.Nastran) 37
2.2.3 Three dimensional model – Explicit Solver (MSC.Dytran) 40
2.2.4 Comparison of the group velocity curves 42
2.3 THE EFFECT OF DAMPING 45
2.4 ENERGY ABSORBING BOUNDARIES 46

THE EXPERIMENTAL SETUP AND VERIFICATION OF THE FINITE ELEMENT MODELS 48

3.1 INTRODUCTION 48
3.2 INSTRUMENTATION FOR THE EXPERIMENTAL SETUP 48
3.2.1 Data acquisition card and software 49
3.2.2 Pulse-echo circuit 50
3.2.3 Amplifier 51
3.2.4 Piezo-ceramic transducers 51
3.2.5 Computer and software for the finite element modelling 52
3.3 THE EXPERIMENTAL TESTING BLOCK 52
3.4 MATERIAL PROPERTIES 54

3.5 UNBOUNDED BOLT 55
3.5.1 Experimental results *56*
3.5.2 Finite element models *59*
3.6 EMBEDDED BOLTS 61

INTERPRETATION OF FAULT SCENARIOS 66

4.1 INTRODUCTION 66
4.2 PARTIALLY ENCAPSULATED BOLTS 66
4.2.1 Finite element models and results *67*
4.2.2 The experimental setup *70*
4.3 LOCAL CORROSION CRACKING 72
4.3.1 Experimental cracked bolt *73*
4.3.2 Finite element models and discussion *75*
A) No defect 76
B) Cracked bolt 77
C) Mortar and resin crack 79
D) Bolt, resin and rock crack 80

CONCLUSIONS AND ECOMMENDATIONS 82

REFERENCES 87

APPENDIX A 91

APPENDIX B 96

APPENDIX C 98

LIST OF FIGURES

Figure 1.1: Tunnel and support elements (Roberts, 1995) 6
Figure 1.2: Resin anchored rock bolt 7
Figure 1.3: Failure mechanisms of a fully grouted roof bolt. 9
Figure 1.4: Photograph showing fully grouted bolts pulled from their holes in a roof fall (Mark et al., 2002) 9
Figure 1.5: Pull test equipment (RMT Ltd, 2003) 13
Figure 1.6: Boltometer (Geodynamik, 2001) 14
Figure 1.7: Schematic diagram of the rock bolt guided wave inspection method 16
Figure 1.8: Picture of the specimens that were used for testing rock bolts in the laboratory (Beard and Lowe, 2003) 17
Figure 1.9: Phase and group velocity curves for a 20 mm rod in a vacuum (Beard, 2002) 22
Figure 1.10: Comparison in CPU time between implicit and explicit integration 29

Figure 2.1: Representation of an axisymmetric model of the rock bolt 33
Figure 2.2: Gaussian windowed sine burst and the FFT of the pulse 34
Figure 2.3: Two different meshes for three different time steps for a 50 kHz Gaussian windowed sine burst 36
Figure 2.4: Three different meshes with three different time steps for a 20 kHz Gauss pulse 37
Figure 2.5: Three-dimensional rock bolt mode with HEX 8 elements 38
Figure 2.6: Displacement plot to show the wave propagating in a 3d model 39
Figure 2.7: Two different meshes with three different time steps 40
Figure 2.8: Comparison between an axisymmetric and a 3d rock bolt model 42
Figure 2.9: Group velocity curves for a bolt in a vacuum from PCdisp 43
Figure 2.10: Group velocity curves for axisymmetric FEM model, Experimental and Pochhammer-Chree frequency equation 45
Figure 3.1: Instrumentation 49
Figure 3.2: Time trace of a 6 cycle Gaussian windowed transmitted signal 51
Figure 3.3: Experimental test block 53
Figure 3.4: Time trace for 40 kHz pulse in a 1.5 m free smooth bolt 57
Figure 3.5: Time trace for a 50 kHz pulse in a 1.5 m free smooth bolt 58
Figure 3.6: Time trace for a 3d model in MSC.Dytran of 1.5 m unbounded bolt 60
Figure 3.7: Time traces for a pulse-echo test on a 1.5 m experimental bolt embedded in mortar 61
Figure 3.8: Axisymmetric model dimensions 63
Figure 3.9: 0.9 m bolt embedded in mortar (40 kHz) 64
Figure 3.10: 0.9 m bolt embedded in mortar (50 kHz) 65
Figure 3.11: 0.9 m bolt embedded in mortar (60 kHz) 65
Figure 4.1: Finite element model details 67
Figure 4.2 a, b, c: Results for the axisymmetric models, with 5 mm elements 68
Figure 4.3 a, b, c: Three-dimensional model results with 10 mm elements 69
Figure 4.4: Experimental partially encapsulated bolt 70

Figure 4.5 a, b, c: Experimental results for a partially encapsulated bolt 72
Figure 4.6: Experimental setup for a representation of a local corrosion crack 73
Figure 4.7 a, b, c : Experimental result for a bolt with a crack 75
Figure 4.8: Finite element model details 76
Figure 4.9 a, b, c: Finite element model results for a 1 m embedded bolt with no defects 77
Figure 4.10 a, b, c: FEM model with a crack in the bolt only 78
Figure 4.11 a, b, c: FEM model with a rock and resin crack 79
Figure 4.12 a, b, c: FEM model with the rock, resin and a bolt crack 80
Figure A1: A typical mechanically end anchored rock bolt (Roberts, 1995). 92
Figure A2: Grout injection arrangements for a mechanically anchored rock bolt 93
Figure A3: A typical straight bar grouted tendon with base plate and nut 94
Figure A4: A typical shepherd's crook grouted tendon (Roberts, 1995) 94
Figure B1: Piezoelectric effect 96
Figure B2: Circuit for pulse-echo tests 97

NOMENCLATURE

c	velocity of wave
ρ	density
E	longitudinal elastic modulus
F	input frequency
λ	wavelength
[M]	mass matrix
[C}	damping matrix
[K]	stiffness matrix
υ	Poisson's ratio
γ	constant for Newmark integration scheme
β	constant for newmark integration scheme
Δt	time step
fmax	maximum frequency of interest
Lmin	shortest wavelength of interest
Le	element length
m	particle mass
x	coordinate
V	bulk longitudinal speed
F	force
a	acceleration
v	velocity
d	displacement
n	number

CHAPTER 1

INTRODUCTION AND LITERATURE SURVEY

1.1. Introduction

Safety is a critical issue for the mining industry. In South African underground mines 1233 ground fall accidents were reported in 2002 with 123 people killed in these accidents (South African Department of Minerals and Energy, 2002). Much attention is therefore focused on the integrity of the roof of mining tunnels. One approach is to stabilize the roof with resin anchored rock bolts. These bolts are essentially steel rods that are fixed into the roof with resin to prevent the roof from collapsing. To support the roof with rock bolts is a costly exercise and the quality and density of the support determines the lifespan and reliability of the tunnels (Roberts, 1995). By way of example, more than 16 million rock bolts are installed each year in the South African mines. Of these 45 percent is resin anchored bolts (Bornman, 2005).

There are however various defects associated with these resin anchored rock bolts that might compromise safety. Examples of such defects include weak rock conditions and corrosion which cause unsatisfactory bonding between the rock and the rock bolt. Poor installation procedures like over-spinning, incomplete mixing and partially encapsulated bolts are also encountered (Mark *et al.*, 2002). For instance from 1996 to 1998 approximately half of the fully grouted bolts were not as effective as they should be (Kelly *et al.*, 1996, Harper and Basson, 1998). The quality of installation and grouting of resin anchored bolts is therefore regarded as a serious problem by the mining industry.

Determining rock bolt integrity has been addressed by various groups around the world. One of the conventional approaches to this issue is the pull-out test. However, it is a time consuming and destructive process. A need therefore arose to develop a non-destructive test that can be used to determine the condition of the bolt *in situ*.

The GRANIT system developed in Scotland, drives a piston that creates a controlled tensile axial impulse that is transferred to the bolts. The vibrational response of the bolt and environment to this impact is measured by an accelerometer that is positioned on the impact device. The acceleration signals that arise from this impulse are interpreted by neural networks to determine the condition of the bolt (Starkey *et al.*, 2003). The disadvantage of the GRANIT system is that it can only work on rock bolts that have been characterised at installation. Furthermore research studies have suggested that ultrasonic testing would be the most promising non-destructive technique (Kelly *et al.*, 1996). Such a product, the Boltometer, developed in Sweden is an instrument that can be used on cemented grouted bolts and also on polyester and some other resin grouts. The Boltometer uses a sensor with piezoelectric crystals, and transmits compressional and flexural waves into the bolt. The waves propagate through the bolt, reflect at the bolt end and the echo is received by the sensor. It relies on the principle that good grouting will absorb most or all of the wave energy into the rock, leaving only small echoes returning to the sensor, whereas insufficient grouting will result in a distinct echo. The Boltometer can indicate bad grouting, but if the impedance between the grout and surrounding rock are the same; wave energy will dissipate into the rock before it could reach a major defect, reporting good grouting (Thurner, 1996).

Subsequently, non-destructive testing of rock bolts using guided ultrasonic waves has been proposed as a feasible approach for detecting resin defects (Beard and Lowe, 2003). Guided wave propagation refers to ultrasonic waves that propagate in solid media with boundaries. These ultrasonic waves experience reflection and refraction with the boundary of the solid, which cause mode conversion between longitudinal and shear waves (Rose, 1999). Therefore, different guided wave modes can exist in a cylindrical solid. Each of these modes has a particular wave structure. The wave structure describes the distribution of particle motion in the cylindrical solid. Some modes have large particle motion amplitudes near the surface, while others feature more intense motion near the middle of the cylinder. The wave structure determines the sensitivity of the particular mode to a particular flaw type. Sometimes it may be possible to perform an inspection using only a single mode. One method to generate a single mode, is to employ a Gaussian windowed, sine burst excitation.

Thereby the bandwidth of the signal is reduced and will suppress modes either side of the dominant frequency in the frequency spectrum (Clifford, 2000).

This was recently proposed by Beard and Lowe (2003) who suggested a technique that embraces the following:

A short duration Gaussian windowed sine burst is used to excite a guided wave in the bolt on the free end of the bolt, which is then reflected from the bolt end and from any major defects. From the reflection arrival time and knowledge of the wave velocity dispersion curves, the positions of the defects or the bolt length can be calculated. The maximum test range is limited by the extent of the attenuation that the wave experiences as it propagates. The major cause of attenuation for the embedded rock bolt is that ultrasonic energy tends to leak from the bolt into the surrounding rock. With guided waves the quality of the grouting and the location of the defect can be determined. Specific modes can be selected that are less sensitive to difference in impedance as in the Boltometer. It is also not necessary that previous data of the specific rock bolt should be available, because guided wave testing requires only baseline measurements.

Beard and Lowe further investigated the effect of guided wave modes, frequencies and excitation periods to find the best guided wave mode for defect detection. The selection of suitable modes and frequencies were done by means of analytically based dispersion curves, calculated for a simple cylinder. They established that embedded bolts should be tested by exciting the first axially symmetric longitudinal mode known as the L(0,1) mode, in its low frequency range (30 – 70 kHz), and the first non-axially symmetric longitudinal mode known as the L(1,1) mode, in its high frequency range (2 – 5 MHz). The low frequency test can be used to identify defects such as partial bolt encapsulation and possibly corrosion patches near the bolt surface. On the other hand, the high frequency test is not sensitive to surface defects, but can give a reliable indication of the bolt length (Beard and Lowe, 2003).

This earlier study by Beard and Lowe (2003) focused primarily on the identification of suitable modes which are not significantly influenced by the embedding rock modulus, the epoxy thickness and modulus and the bolt-epoxy bond quality. With

the limitations of the analytical model, it was not possible to simulate complex defect scenarios.

To deal with more complicated defects and geometries, the finite element (FE) method is commonly used to model wave propagation. The primary advantage of the finite element method is that there are numerous commercial FE codes available, thus eliminating any need to develop an actual code. Furthermore, the finite element method offers the advantage that the difficulties associated with complex geometries and defects are simpler to handle. Its availability, user friendliness and the sophisticated pre- and post-processing options, suggest the finite element method as a versatile modelling approach for rock bolt defect simulation. Different defects such as local corrosion cracking and partially encapsulated bolts can be modelled.

The present study extends the previous work to investigate damage in more realistic embedded bolts which deviate from pure cylinders, using the guided wave testing modes and frequencies suggested by Beard and Lowe (2003). This is done through the use of finite element models of various defect scenarios, which are simulated and compared to experimental measurements on bolts. The time traces of the different finite element defect scenarios could be directly compared to experimental time traces which distinguish this study from the analytical approach. Once the integrity of models such as these have been established, the models could in principle be used to train neural networks for use in commercial equipment. The present study was limited to lower frequencies because of computer resource limitations. Basic principles and modelling issues could however be addressed and it may be expected that these principles could soon be extended to higher frequencies with a new generation of computers.

The document consists of 5 chapters. The rest of the first chapter reviews the literature and highlights the different opportunities for research on ultrasonic testing of rock bolts and their modelling.

Chapter 2 deals with modelling issues for bolts in air (unbounded bolts) as well as embedded bolts. The effect of the time step, element size, and boundary condition is discussed in detail.

In chapter 3 the experimental setup, instrumentation and associated problems are presented. The experimental unbounded bolt and an embedded bolt are discussed. The finite element models for an unbounded bolt and an embedded bolt are compared to the experimental and Pochhammer-Chree frequency equation dispersion curves.

Chapter 4 deals with the modelling of the different defects and the comparison of the finite element models to the experimental setup.

The work is concluded in chapter 5 and recommendations for future work are discussed. Some background information on rock bolts and ultrasonic equipment are presented in the appendix.

1.2 Background to roof support and rock bolt types

The history of roof support can be traced back prior to the 1940s when underground roof support methods such as timber support were used (Yassien, 2003). These supports were external and passive and it was Weigel in 1943 who was the first to propose the main concepts of roof bolting to support the weak roof strata. In the 1970s, there was a rapid increase in the use of roof bolting and it became the primary roof support.

To support the tunnels with rock bolts is a costly exercise and the quality and density of the support determines the lifespan and reliability of the tunnel. Large stresses cause the tunnels to close up over time. Furthermore, injuries and fatalities to personnel often occur in tunnels, mostly due to the sudden advent of rock burst and consequent failure of the support system (Roberts, 1995).

The tunnel support systems in the South African gold and platinum mines are comprised of the following elements: tendons, wire mesh and wire rope lacing (Roberts, 1995). Shotcrete and steel sets are also used under certain conditions. These elements are combined into a system as illustrated in figure 1.1. Tendons can

be any form of reinforcing or support in the form of a bar; cable or tube inserted into bore holes in the rock mass and anchored there by grouting, friction or mechanical means. Some of the tendons are equipped with a base plate where the protruding end of the tendon is secured. This base plate sometimes has a ring built into it or the end of the tendon itself may be formed into a ring. The wire rope is then laced through these rings in a certain pattern. After this operation wire mesh is installed between the lacing and the rock for containment.

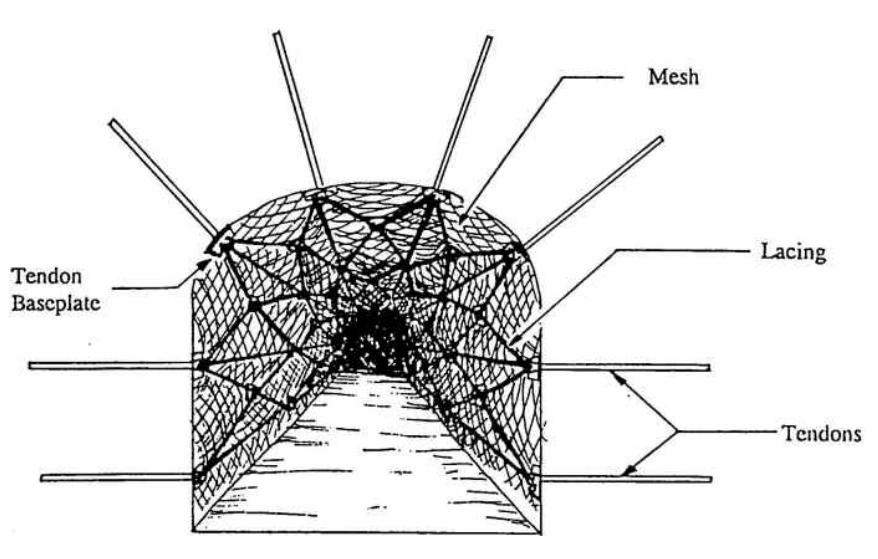

Figure 1.1: Tunnel and support elements (Roberts, 1995)

Different types of tendons (rock bolts) exist and the selection is based on the roof conditions. Yassien (2003) classifies the different types into five categories. These types are:

- Mechanical anchor bolts
- Resin-assisted mechanical anchor bolts
- Fully grouted resin rebar
- Torque-tension bolts
- Combination bolts

In Australia, the fully grouted resin bolt is currently the most common rock bolt (Gamboa and Atrens, 2003). In the U.S resin and fully grouted anchored rock bolts

comprise 80 percent of the bolt consumption (Yassien, 2003). Approximately 1.4 million bolts are installed monthly in South Africa, of which 600 000 are resin anchored bolts. The rest are mechanical and cementitious grouted bolts like shepherd crooks (Bornman, 2005). In this research, the focus will be on resin anchored bolts mostly used in the coal and platinum mines. For a more detailed discussion on the various types of bolts and the associated problems, refer to Appendix A.

The resin anchored bolt is installed using a rotary-percussive drill that drills a hole with a larger diameter than the bolt's diameter and a shorter hole depth than the bolt's length (Haarhoff, 2003). A plastic cartridge containing a resin and a catalyst are pushed to the end of the drill hole ahead of the bolt, which is then spun into hole. The plastic sheath of the cartridge is broken and the resin and catalyst are mixed by this spinning action. Setting of the resin occurs within a few minutes (depending upon the specifications of the resin mix) and a very strong anchor is created. This type of anchor will work in most rocks, including the weak shales and mudstones in which expansion shell anchors are not suitable (Hoek, *et al.*, 1995). In figure 1.2 such a bolt and resin compartment can be seen.

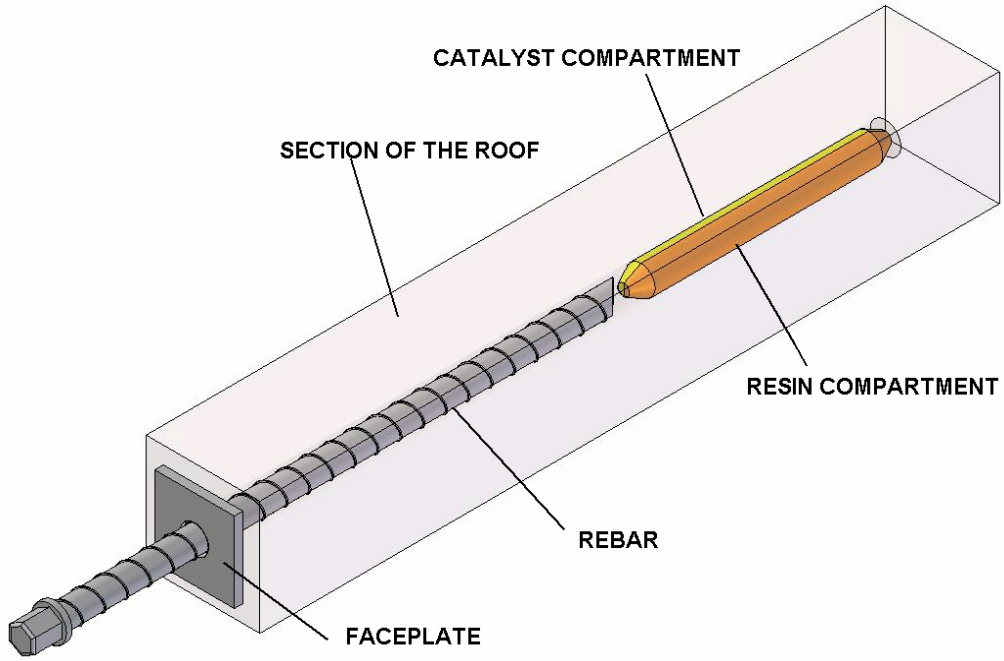

Figure 1.2: Resin anchored rock bolt

The high unit cost of resin cartridges is offset by the speed of installation. The process described above results in a completely tensioned and grouted bolt installation in one operation, something that cannot be matched by any other available system. However, as will become clear from the discussion, there are potential problems with the resin anchored bolts (Hoek, *et al.*, 1995).

1.3 Failure mechanisms of resin anchored bolts

Most resin/catalyst systems have a limited shelf life which, depending on the storage temperature and conditions, may be as short as six months. Breaking the plastic sheath of the cartridges and mixing the resins effectively can also present practical problems. Cutting the end of the bolt at an angle to form a sharp tapered point will help in this process. Once the setting process has been initiated, the structure of the resin can be damaged and the overall installation weakened by additional spinning. In some weak argillaceous rocks, the drill hole surfaces become clay-coated during drilling. This causes slipping of the resin cartridges during rotation, resulting in incomplete mixing and an unsatisfactory bond. In highly fractured rock masses, the resin may seep into the surrounding rock before setting, leaving voids in the resin column surrounding the bolt (Hoek, *et al.*, 1995).

Fully grouted bolts are loaded by the movement of the rock strata (Mark *et al.*, 2002). This movement may be vertical sag, shear along a bedding plane, or dilation of a roof layer buckled by horizontal stress. The movements cause tensile and bending forces in the bolt. The failure of the bolts is dependent on where the roof movements are concentrated and can fail in one of three ways. The head or the plate can fail, the bolt may break, either in tension, or a combination of tension and bending and lastly the anchorage may fail. These three failure mechanisms are shown figure 1.3.

In figure 1.4 one can see a typical roof support failure. In this example it was the grout-rock interface that failed.

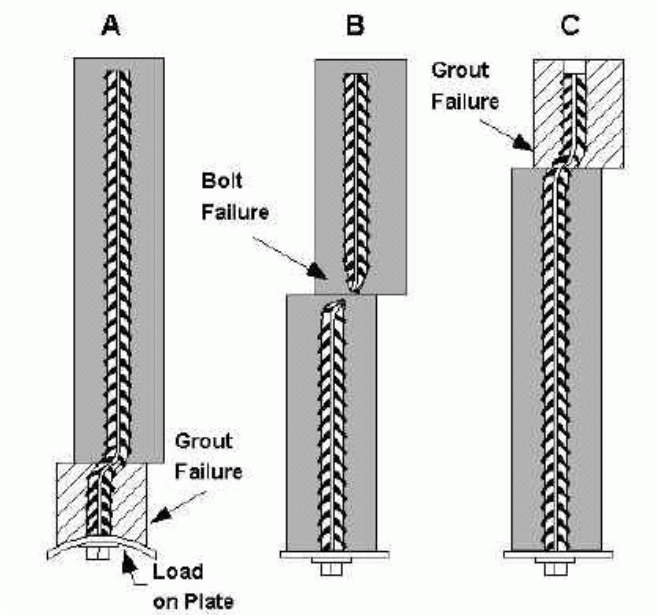

Figure 1.3: Failure mechanisms of a fully grouted roof bolt.
(A) Roof movement near head; (B) Roof movement in central portion; (C) Roof movement in anchorage zone (Mark *et al.*, 2002).

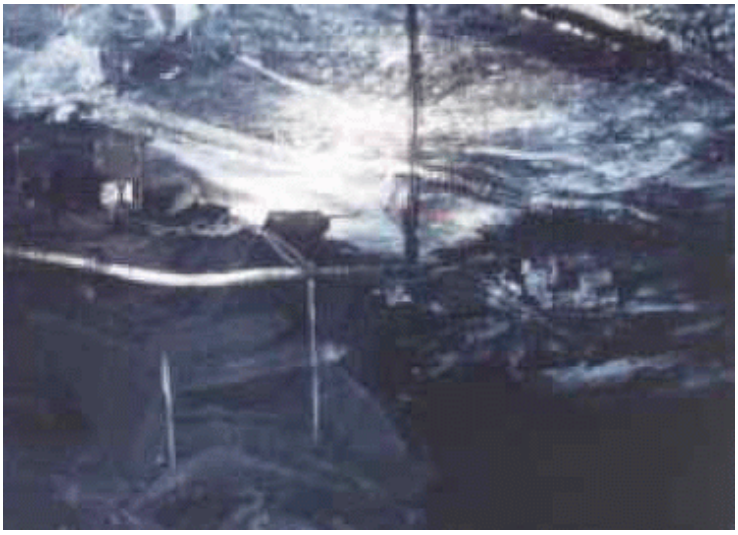

Figure 1.4: Photograph showing fully grouted bolts pulled from their holes in a roof fall (Mark et al., 2002)

1.3.1 Anchorage failure

One of the major problems is anchorage failure when roof movement occurs near the top of the hole (Mark *et al*., 2002). If the load applied to the bolt exceeds the strength

of the grout anchor, the top of the bolt will be pulled out of the hole. There are mainly three causes for poor anchorage namely: weak rock, poor installation and corrosion.

- **Weak Rock**

Testing results have consistently shown that weaker rock requires a longer grouted length to achieve the same anchorage as strong rock.

- **Poor installation**

A number of factors can result in poor anchorage with fully grouted bolts. The first is defective grout where the grout was not properly stored (for example too hot, too cold, too wet, or shelf life exceeded). The second is improper mixing when required spin time is not followed. Under-spinning can result in inadequate mixing, while over-spinning can destroy the partially cured resin. Improper mixing can also occur with long bolts where the top of the hole has less time to mix before the bottom sets up. The temperature of the resin at the time of installation can also affect the cure time. The third is improper holes where the holes can be too deep, too short, too large, or too smooth. The proper grout cartridge should also be matched to the hole and bolt size. Finger gloving where the plastic cartridge wrapper remains unbroken around the hardened resin is another installation associated problem (Mark *et al.*, 2002).

- **Corrosion**

Another source of failure that is attracting more and more attention is the phenomenon of corrosion of rock bolts in an underground environment.

There is some uncertainty about long-term corrosion protection offered by resin grouts and also about the reaction of some of the resins with aggressive groundwater. For typical mining applications these concerns are probably not an issue because of the limited design life for most bolt installations. However, where very long service life is required, current wisdom suggests that cement grouted bolts may provide better long-term protection (Hoek, *et al.*, 1995).

Field observations have shown that unprotected rock bolts corroded freely and rapidly under certain conditions (Charrette, 2004). Water conditions are often not taken into account because the water supply is non-corrosive at the source. But the

process of recirculation of water, often gathers corrosive ions and renders the water more aggressive toward steel components.

Corrosion can be either uniform or very localized. Uniform corrosion is characterized by a regular loss of metal from the corroding surface. For example a rock bolt will be radially thinned from the outside to the inside, or, in the case of split tube stabilizers, from both sides. Localized corrosion will produce metal loss in a very confined area of the exposed surface. For example pitting can be seen in areas where the bolt surface is metallurgically non-homogenous, or where certain types of rock minerals are in contact with the bolt.

From the above discussion it can be seen that it is important to do research on the different defects associated with resin anchored bolts. Furthermore, a non-destructive test will help to improve the safety and productivity in the mining industry.

1.4 The history of rock bolt condition monitoring

In 1996 to 1998 approximately half of the fully grouted bolts were not as effective as they should be (Kelly *et al*., 1996; Harper and Basson, 1998). The quality of installation and grouting of rock reinforcing tendons is regarded as a serious problem by the mining industry.

These ineffective grouted tendons increase the risk of ground falls and hence constitute a hazard of death or injury and influence the productivity.

The method presently used in South African mines to test a rock bolt's integrity, is the pull-out test. This is a destructive test and time-consuming (Kelly *et al*., 1996). There is thus a need for a quick non-destructive test.

Since 1977 studies were undertaken to develop a non-destructive testing method to determine a rock bolt's integrity. Some looked at electromagnetic techniques and others at acoustic techniques. By far the greatest effort of these studies went into measurement techniques based on sound waves. The acoustic principle offers

promise in that sound waves are directly influenced by mechanical coupling, which lies at the heart of the problem of grouting effectiveness. (Kelly *et al*., 1996).

In the next section the different approaches to determine the bolt's integrity are summarized and evaluated.

1.5 Review of destructive rock bolt testing

1.5.1 Pull-out test

The pull-out test is widely used to test the integrity of bolts. Different products exist, varying on the type of tendons that it can test. In figure 1.5 one such product can be seen.

The working principle is to connect a hydraulic jack to the nut and pull the bolt from the roof, while the load versus extension is recorded. Two categories of pull out requirements can be used. The first is to see if the bolt can withstand a required level of load and stop the test. The second is to see the actual bonding strength and pull the bolt until it fails. Because of the bonding strength of fully grouted bolts, it is impossible to pull the bolt out of the roof before the bolt itself will fail. The Critical Bond Length (CBL) is the critical length of grout coverage to pull the bolt out of the hole rather than to break the bolt (Kelly *et al.*, 1996).

It is apparent that such a test cannot provide a good indication of the effectiveness of the fully grouted bolt.

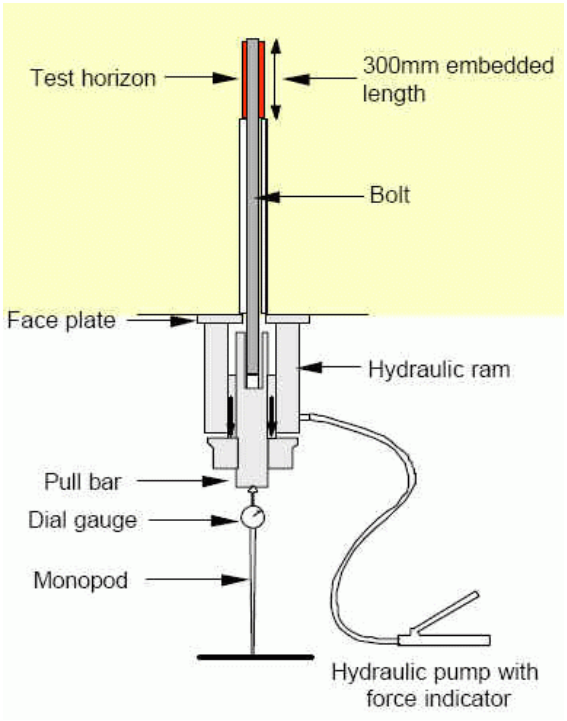

Figure 1.5: Pull test equipment (RMT Ltd, 2003)

1.6 Review of non-destructive rock bolt testing

The most promising non-destructive testing techniques are discussed below.

1.6.1 Boltometer

The Boltometer is an ultrasonic device developed by Geodynamik in Sweden; it has been in used since 1979 and is designed for full bar anchors preferably with diameters between 20 and 30 mm. The instrument can be used on cemented grouted bolts and also on polyester and some other resin grouts (Thurner, 1996). The instrument can be seen in figure 1.6.

Figure 1.6: Boltometer (Geodynamik, 2001)

The Boltometer uses piezoelectric crystals to transmit elastic waves (compressional and flexural waves) into the bolt. The waves propagate through the bolt, reflect at the inner end and the echo is received by the sensor. If the grouting is good most or all of the wave energy disappears into the rock, leaving a small or zero echo to the piezoelectric crystal. Insufficient grouting will result in a distinct echo, which is easy to read on the paper printout (Thurner, 1996).

The Boltometer can indicate bad grouting, but if the impedance between the grout and surrounding rock are the same; wave energy will dissipate into the rock before it could reach a major defect, reporting good grouting. Furthermore, the penetration length is dependent on the type or density of the grout. Polyester resin, for example, can permit a penetration of almost 10 m, very often giving indication of the number of resin cartridges, which cause small echoes. Cement grout can be penetrated up to 5 m and epoxy grout and thermoplastic has a penetration length of about 1 m (Thurner, 1996). Another limitation is the inability to measure shepherd's crooks and a reduced performance in the presence of mesh, lace and washers (Kelly et al., 1996).

1.6.2 JK rockbolt tester

The JK rock bolt tester is a device developed by the JKMRC at the University of Queensland and is based on the measurement and analysis of the complete dynamic response of the bolt. The essence of the method is to measure the frequency response function of the bolt. This function can be considered as the signature of the bolt *in situ*. Resonant frequencies and associated damping ratios are primarily determined by the mechanical characteristic of the bolt *in situ*, resin grout and the rock (Djordjevic, 1999).

1.6.3 GRANIT

The ground anchorage integrity testing (GRANIT) system was developed at the University of Aberdeen in Scotland and is a patented solution. This testing system applies an impulse of known force by means of an impact device that is attached to the tendons. The vibration signals that arise from this impulse are complex in nature and require analysis to be performed. Novel artificial intelligence techniques are used in order to learn the complicated relationships that exist between an anchorage and its response to an impulse. The system has a worldwide patent and is currently licensed commercially (Starkey *et al.*, 2003).

The operating principle of the GRANIT system is as follows: A loading device named the universal impact device is attached to the tendon (on this device an accelerometer is attached). A single axial impulse load is generated at the head of the tendon. A set of datum response signatures for different post-tension levels is recorded for the anchorage immediately after installation. The condition of the tendon at any later date can be determined by comparing the datum with the characteristics of the subsequent response signatures. A change in characteristics indicates a potential change in the integrity of the anchorage. It is difficult determining the relationship between the dynamic response of the anchorage and its post-tension level. Therefore, neural networks are implemented, which suit the task of learning such complicated non-linear relationships. The neural network, trained on a single tendon, may be used to diagnose the post-tension level of a number of tendons (Starkey *et al.*, 2003). The disadvantage of the GRANIT system is that it can only work on rock bolts that have been characterised at installation.

1.6.4 Ultrasonic Guide Wave Testing

A study was conducted by Imperial College in England and they developed what seems to be the most promising technique. The inspection technique is an ultrasonic pulse echo test, carried out from the free end of the bolt. A schematic diagram of the rock bolt guided wave inspection method is shown in figure 1.7. A picture of the laboratory testing facility used in this research is shown in figure 1.8. The research showed that the proposed approach could determine the bolt length and identify major defects such as loss of resin encapsulation, necking and deformation (Beard and Lowe, 2003).

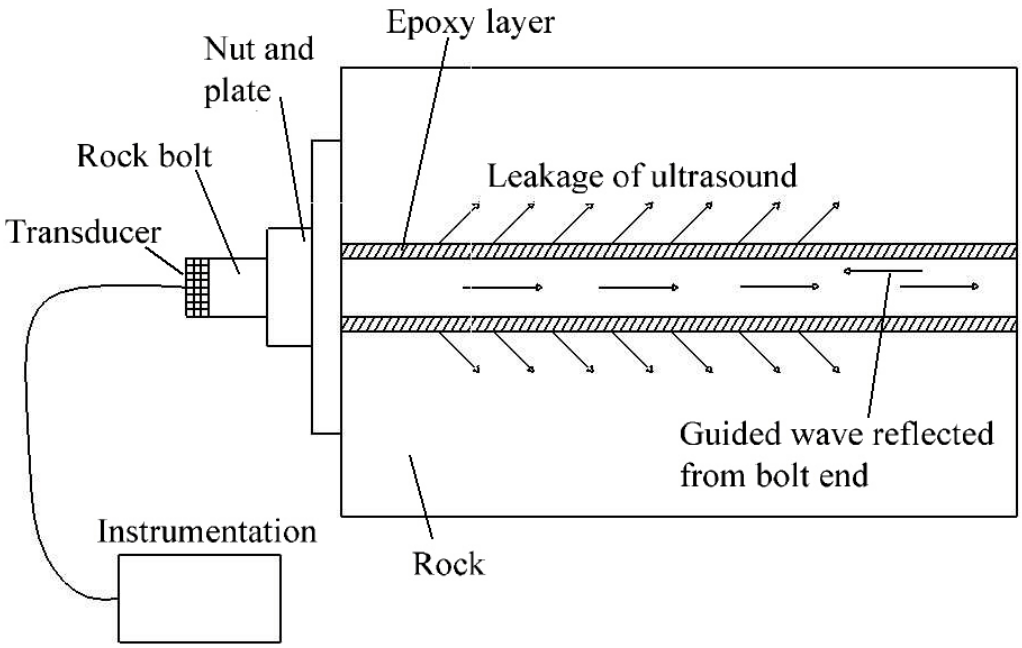

Figure 1.7: Schematic diagram of the rock bolt guided wave inspection method (Beard and Lowe, 2003)

The following procedures are followed: An ultrasonic transducer is clamped onto the end of the bolt and connected to a pulse-echo instrument. A short duration Gaussian windowed sine burst is used to excite a guided wave in the bolt, which is then reflected from the bolt end and from any major defects. The reason for using a Gaussian windowed sine burst signal is that the excitation frequency can be tightly controlled and thereby excite specific modes. From the reflection arrival time and knowledge of the wave velocity dispersion curves the positions of the defects or the

bolt length can be calculated. The maximum test range is limited by the amount of attenuation that the wave experiences as it propagates. The major cause of attenuation is the fact that ultrasonic energy tends to leak from the bolt into the surrounding rock.

Different studies were undertaken to find the best guided wave mode, frequencies and excitation time duration. The selection of suitable modes and frequencies was done by inspection of dispersion curves.

The study concluded that the bolts should be tested in its low frequency range (30 – 70 kHz) as well as in its high frequency range (2-5 MHz). The low frequency test can be used to identify defects such as partial bolt encapsulation and possibly corrosion patches near the bolt surface. On the other hand, the high frequency test is not sensitive to surface defects, but can give a reliable indication of the bolt length. The fact that high frequency waves are attenuated by curvature also allows the possibility of determining whether or not bolts are deformed (Beard and Lowe, 2003).

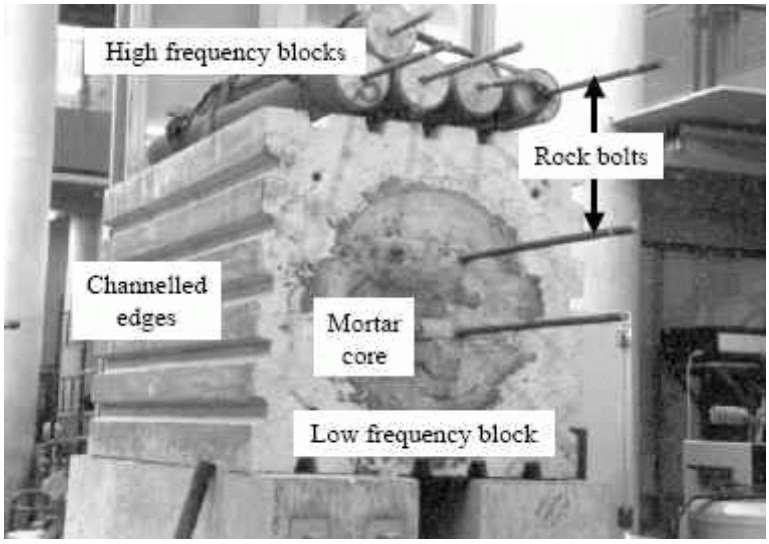

Figure 1.8: Picture of the specimens that were used for testing rock bolts in the laboratory (Beard and Lowe, 2003)

It was not possible with their modelling tools to determine the dispersion relationships for bars with 3 dimensional features. Because the rock bolt end and certain defects are not always axially symmetric it may be necessary to model the bolt with three-

dimensional finite elements (Beard, 2002). Furthermore the study focused primarily on the identification of suitable modes which are not significantly influenced by the embedding rock modulus, the epoxy thickness and modulus and the bolt-epoxy bond quality. With the limitations of the analytical model, it was not possible to simulate complex defect scenarios.

It is thus necessary to model certain defects with finite elements to contribute to the development of guided wave inspection of fully grouted bolts.

1.7 Physics of ultrasonic guided waves

Ultrasonic guided waves offer the potential to transmit guided wave modes in a bolt, which are more sensitive to resin and surface defects than any other non-destructive test. Guided waves seem to be the most promising technique presently available to determine the integrity of resin anchored rock bolts. The following topics deal with ultrasonic principles, especially guided waves and the modelling of their wave propagation.

Ultrasonic testing is based on the analysis of time varying deformations in materials, which is generally referred to as acoustics. Acoustics focus on particles that contain many atoms that move in unison to produce a mechanical wave. When the particles of a medium are displaced from their equilibrium positions, internal restoring forces arise. These elastic-restoring forces, combined with the inertia of the particles, lead to oscillatory motions of the medium (Auld, 1973). In gases the oscillatory motion of the medium cause compression and rarefaction areas in the gas and energy travels in the direction of oscillation. However, in solids, molecules can support oscillations in other directions and different types (modes) of waves are possible. The longitudinal and shear waves are surely the most widely used in ultrasonic testing, but at surfaces and interfaces, various types of elliptical or complex vibrations of the particles make other waves possible (NDT Resource Center, 2001).

Ultrasonic waves can be distinguished into two categories. These are bulk and guided waves. Bulk waves are waves that travel in the bulk of the material (thus,

away from the boundaries) and are limited to longitudinal and shear waves. Guided waves on the other hand need a boundary to exist (Rose,1999). The reflection and refraction with the boundaries, cause mode conversion between longitudinal and shear waves giving rise to numerous modes of propagation that are called guided waves. It is these types of waves that will propagate in a rock bolt.

The physics of guided waves can be explained by the example of plate waves. Impinging the plate with a tone-burst by a transducer generates the guided wave. The resulting refraction and reflection at the interfaces (boundaries) of the plate let mode conversion occur. After some travel in the plate, interference cause the formation of "wave packets" that are known as guided wave modes in a plate. By adjusting the entry angle and frequency, different modes can be generated in the plate. Guided wave modes can also be transmitted in rods, tubes and embedded layers (Rose, 1999).

Many guided wave modes can exist in a particular component. Each of these modes has a particular wave structure. The wave structure describes the distribution of particle motion through the thickness of the layer. Some modes have large particle motion amplitudes near the surface, while others have more intense motion near the middle of the layer. The wave structure determines the sensitivity of the particular mode to a particular flaw type. Therefore the selection of the appropriate mode is very important to inspection optimization. Sometimes it may be possible to perform an inspection using only a single mode. To generate a single mode a narrow band transducer should be used to limit the number of generated modes. By employing sine burst excitation the bandwidth of the signal may be reduced. Theoretically, a sine burst enclosed in a 'Hanning Window' would help to suppress modes either side of the dominant frequency in the frequency spectrum. In this way single mode generation is more likely to be achieved (Clifford, 2000). Multimode guided wave testing requires broad bandwidth transducers but yields additional information in more difficult test situations (Krautkramer, 1998).

The velocity of propagating waves is one of the most important parameters in ultrasonic testing. In bulk waves it is constant and can be calculated with equation

1.1, but in guided waves it changes with frequency and this relationship is represented as a dispersion curve (Staszewski *et al.*, 2004).

The relationship between velocity and the elastic properties and density can be given as:

$$c^2 = \frac{E}{\rho} \tag{1.1}$$

where c is the velocity of the wave and *p* is the density of specimen and E is the longitudinal modulus.

Ultrasonic waves can travel long distances in solid materials. However, the acoustic energy decreases with the distance of propagation. This is called attenuation. Propagating waves are scattered or reflected and are absorbed by different material/structural boundaries. When a wave passes between different media, the velocity of the propagation changes according to Snell's Law. Additionally, various mode conversions occur. Ultrasonic testing utilizes wave attenuation, reflection and refraction for damage detection. It is important for successful damage detection that the wavelength of ultrasound used for testing is of the order of the defect's size. The wavelength λ can be calculated with equation 1.2 as:

$$\lambda = \frac{c}{f} \tag{1.2}$$

where f is the input frequency (Staszewski *et al*., 2004).

The problem in imbedded structures is leakage of ultrasonic energy into the surroundings. Propagation distances of guided waves in steel pipes or bars in air are many tens of meters but when the bar or pipe is surrounded by a fluid or solid, leakage of energy into the material is possible. The attenuation rate can be very high when the acoustic impedances of the waveguide and the surrounding solid are similar. This is exactly the case with the rock bolts in the mining industry (Pavlakovic, *et al*., 2001). With the modelling tool Disperse they showed that there exist guided

wave modes with minimum attenuation, which could be used for ultrasonic inspection of rock bolts.

1.8 Modelling of ultrasonic waves

The general governing equation describing wave propagation in an infinite medium is Navier's wave equation. For wave propagation in an infinite rod, Navier's equation is formulated in cylindrical coordinates (Rose, 1999). The Navier's-equation is a second order linear partial differential equation and a solution subject to certain boundary conditions is needed. A variety of different techniques could be used to solve the second order partial differential equation (Rose, 2003).

One technique is to propose a particular solution and substitute it into the governing equation to check if the governing equation is satisfied. If a harmonic solution is assumed and the boundary conditions are satisfied, a system of homogeneous equations evolves. In order to find a nontrivial solution, the system of homogeneous equations must have the determinant of the coefficient matrix set equal to zero. By extracting the roots, solutions for phase velocity (the velocity of a particular wave in a packet of waves) versus frequency are set up. These values are plotted on a dispersion curve, so named because the velocity changes with frequency and pulses tend to become stretched or dispersed as they propagate (Rose, 2003).

Every natural wave guide like the rock bolt has associated with it, a set of dispersion curves that presents to us the wave propagation possibilities in the structure. Some modes at a specific frequency are much better than others for improved reception, sensitivity and penetration power (Rose, 2003; 2004).

1.8.1 Dispersion curves

The complex effect of the boundaries means that energy propagates in modes that have predictable frequency-dependent properties, which can be calculated by the solution of the wave propagation equation as discussed above. The mathematical

solution to the propagation equation yields a number of solutions that form continuous propagating modes (Beard, 2002).

The velocity is not only dependent on the material (like longitudinal, shear and surface waves) but also the thickness of the material and frequency. Dispersion curves are used to describe and predict the relationship between frequency, phase velocity and group velocity, mode and thickness (Rose, 2003). An example of the phase and group velocity curves for a 20 mm diameter perfectly elastic rod in a vacuum is shown in Figure 1.9.

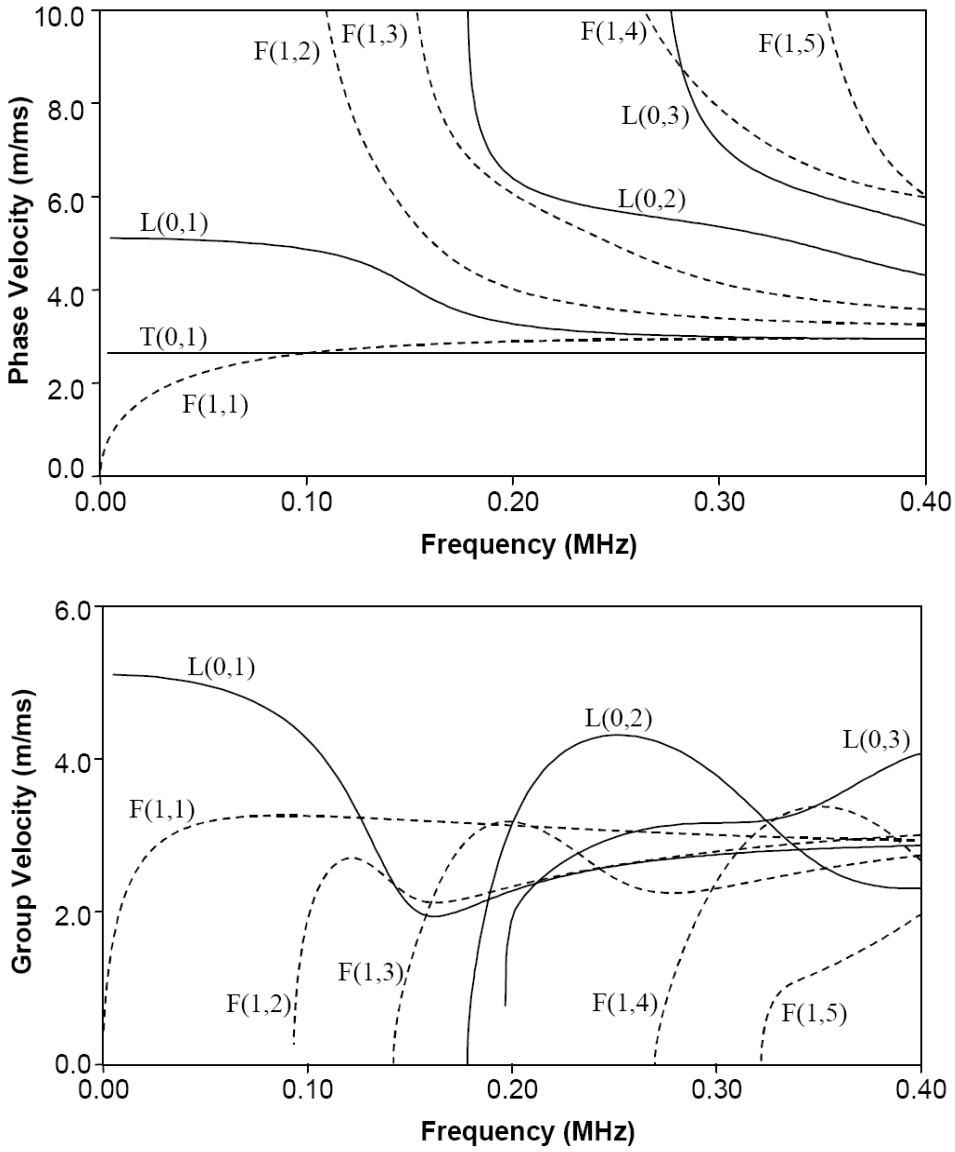

Figure 1.9: Phase and group velocity curves for a 20 mm rod in a vacuum (Beard, 2002)

The velocity of a wave packet is called the group velocity. The group velocity can differ from the phase velocity and changes drastically as we move along each mode as frequency is swept. It is the group velocity that is measured in a laboratory in order to carry out location analysis for a particular discontinuity. The group velocity is derived from the phase velocity curve (Rose, 2003). The group velocity curves show the variation in the velocity over a frequency range. Thus it shows how dispersive a mode is (Beard, 2002).

As discussed in section 1.6 the general purpose modelling software, Disperse, was developed by Pavlakovic, *et al*. (2001) for the prediction of the dispersion curves of systems having either flat or cylindrical geometries with an arbitrary number of layers. The software can solve for both axisymmetric and non-axisymmetric wave propagations like longitudinal, torsional, and flexural modes and can also model leakage into a solid or liquid medium.

The convention used by the Disperse Software follows the Silk and Bainton format. Each mode is identified by the use of a letter and two reference numbers. The longitudinal modes are numbered in the series L(m,n), and the flexural modes are numbered in the series F(m,n). The ‘m’ variable refers to the variation in the displacement around the circumference of the bar. This variable is zero by definition for the axially-symmetric longitudinal modes. For the flexural modes the ‘m’ variable is determined by the number of displacement cycles around the outside of the bar, hence the displacement varies as cos(mϴ) around the circumference. The second number ‘n’ is a counter variable, the modes being numbered sequentially as they appear with increasing frequency. The lowest frequency axially symmetric mode is therefore L(0,1) (Beard, 2002).

The first investigators of the mathematically equations of guided wave propagation in cylindrical waveguides were Pochhammer and Chree, and their names are still associated with the equations that describe the modes in a solid cylinder. Leaky cylindrical systems have been much more difficult to model than their free counterparts. Much of the difficulty arose from the need to calculate complex Bessel functions, which were not readily available. This has however now changed and can be solved (Pavlakovic, *et al*., 2001). No analytical equations can be set up for

complex geometries and defects in cylindrical waveguides. It is therefore necessary to use other approaches. Furthermore guided waves can encompass many different modes that propagate independently through a structure. These wave packets interact with defects and geometrical features such as curved corners or surfaces, causing reflections, refraction and thus mode conversion. The propagation of guided waves in a complex structure is a complicated process that is difficult to understand and interpret. Therefore, computer simulation and visualization of guided waves are effective tools to clarify such complex ultrasonic wave motions (Moser *et al*., 1999).

1.9 The Finite Element Method

The boundary element (BE) method and the finite element (FE) method are commonly used to model wave propagation.

The BE method has the advantage that only the surface of the specimen needs to be discretised; the numerical problem itself is therefore reduced by one dimension. The primary advantage of the finite element method is that there are numerous commercial FE codes available, thus eliminating any need to develop actual code. These commercial FE codes have the additional advantages of being very user friendly, and providing sophisticated pre- and post-processing options. For example, a snapshot of the displacement field or a colour plot of the stress distributions can give new insights into wave propagation phenomena (Moser *et al*., 1999).

According to Kishore *et al*. (2000) previous researchers have concluded that the finite element method (FEM) is superior to the other methods because of its versatility to model flaws of arbitrary shape and size, and its ability to incorporate anisotropic and inhomogeneous material characteristics with ease. However, the disadvantage of the FE technique is that it is computationally demanding (Hill *et al*., 2004). But with the evolution of processor speed it will become increasingly attractive to model different wave propagation problems.

In addition, the research of Moser *et al*. (1999) clearly demonstrated the effectiveness of using the FE method to model 2D guided wave propagation problems, specifically demonstrating the potential of the commercial FE package for

problems when an analytical solution is not possible because of a 'complicated' component geometry.

If the frequencies are high a high time resolution is needed. In addition, these high frequencies have very short wavelengths, so the numerical model must have small element lengths to accurately resolve these spatial features. This high spatial resolution implies very small elements. An additional complication of this small element size is that a large number of elements (and thus a large system of equations) are needed to model a realistic component. As a result, the FE solution requires the inversion of a large stiffness matrix, if an implicit integration is used, leading to a requirement for significant computational power (Moser *et al*., 1999). There are also explicit methods that do not require inversion of the stiffness matrix and can reduce the computation time required. To understand the different solution methods a short discussion of these are given in the following sections.

1.9.1 Implicit Integration

The MSC software offers various options to solve the FE equation of motion. The implicit solver is based on the Newmark scheme and the explicit solver is based on the central difference scheme. To clearly see the benefit of each a short description of each is given below and can also be seen in the MSC Document library, (2005).

If the current time step is n, a good estimate of the acceleration at time n+1 will satisfy the following equation of motion:

$$Ma'_{n+1} + Cv'_{n+1} + Kd'_{n+1} = F^{ext}_{n+1} \qquad (1.3)$$

where

M	=	mass matrix of the structure
C	=	damping matrix of the structure
K	=	stiffness matrix of the structure
F^{ext}_{n+1}	=	vector of externally applied loads at step n+1
a'_{n+1}	=	estimate of acceleration at step n+1

v'_{n+1} = estimate of velocity at step n+1

d'_{n+1} = estimate of displacement at step n+1

where the prime denotes an estimated value.

The estimates of the displacement and velocity are given by:

$$\begin{aligned} d'_{n+1} &= d^*_n + \beta a'_{n+1}\Delta t^2 \\ v'_{n+1} &= v^*_n + \gamma a'_{n+1}\Delta t \end{aligned} \qquad (1.4)$$

where Δt is the time step and β and γ are constants.

The terms d^*_n and v^*_n are estimates based on previously calculated values.

Substituting these values in the equation of motion results in:

$$\begin{aligned} &\left[M + C\gamma\Delta t + K\beta\Delta t^2\right] a'_{n+1} = F^{ext}_{n+1} - Cv^*_n - Kd^*_n \\ &\therefore M^* a'_{n+1} = F^{residual}_{n+1} \\ &\therefore a'_{n+1} = M^{*-1} F^{residual}_{n+1} \end{aligned} \qquad (1.5)$$

This is analogous to decomposing the stiffness matrix in a linear static analysis, but with mass and damping terms also present.

Temporal and spatial resolution of the finite element model is critical for the convergence of these numerical results (Moser *et al*., 1999).

The integration time step, Δt, is the step size for which the equation of motion is solved. Choosing an adequate integration time step, Δt, is very important for the accuracy of the solution. In general, the accuracy of the model can be increased with increasingly smaller integration time steps. With time steps that are too long, the high frequency components are not resolved accurately enough. On the other hand, too small time steps are a waste of calculation time. Therefore, a compromise must be found. For the Newmark time integration scheme, this compromise is 20 points per cycle of the highest frequency. This gives accurate solutions in an efficient manner. This rule is expressed as:

$$\Delta t = \frac{1}{20 f_{max}} \tag{1.6}$$

If the input function gets close to a step function, the ratio given in Eq. 1.6 might not provide sufficient temporal resolution. In such case the time step must be reduced as small as $\frac{1}{180 f_{max}}$.

The size of the elements are chosen in a manner so that the propagating waves are spatially resolved, it is recommended that:

$$L_e = \frac{L_{min}}{20} \tag{1.7}$$

where L_e is the element length and L_{min} is the shortest wavelength of interest (Moser *et al*., 1999).

1.9.2 Explicit Integration

MSC Dytran is an explicit method and does not require matrix decompositions or matrix solutions. A short discussion follows to explain the basic principle of this explicit software.

The equation of motion:

$$Ma_n + Cv_n + Kd_n = F_n^{ext} \tag{1.8}$$

can be rewritten as:

$$Ma_n = F_n^{ext} - F_n^{int}$$

$$\therefore a_n = M^{-1}(F_n^{ext} - F_n^{int})$$

$$a_n = M^{-1}F_n^{residual}$$

where

F_n^{ext} = is a vector of externally applied loads

F_n^{int} = is a vector of internal loads $F^{int} = Cv_n + Kd_n$

M = mass matrix

Thus the accelerations can be found by inverting the mass matrix and multiplying it by the residual load vector. If M is diagonal, its inversion is trivial, and the matrix equation is the set of independent equations for each degree of freedom:

$$a_{ni} = \frac{F_{ni}^{residual}}{M_i} \tag{1.9}$$

By assuming that the accelerations are constant over the time step and using the central difference scheme to advance in time, the velocity and displacement can be calculated:

$$v_{n+1/2} = v_{n-1/2} + \frac{a_n(\Delta t_{n+1/2} + \Delta t_{n-1/2})}{2}$$
$$d_{n+1} = d_n + v_{n+1/2}\Delta t_{n+1/2} \tag{1.10}$$

Implicit methods can be made unconditionally stable, regardless of the size of the time step. However, for explicit codes to remain stable, the time step must subdivide the shortest natural period in the mesh. This means that the time steps must be less than the time taken for a stress wave to cross the smallest element in the mesh (MSC.Dytran Theory Manual).

Figure 1.10 shows the comparison in CPU time cost against problem size for the implicit and explicit solvers respectively.

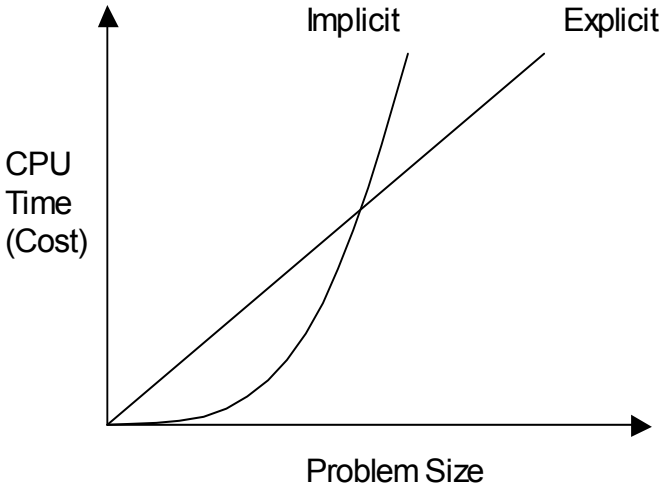

Figure 1.10: Comparison in CPU time between implicit and explicit integration

1.10 Summary of the literature study

Different types of bolts are in use but the most commonly used is the resin anchored bolt because of its load bearing capacity and ease of installation. These bolts have different problems associated with them like corrosion, over-spinning, voids and cracks. Currently there is no reliable no non -destructive test available in South Africa to determine the condition of a rock bolt.

Different techniques and research studies on the condition monitoring of rock bolts were discussed and evaluated. The most promising technique was based on guided ultrasonic waves.

Guided waves can consist of many different modes that propagate independently through a structure. These wave packets interact with defects and geometrical features, causing reflections, refraction and thus mode conversion. The propagation of guided waves in a complex structure is a complicated process that is difficult to

understand and interpret. Therefore computer simulation and visualization of guided waves are effective tools to clarify such complex ultrasonic wave motions.

The finite element method seems to be a promising modelling tool because of its availability, user friendliness and the sophisticated pre- and post-processing options that are available. Different integration techniques exist to solve the equation of motion. The explicit solver seems to be the most promising one for large wave propagation problems.

1.11 Scope

The aim of this study was to extend the previous work by Beard and Lowe (2003) to investigate damage in more realistic embedded bolts which deviate from pure cylinders. The fundamental L(0,1) mode in its lower frequency range suggested by Beard and Lowe will be utilized. This is done through the use of finite element models of various defect scenarios, which are simulated and compared to experimental measurements on bolts. Defects like loss of resin encapsulation, voids and local corrosion cracks will be addressed. The time traces of the different finite element defect scenarios could be directly compared to experimental time traces which distinguish this study from the analytical approach. Three dimensional and axisymmetric models using commercially available finite element software will be compared. Different solver algorithms will be utilized to determine the best solver for solving large finite element models.

Once the integrity of models such as these have been established, the models could in principle be used to train neural networks for use in commercial equipment. The present study was limited to lower frequencies because of computer resource limitations. Basic principles and modelling issues could however be addressed and it may be expected that these principles could soon be extended to higher frequencies with a new generation of computers.

CHAPTER 2

MODELLING ISSUES

2.1 Introduction

Modelling guided wave propagation in rock bolts can be done using full three dimensional models or axisymmetrical models. By assuming axial symmetry of the geometry, load, boundary conditions and materials, the axisymmetric model allows one to analyze the three dimensional bolt and surrounding rock mass with a two dimensional model. However, defects can occur that are not symmetric around the axis and in which case a three-dimensional model of the rock bolt will be necessary.

Choosing of an appropriate integration time step and element size is critical to the success of a finite element solution. In general, the accuracy of the model can be increased with increasingly smaller integration time steps. With time steps that are too long, the high frequency components are not adequately resolved. On the other hand, too small time steps are a waste of calculation time. The size of the elements is chosen in a manner so that the propagating waves are spatially resolved. In this chapter issues such as the influence of the mesh density and time step size on the finite element modelling of guided waves in bolts and embedded bolts are investigated. The effect of damping and the effect of boundaries on the finite element models are discussed. The finite element model of an unbounded bolt was compared to the well known group velocity curve for an unbounded bolt. This was to verify the accuracy of the modelling approach. This chapter provides the foundation for finite element modelling of guided waves in defective rock bolts.

2.2 The influence of mesh density and time step size

To be computationally efficient, it is important to know what the efficient mesh density and time step is. The effect of the mesh density and time step size on an axisymmetric as well as a three-dimensional model was investigated. The three dimensional model was solved in MSC.Nastran and MSC.Dytran to compare the different solving algorithms. The former is an implicit and the latter an explicit solver.

2.2.1 Axisymmetric model

An axisymmetric model of a 1.5 m long rock bolt with a diameter of 20 mm was built to study the effect of different time steps and mesh densities as illustrated in figure 2.1. A surface was generated in MSC.Patran with a size of 1.5 m x 0.01 m, which is the cross sectional surface of the bolt. The surface was meshed with TRIA 6 elements with the axisymmetric properties defined. The material was steel with a density, elastic modulus and Poisson's ratio of 7850 kg/m³, 206 GPa and 0.3 respectively.

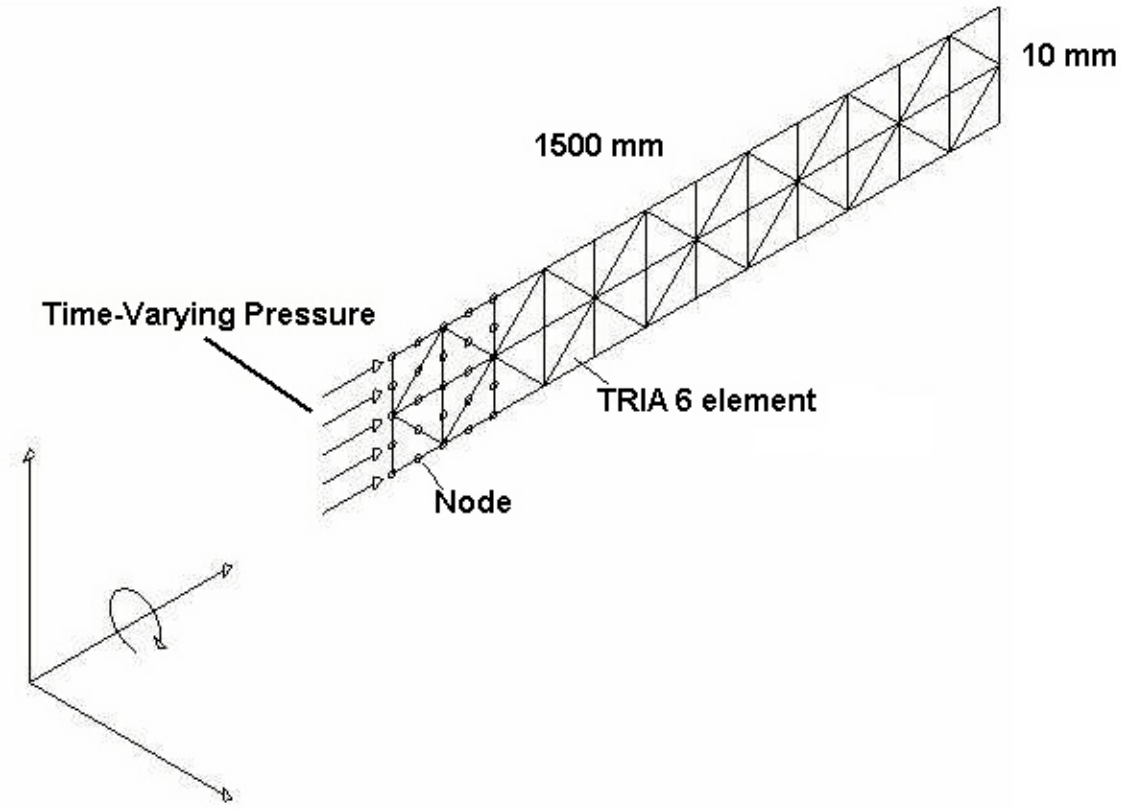

Figure 2.1: Representation of an axisymmetric model of the rock bolt

A time-varying pressure load of 1 Pa was applied to the one edge. The time-varying pressure was defined by a field, which was imported from a text file. The time varying signal can be seen in figure 2.2. The dispersive nature of the guided waves causes each frequency component of the wave to travel at its own speed and thus influencing the shape of the reflecting signal (Beard, 2002). The reason for the Gaussian windowed sine burst of the input signal is to control the frequency bandwidth of the input signal and thereby reduce the effect of dispersion.

To effectively transmit a specific guided wave mode, the displacement of the transducer should match the displacement of the mode profile. Dispersion cause different frequency contents of a transmitted signal to travel at different speeds. It is therefore important to transmit a signal with a very narrow frequency band. There are two ways of doing it; the first is to transmit a signal with a large number of cycles. The problem with a many cycles is that it will conceal early reflections. Thus the number of cycles influences the distance away from the free edge at which the closest defects can be detected. The second is to use a windowed sine burst. A 6 cycle sine

burst and a 6 cycle Gaussian windowed sine burst were transmitted in an experimental unbounded bolt. It is noteworthy that it was difficult to distinguish the end reflections for the sine burst, but for the Gaussian windowed sine burst there was a clear reflection. The effects of the discontinuities at the start and end of the transmitted signal are reduced by using a Gaussian windowed sine burst. Thus, the Gaussian windowed allows more energy to be focussed at a particular frequency. In figure 2.2 a 50 kHz Gaussian windowed sine burst and its Fast Fourier Transform are presented.

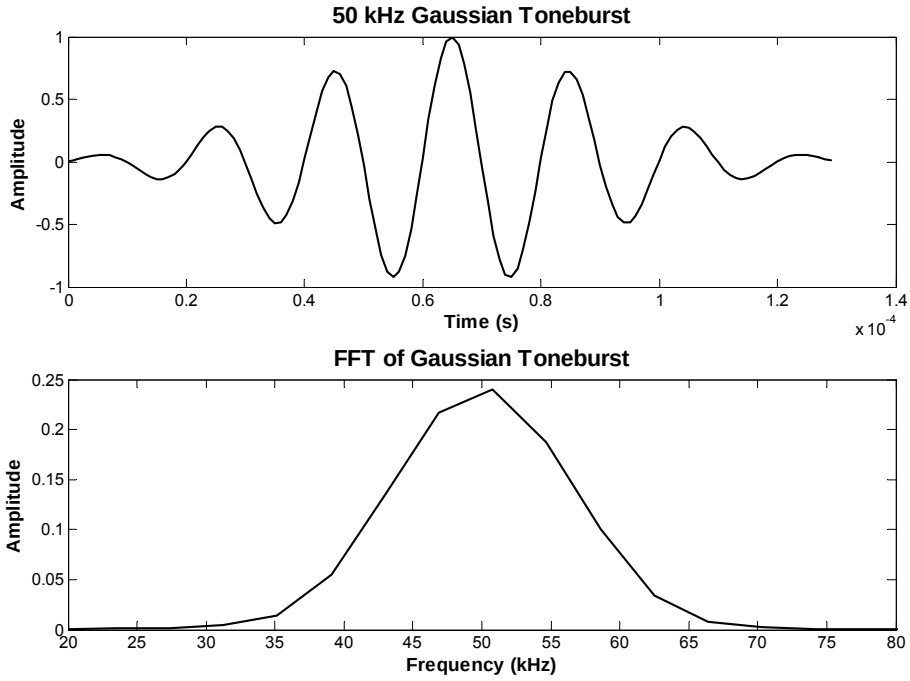

Figure 2.2: Gaussian windowed sine burst and the FFT of the pulse

Two axisymmetric models, one with a 50 kHz time-varying pressure and another with a 20 kHz time-varying pressure, were analysed to investigate the effect of mesh density and time step size.

Axisymmetric 50 kHz model

Two different meshes with three different time steps were modelled. The first model's element size was the recommended 20 nodes per wavelength (Moser *et al*., 1999). The second mesh element size was half of the first element size. For this mesh density three different time steps were chosen. The first was the recommended 1/20f, the second 1/40f and the third 1/80f.

The longitudinal bulk sound speed in steel can be calculated as follows:

$$c = \sqrt{\frac{E}{\rho}} = \sqrt{\frac{206\,x10^{9}}{7850}} = 5123 \ \ m/s\,.$$

The element size for the 50 kHz pulse is calculated in the following way:

$$\lambda = \frac{c}{20f} = \frac{5123}{20\ x\ 50000} = 5\ mm\,.$$

The required time step was calculated as follows:

$$\Delta t = \frac{1}{20f} = \frac{1}{20\ x\ 50000} = 1\ \ \mu s$$

The second mesh's element length was 2.5 mm. The second and third time step was 0.5 µs and 0.25 µs respectively.

In figure 2.3 a portion of the pulse computed at a distance along the rod can be seen. The red lines represent the 1 µs time step for the first and second mesh. The magenta lines represent the 0.5 µs time step for the first and second mesh. The blue line represents the 0.25 µs time step for the two meshes. Undoubtedly, the accuracy

of the solution is more influenced by the time step than the element length. It is also noticeable that as the time step becomes smaller, the solution converges. It also proves the result from the study by Moser *et al.* (1999) that the element size is not as critical as the time step size.

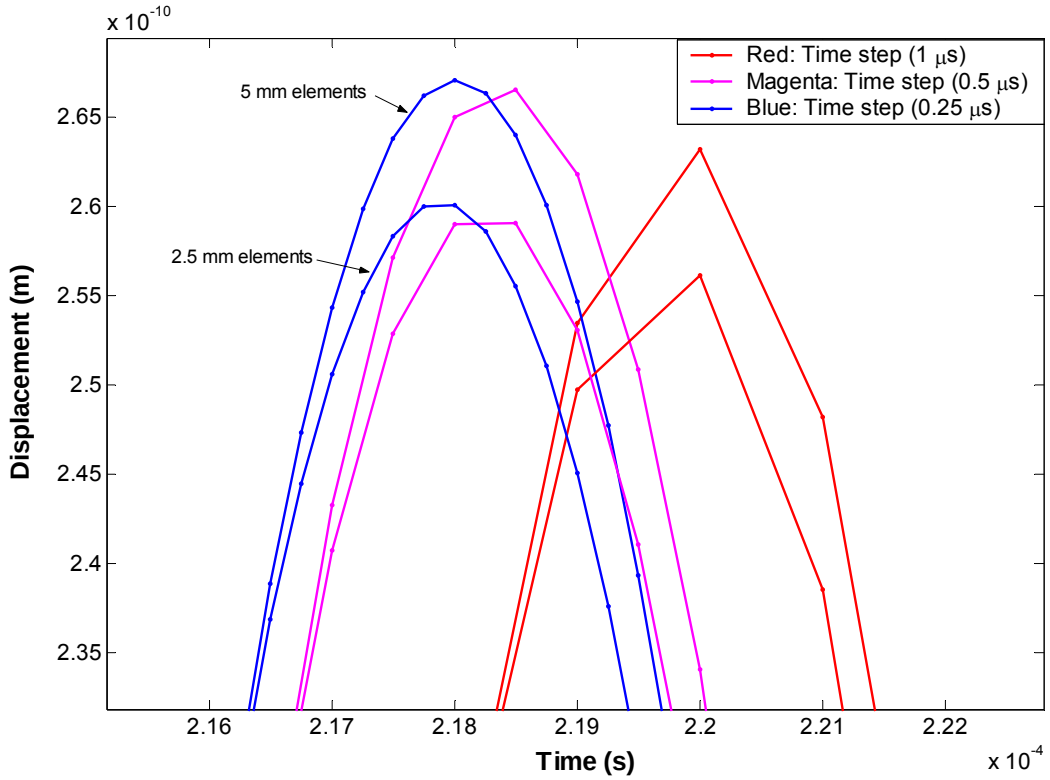

Figure 2.3: Two different meshes for three different time steps for a 50 kHz Gaussian windowed sine burst

Axisymmetric 20 kHz model

The same procedure was followed to calculate the element size and time step for the 20 kHz pulse. The first mesh element size was 10 mm and the time step was 2.5 μs. The second and third mesh's element size was 5 mm and 2.5 mm respectively and the second and third time step were 1.25 μs and 0.625 μs respectively.

In figure 2.4 a portion of the pulse can be seen. The different colour lines represent the different time steps for the different meshes. It is clear that the time step influences the accuracy of the solution more than the mesh density does.

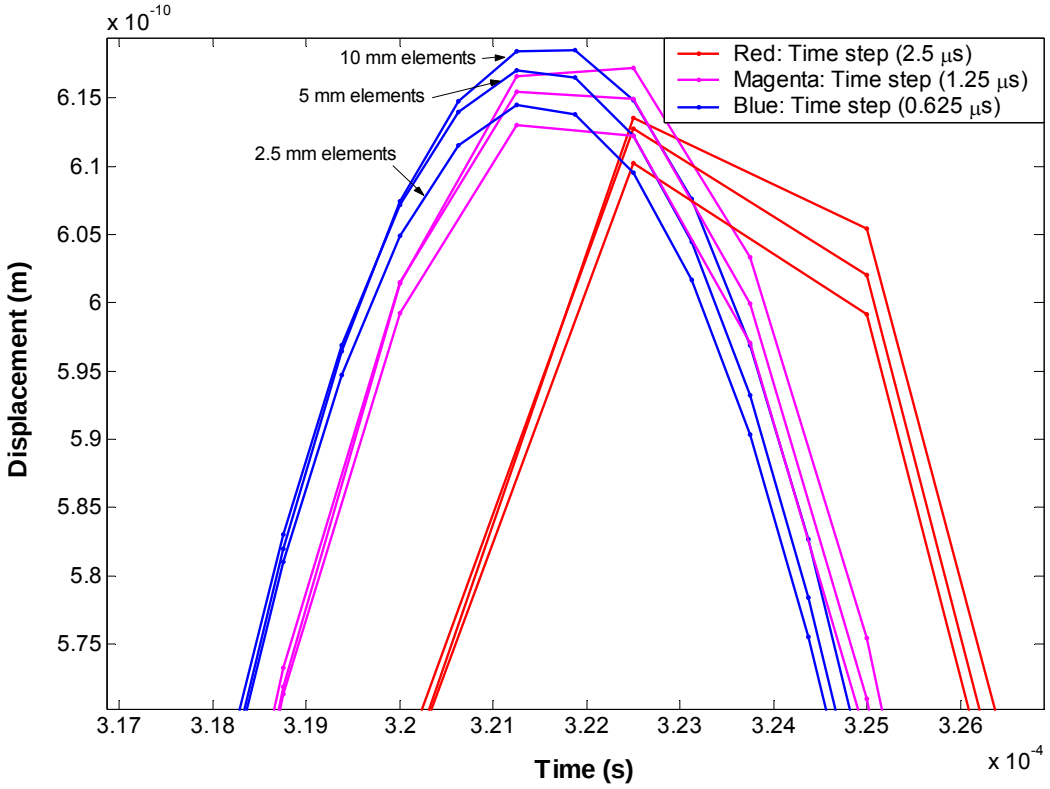

Figure 2.4: Three different meshes with three different time steps for a 20 kHz Gauss pulse

2.2.2 Three Dimensional model – Implicit Solver (MSC.Nastran)

To examine if the mesh density and time step influence the results of a three-dimensional model when using an implicit solver, a solid cylinder was generated in MSC.Patran and solved with MSC.Nastran. The size of the solid was 1.5 m long and

with a diameter 0.02 m. The solid was meshed with HEX 8 elements and part of the model is presented in figure 2.5. The material was steel with a density, elastic modulus and Poisson's ratio of 7850 kg/m³, 206 GPa and 0.3 respectively. A time-varying pressure load of 1 Pa was applied on the one face. The time-varying pulse was defined by a field which was imported from a text file. The time varying signal is the same as in the axisymmetric models.

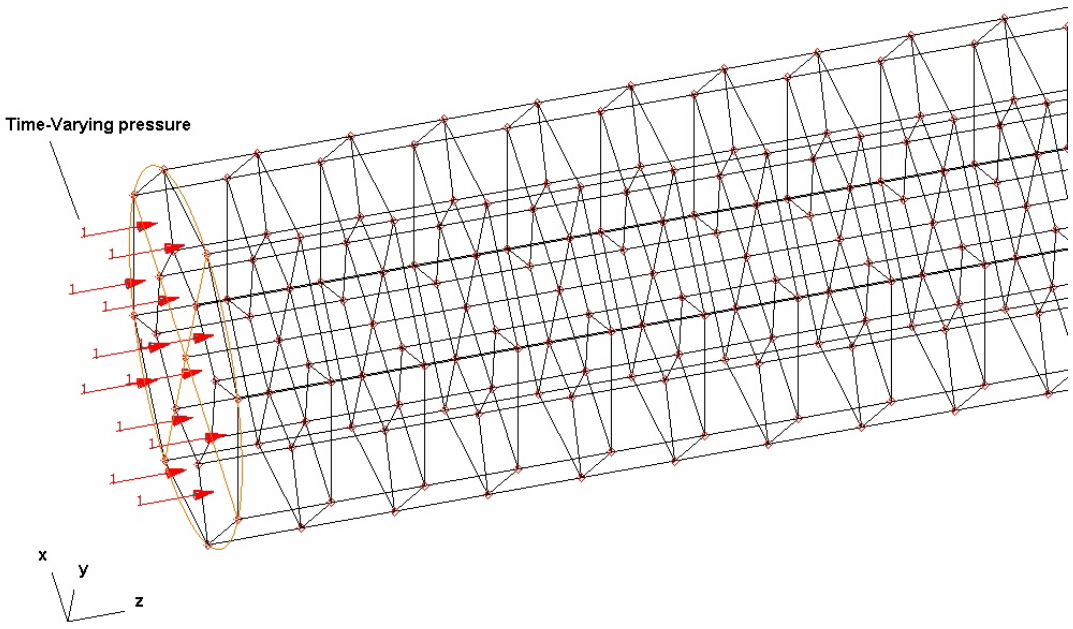

Figure 2.5: Three-dimensional rock bolt mode with HEX 8 elements

The displacement of the bolt at time 0.25 ms is shown in figure 2.6. With this plot new insight in the mode shape of the L(0,1) can be gained.

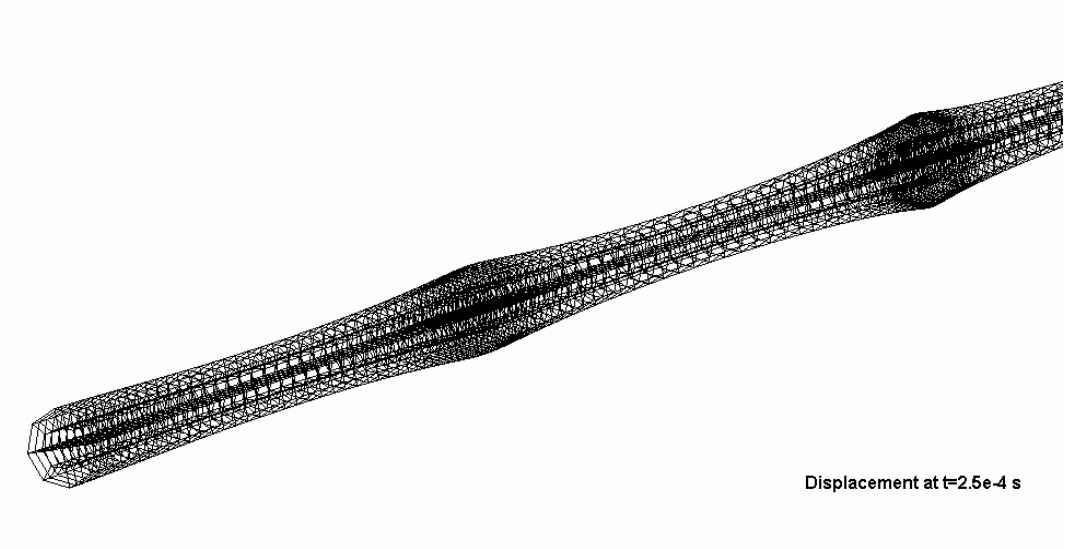

Figure 2.6: Displacement plot to show the wave propagating in a 3d model

In figure 2.7 a portion of the reflecting pulse can be seen. The different color lines represent the different time steps for the different meshes. The three dimensional model is also influenced by the time step rather than the element size. It is clear from the axisymmetric and the three-dimensional model in MSC.Nastran that the time step is the critical aspect when modelling wave propagation with an implicit solver.

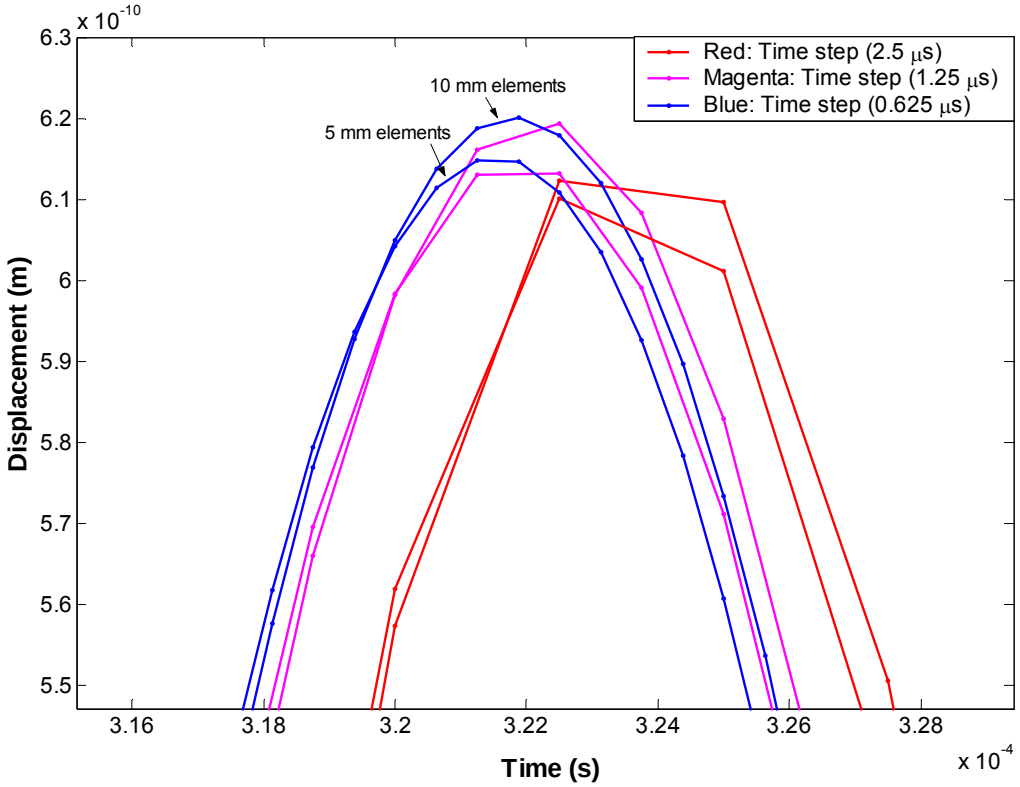

Figure 2.7: Two different meshes with three different time steps for the three dimensional model for a 20 kHz Gauss pulse.

2.2.3 Three dimensional model – Explicit Solver (MSC.Dytran)

To see if the mesh density and time step size influence the results of a three-dimensional model when solved by an explicit solver. The previous problem was solved with MSC.Dytran. The size of the solid was 1500 mm long and with a diameter of 20 mm. In this case the model was defined in millimetres and not in meters was to prevent numerical round-off errors. The solid was meshed with HEX 8 elements. The material was steel with a density, elastic modulus and Poisson's ratio of 7.85×10^{-9} tons/mm³, 206×10^{3} N/mm² and 0.3 respectively. A time-varying pressure load of 30 N/mm² was applied on the one face. The time-varying pulse was defined by a field which was imported from a text file.

The element sizes for the three different meshes were calculated as before and were 5 mm, 2.5 mm and 1.25 mm.

The initial time step was set to $\Delta t_{init} = 0.3 \times \frac{\text{element size}}{5123}$ which is the time a

pressure pulse will travel through an element. MSC.Dytran will automatically change the time step to this value if it is too small, but will return an error if it is too big.

If the element size reduces, the maximum required time step also becomes smaller and the results will eventually be more accurate. A comparison of the reflecting signal of a three-dimensional model in MSC.Dytran and an axisymmetric model in MSC.Nastran showed that there is no difference in the results if the element size is the same. With MSC.Dytran the element size influences the results, and it is important to have the correct element size if an accurate answer is required.

In figure 2.8 a comparison between an axisymmetric model and a three dimensional model is presented. It is apparent that the axisymmetric and the three-dimensional models produce the same results. Thus for a case where the model can be reduced to an axisymmetric case it will save significant computer time. However in the rock bolt there exist numerous scenarios that are not axisymmetric. In this study the possibility of three-dimensional modelling of an embedded bolt will be investigated.

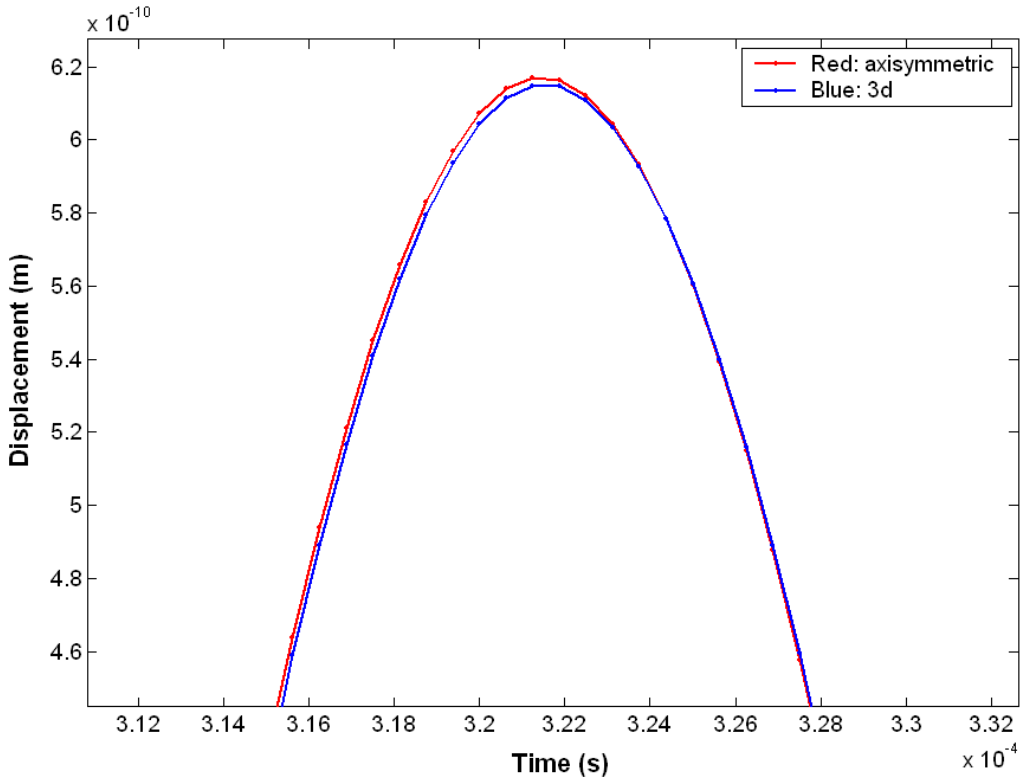

Figure 2.8: Comparison between an axisymmetric and a 3d rock bolt model with the same element size and a 20 kHz Gauss pulse.

In the following section the Pochhammer-Chree frequency equation, finite element and the experimental results are compared based on group velocity curves.

2.2.4 Comparison of the group velocity curves

It is important to verify the group velocity curves of the experimental and finite element models against the Pochhammer-Chree frequency equation solution. Furthermore, the group velocity curve and attenuation curves are good measures to find an optimum frequency for guided wave testing (Beard, 2002). The generation of group velocity curves for an unbounded bolt is discussed in this section.

PCdisp is an open source MATLAB program written by Seco *et al.* (2002). This was used to generate the Pochhammer-Chree frequency equation dispersion curves. The Pochhammer-Chree frequency theory deals with wave propagation in structures with cylindrical symmetry. The software uses the Pochhammer-Chree frequency equation

and solved it numerically (Seco *et al.*, 2002). The input for the software was the frequency range, the bolt diameter, the modes wanted and the material properties. The same material properties and model dimensions were used as in the finite element model.

The Pochhammer-Chree frequency equation group velocity curves for a bolt in a vacuum are shown in figure 2.9. The frequency range was chosen to be 0 Hz to 400 kHz. Only the longitudinal modes and the flexural modes were considered.

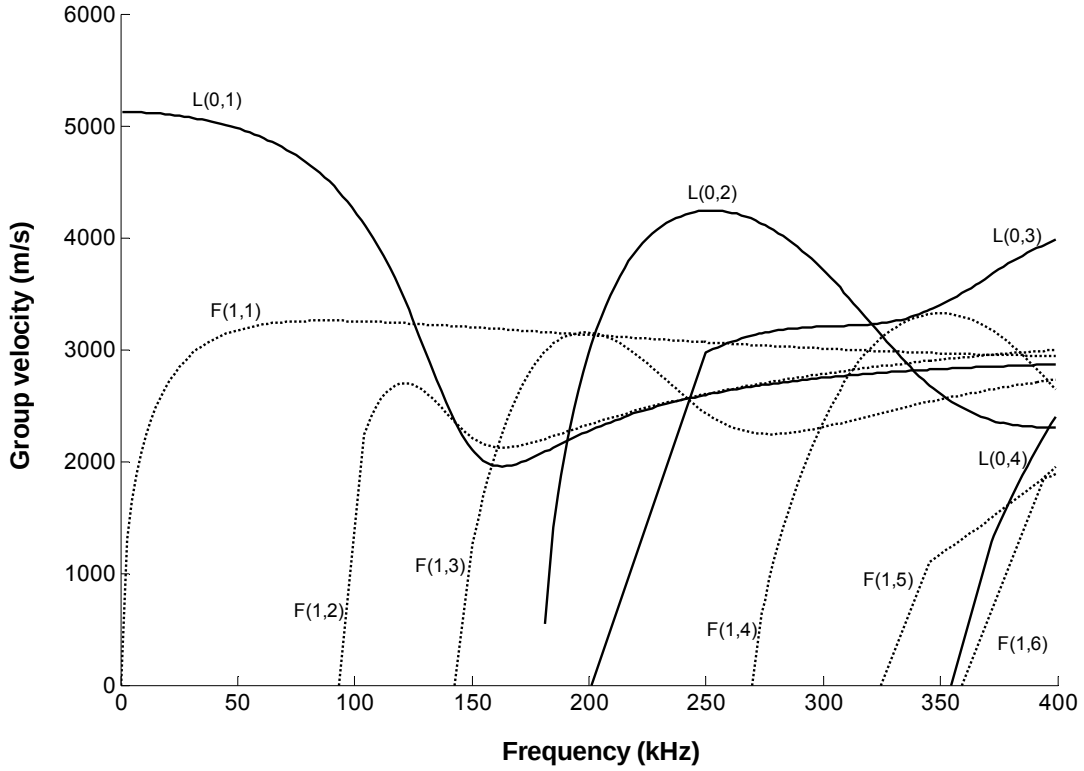

Figure 2.9: Group velocity curves for a bolt in a vacuum from PCdisp

To determine the group velocity curves of the first longitudinal mode, L(0,1) from the finite element method, a six-cycle sine burst was transmitted to the end of the bolt.

The excitation frequency was swept from 30 kHz to 90 kHz.

An axisymmetric model was used to determine the group velocity curves. A surface was generated with dimensions of 1500 mm x 10 mm, which represented the axisymmetric surface of a 20 mm bolt with a length of 1.5 m. TRIA 6 elements were used with the axisymmetric properties defined. The material properties were that of mild steel. A time-varying pressure with amplitude of 30 Pa was applied to the one edge. The element size and time step size was chosen according to the results in section 2.2.1 where the trade-off between accuracy and computational time was investigated. From the results in section 2.2.1 an element size of half the recommended size was chosen, i.e. 40 elements per wavelength. This gives good accuracy with less computational power. The time step was also chosen to be half the recommended step size, i.e. 40 steps per cycle.

The time of arrival of each end-reflection was used to calculate the group velocity at the specific frequency. The time of the peak of the outgoing tone-burst and the peak of the first end-reflection was taken to calculate the first time of travel. The second reflection's peak and the peak of the first end reflection were used to calculate the second time of arrival. The average of the time of travel of four end-reflections was used to accurately determine the group velocity. The comparison of the Pochhammer-Chree frequency equation, FEM and the experimental results can be seen in figure 2.10.

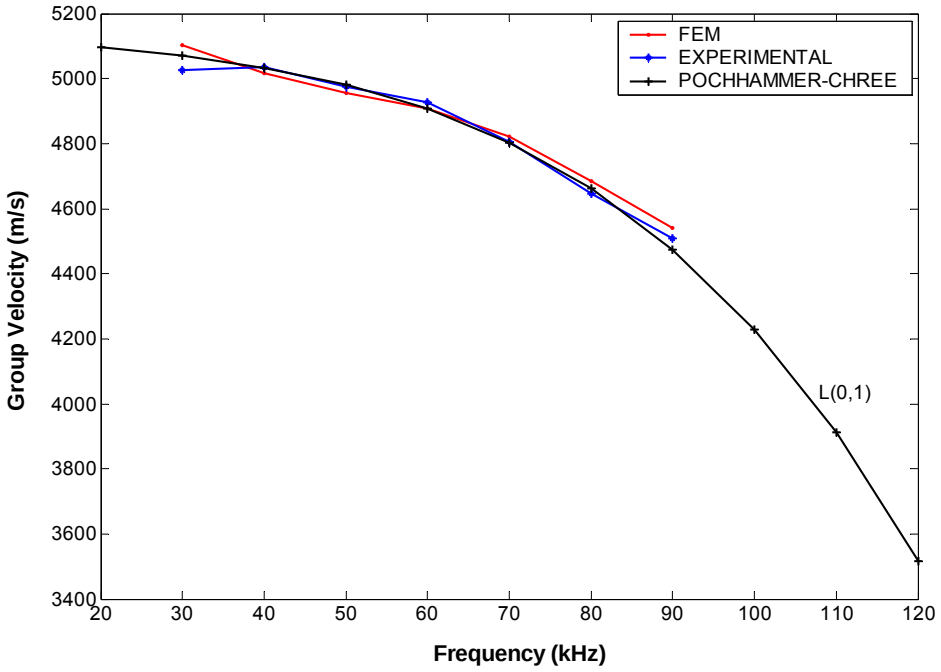

Figure 2.10: Group velocity curves for axisymmetric FEM model, Experimental and Pochhammer-Chree frequency equation

It is noticeable that the curves differ slightly and the maximum difference is 1.2 %, which is very small. Some reasons for the difference may be the effect of dispersion, sample rate, element size, noise and uncertainty of material properties.

The group velocity curve can also be used to determine which wave was received if multiple reflections are seen. The time for each reflection is then determined and the speed is calculated for the reflection. From the speed of the reflection it can be noticed whether it is a flexural or longitudinal wave. For this research it is not necessary to know which wave is reflecting. If a reflection arrives before the end reflection, it indicates a potential defect.

2.3 The effect of damping

Damping is an important factor when doing transient analysis and an accurate estimate is crucial if amplitudes are to predicted. It will however complicate the equation of motion and will therefore be time-consuming for solving the system of equations. Secondly, material attenuation values are difficult to measure, particularly

in highly attenuative materials such as epoxy and rock.

The overall attenuation of a guided wave in imbedded rock bolts is dominated by leakage at low frequencies, which is not significantly affected by material damping. (Beard, 2002). However at high frequencies damping does contribute significantly to the overall attenuation, but since the ultrasonic energy at these frequencies is travelling mainly in the steel bar, only the steel properties are necessary. This study focussed only on the lower frequencies and therefore neglect the effect of damping in the models. And as a consequence the amplitudes could not exactly compared to the experimental bolts.

2.4 Energy absorbing boundaries

For the rock bolt model the finite boundary of the finite element model will cause the waves to be reflected and superimposed on the progressing waves. Therefore, it is necessary to create a boundary, which is perfectly radiating to outgoing waves. Ideally, the boundary should be as close to the finite structure as possible for computational efficiency.

A simple solution to the problem is to move the boundary a great distance away from the finite structure so that the boundary does not influence the results (Ross, 2004). This is not computationally efficient and the need arise to use an artificial boundary condition. There appears to be two basic approaches to modelling boundary condition. The first is to create boundary elements with special properties to absorb the outgoing waves. The second approach is to create infinite elements. The boundary element approach can be divided into: plane wave approximation, viscous damping boundary method, and perfectly matched layers (Ross, 2004).

In general commercial finite element packages these artificial boundaries are not available. Therefore, the only way to model the rock bolt and the surrounding rock is to increase the rock's boundary distance so that the reflecting waves from the boundaries arrive later than the end reflection of the bolt. This however will cause the model to become very large, if the same element size is used for the rock and the bolt and the solving will be very time-consuming. If a mesh of uniformly distributed nodes is used as well as one with an increasing element length size, the reflecting signal will arrive at the same time but the wave form will not be that accurate. A study was conducted to investigate the influence on the results when the rock is meshed coarsely. This study will be discussed in chapter 4.

CHAPTER 3

THE EXPERIMENTAL SETUP AND VERIFICATION OF THE FINITE ELEMENT MODELS

3.1 Introduction

The preceding chapter has laid the foundation for the finite element models. It showed the effect of the element and the time step size. Secondly the effect of damping was discussed. Finally the treatment of the boundary conditions for embedded bolts was considered. In this chapter, results from the finite element models of an unbounded bolt, as well as perfectly embedded bolts are compared to experimental results. Certain recommendations and precautions for the instrumentation are discussed. The design and manufacturing of the testing block, the materials used and their properties, are given. To verify the study the group velocity curves from the theory, the finite element models and the experimental tests are compared.

3.2 Instrumentation for the experimental setup

The instrumentation used in this study were the following:

- A computer with a data acquisition card
- A Piezo-Amplifier for amplifying the outgoing pulse
- A Circuit for pulse echo switching and noise minimization
- Piezo-ceramic transducers
- Computer and software for the finite element modelling

In figure 3.1 the computer with the data acquisition card, amplifier, pulse-echo circuit and a connector block can be seen.

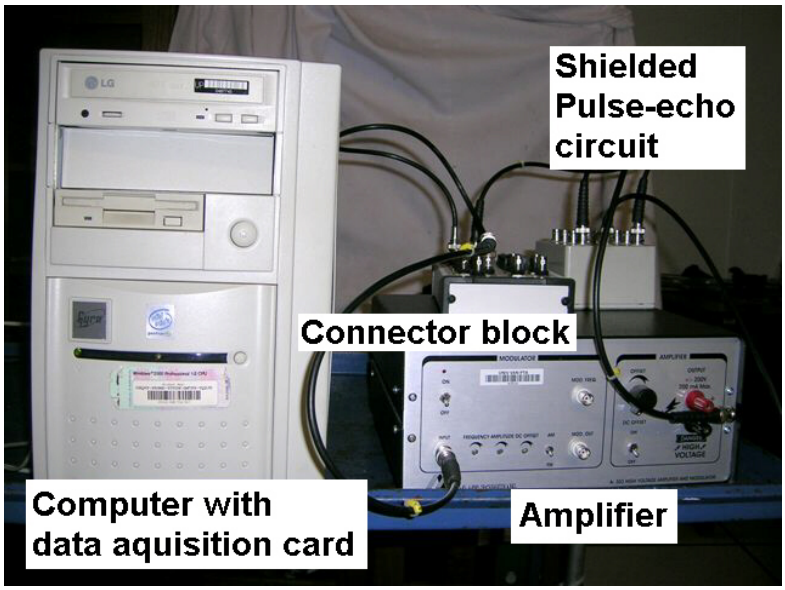

Figure 3.1: Instrumentation

3.2.1 Data acquisition card and software

A 500 MHz PC with 500 MB of RAM was used with the National Instruments, PCI 6110, data acquisition card. The card has 4 input channels and 2 output channels. The maximum sample rate on the input channels is 5 MHz. At least 20 samples per period are needed if a good representation of the amplitude is required. Therefore, the maximum frequency is limited to 250 kHz. The output channels' maximum frequency is 4 MHz and it limited the output signal to 200 kHz. It was therefore decided that only the lower frequency tests, recommended by Beard (2002), will be considered. The maximum output voltage of the card was limited to ± 10 V and an amplifier was necessary to drive the piezoelectric transducer. The data acquisition

card was controlled by MATLAB's data Acquisition Toolbox. Matlab programs were written to generate different output frequency pulses and to measure the time of arrival. These programs are attached in Appendix C.

3.2.2 Pulse-echo circuit

Only one end of the bolt can be used to excite guided waves in the bolt. It was therefore necessary to use the same transducer as a transmitter and receiver. The piezo-ceramic transducer was connected to a circuit that was built to utilize the transducer as a transmitter and receiver. The circuit had an input side which is connected to the amplifier. The amplifier was connected to the output of the data acquisition card. The output side of the circuit was connected to the input of the data acquisition card. The transducer is also connected between the input and output of the circuit, so that it can transmit and receive signals. The signal from the output of the data acquisition card is amplified and the circuit sees a high voltage signal. This signal excited the transducer. The output side of the circuit also sees this voltage but diodes clip the signal to ± 0.2 V. The reflected waves return after a few milliseconds and excites the transducer so that it produces a voltage signal. The voltage generated by the reflections is smaller than 0.2 V and the signal can be measured at the output side of the circuit. The resistors and diodes were chosen such that the noise was reduced and the recovery time of the circuit after excitation was short enough. The time trace of a 50 kHz signal is shown in figure 3.2 to demonstrate these concepts. The circuit for the pulse echo configuration can be seen in Appendix B.

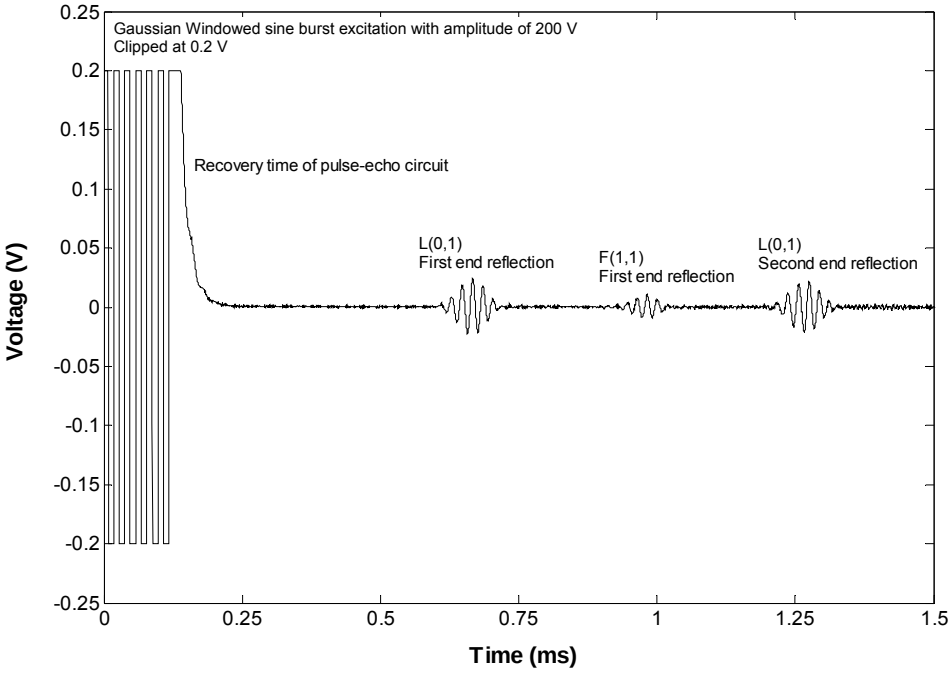

Figure 3.2: Time trace of a 6 cycle Gaussian windowed transmitted signal

3.2.3 Amplifier

A A-303 Piezo Amplifier from AA Lab Systems was used. This amplifier is a high voltage, high-speed linear piezo driver. The amplifier is capable of driving up to ± 200 V at 200 mA at frequencies from DC to 450 kHz. The amplifier is connected to the pulse-echo circuit to amplify the input signal to the transducer. The maximum amplification achieved, was 26 dB.

3.2.4 Piezo-ceramic transducers

The piezo-ceramic transducer was manufactured by the CSIR Materials Science and Manufacturing operating unit, and consisted of a ceramic disc that was cut with thin blades into small pillars. The space between the pillars was filled with a polymer material. This material is known as 1-3 piezocomposite and was used to avoid the radial vibration modes that occur in piezoelectric ceramic discs. These blocks can be individually controlled if necessary. In this study only the fundamental longitudinal mode was considered, which is predominately axially. To excite this mode the flat surfaces were covered with silver plating and wires were soldered onto each end. For an explanation of the working principle of piezo transducers, refer to Appendix B.

3.2.5 Computer and software for the finite element modelling

The computer for the finite element modeling was acquired specifically to run large models. The configuration of the computer was as follows: A Pentium 4, 3.2 GHz with 3 GB of RAM. The MSC.Software package was installed on the computer. The package included MSC.Patran, MSC.Nastran and MSC.Dytran. This allowed access to an explicit as well as an implicit solver.

3.3 The experimental testing block

Elastic wave propagation in free and embedded bolts was investigated by different researchers in the past. Most of these studies utilize the Pochhammer-Chree frequency equations and plot dispersion curves for the bolts. Modes can be identified, from the dispersion curves, that will perform well when used to detect defects. The Pochhammer-Chree frequency equation solutions narrow such investigations to axisymmetric and simple geometry models. The study by Simmons *et al.* (1992) applied the numerical solution of the Pochhammer-Chree frequency equation to study the axisymmetric modes in embedded bolts. The possibility of using three-dimensional models to model non-axisymmetric defects was considered in this study. Before different fault scenarios can be considered, some fundamental concepts should be reviewed.

To test and verify fundamental concepts of embedded bolts, it was necessary to have a laboratory test block. A concrete block was cast and bolts were installed into it. In figure 3.3 the testing block can be seen.

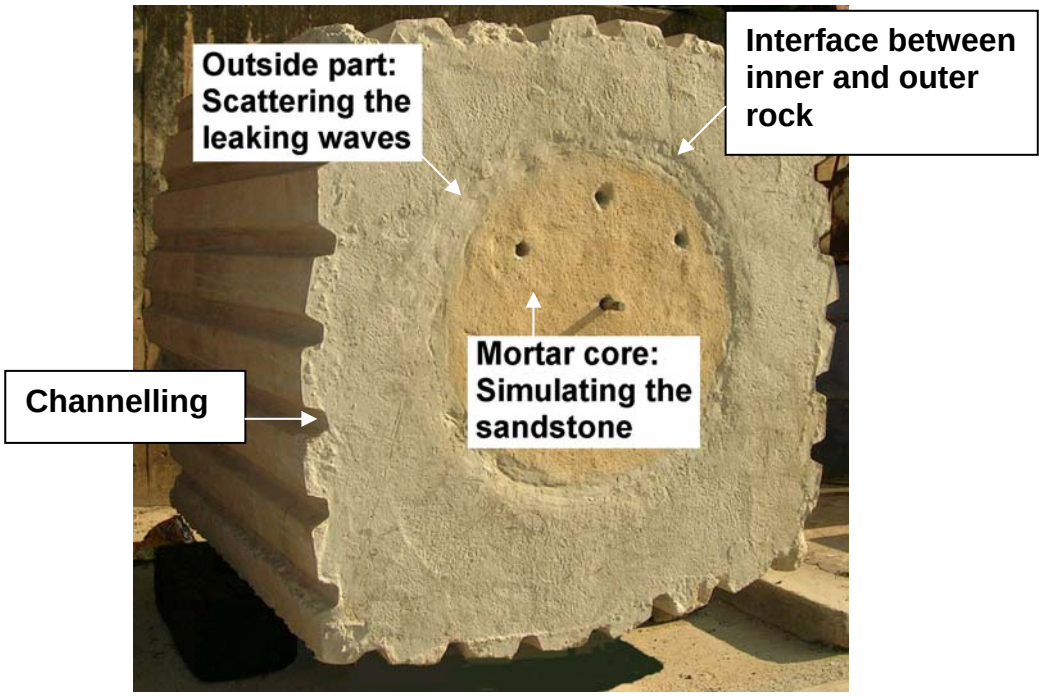

Figure 3.3: Experimental test block

The configuration of the testing block was essentially the same as the testing block at Imperial College (Beard, 2002). Simulating the infinite mass of the roof was problematic and therefore the testing block had to consist out of an inner and an outer “rock”. The inside part of the block, was to model the sandstone and the outer part was to scatter the leaking waves to prevent them interfering with the waves propagating in the bolt. At high frequencies the wavelength is small and the waves are easily scattered. However at low frequencies the wavelength is much longer, in the order of 0.1 m and the waves are scattered less, requiring a larger test block.

In South Africa different variations of sandstone are present in the coal and platinum mines. A 3:1 mixture of sand and concrete was used to simulate the sandstone properties. The majority of rock bolts installed in the South African coal and platinum mines are between 0.9-1.5 m in length (Bornman, 2005). The block‘s length was chosen to be 1.4 m to have an embedded length of at least 1.2 m. The width of the block was chosen to be 1.2 m to prevent reflections from the boundaries of the block interfering with the waves propagating in the bolt. Two other precautions were taken to prevent any edge-reflections interfering with the end-reflections. The first precaution was to channel the edges of the block to minimize the coherence of the

reflected waves and the second was to cast the outer part with aggregate to scatter the waves. The installation holes were cast rather than drilled, to prevent any oversize drilling and crooked holes. Seven holes were cast. To cast the holes a PVC pipe was greased with concrete mould oil. This helped with the removal of the pipes after the concrete had set. The inside rock was made up of mortar only and was cast first. The outside was cast while the inside was still green, thus improving the bonding between the surfaces and reducing the possibility of reflections being detected from this interface.

Two bolts without defects were installed to compare and use them as references. A 1.5 m bolt was installed protruding on both ends of the block. This allowed pitch-catch testing. The other bolt was 0.9 m long and was installed in a 1.2 m blind hole.

To model the defects accurately and experiment with different scenarios, a fluid type resin with a slower reaction time was sought. Fibreglass resin was a potential solution with basically the same acoustic properties as the rock bolt resin in the mining industry.

To install the bolts, the block was slightly tilted with a hydraulic jack. The fibreglass resin and catalyst were mixed and poured into the hole. An end cap designed to fit tightly to the protruding end, was placed against the concrete wall, and fastened with rawlplugs. After that the bolt was pushed through the cap and to the end of the blind hole. The fibreglass resin was pressed past the bolt end to the opening of the hole. The end cap had a grease nipple to enable the rest of the resin to be pumped into and fill the hole.

3.4 Material properties

To determine the material properties small samples were taken of the mortar, the fibreglass as well as the rock bolt resin (from Minova, one of South Africa's biggest rock bolt resin suppliers). The rock bolt resin properties were only for comparison between the fibreglass and the rock bolt resin and were not used in installation. To

determine the volume accurately, the fibreglass and rock bolt resin was machined in a lathe to a specific diameter and length. The mass was measured on a high sensitivity scale and the density was calculated. A compression test was done on a 100 kN Shenck Hydropulse to determine the elastic modulus of the rock bolt resin, fibreglass and mortar. The values for steel were taken from the steel construction handbook (SAISC, 1987). The Poisson's ratio for the rock bolt resin, fibreglass and mortar, could not be measured and typical values were chosen for the materials. The results for material properties are given in table 3.1:

Table 3.1: Measured material properties

Property/Material	**Steel**	**Fibreglass resin**	**Rock bolt resin**	**Mortar/ Sandstone**
Elastic Modulus E (GPa)	206	10	12	20
Density, ρ (kg/m^3)	7850	1200	2000	2500
Poisson's ratio ν	0.3	0.3	0.3	0.25
Bulk longitudinal Speed, V (m/s)	5123	2887	2450	2828

3.5 Unbounded bolt

For the experimental unbounded bolt the instrumentation as described in section 3.2 was utilized. A 20 mm diameter 1.5 m long mild steel bolt, having the material properties summarized in table 3.1 was used. An 18 mm piezo-ceramic transducer was bonded to the bolt at both ends so that pitch-catch measurements could also be performed. Superglue was used to bond the transducer to the bolt. During bonding it was ensured that the transducer was exactly in the middle of the bolt. The amount of glue was equally distributed over the surface of the transducer. If that was neglected, the transducer would not be equally bonded to the surface of the bolt, causing bending of the transducer and exciting flexural modes. The amount of glue is also

important; the more glue on the surface the more energy is lost. For the embedded bolt, energy loss could not be afforded.

A MATLAB program was written to transmit different frequency pulses and to measure the time of arrival. The number of cycles reduces the bandwidth and clearer reflections will be obtained. The reason for that is that the different frequency components of the wave are travelling at different speeds, which is the effect of dispersion. This effect becomes apparent if the dispersion curves (group velocity vs. frequency plots) are examined. A study of the number of cycles was conducted, using less than 6 cycles caused the reflecting signal to be come distorted. More than 6 cycles for the lower frequencies limited the detection length of the bolt. The optimum number of cycles for the 1.5 m bolt with a testing frequency range of 30-90 kHz, was a 6 cycle pulse.

3.5.1 Experimental results

A 1.5 m mild steel bolt with a 20 mm diameter was used in these experiments. The transducer was bonded to the one end of the bolt and was used as a transmitter and receiver. Six cycle Gaussian windowed sine bursts with frequencies ranging between 30 kHz and 90 kHz were used to excite the one end of the bolt. The L(0,1) mode was excited by applying the voltage to the whole face of the transducer so that the 18 mm transducer expanded mainly axially. The sampling time was increased so that four end reflections could be seen. Ten averages were taken to produce the results shown in the figures.

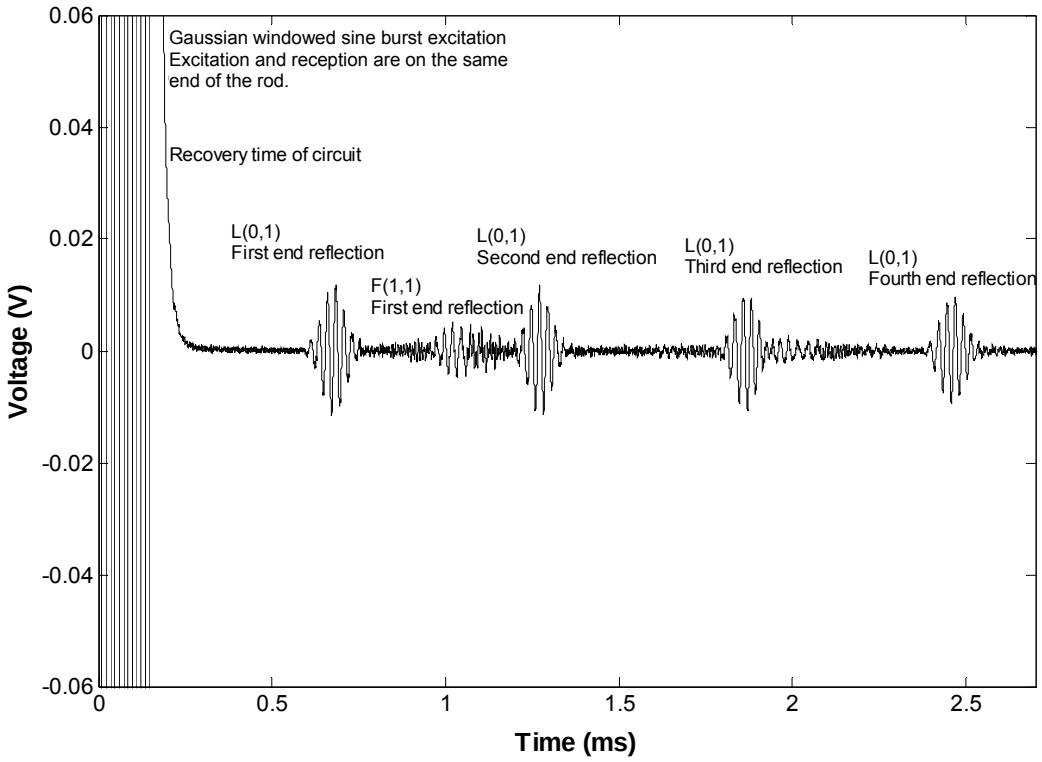

Figure 3.4: Time trace for 40 kHz pulse in a 1.5 m free smooth bolt

If the Pochhammer-Chree frequency equation group velocity curve is examined, the speed of a group of waves at 40 kHz is around 5033 m/s, hence the first L(0,1) end reflection should return at:

$$t = \frac{2 \text{ x } 1.5}{5033} = 0.6 \text{ ms}$$

This is the case for the 40 kHz time trace in figure 3.4. Another reflection can be seen between the first L(0,1) end reflection and the second L(0,1) reflection. It was suspected that it may be the F(1,1) mode's end-reflection. If one examines the dispersion curve, the speed of the F(1,1) at a frequency of 40 kHz is 3092 m/s. Thus, the time of arrival for the first F(1,1) end-reflection will be back at:

$$t = \frac{2 \text{ x } 1.5}{3092} = 0.97 \text{ ms}$$

This matches the reflection seen in figure 3.4. The attenuation of the F(1,1) is approximately 50 dB/m more at 50 kHz than the L(0,1) mode (Beard, 2002). This is the reason for seeing it only once as it attenuates very quickly.

Misalignment of the transducer or non-homogenous bonding of the transducer to the bolt may be the reason why the F(1,1) mode is present.

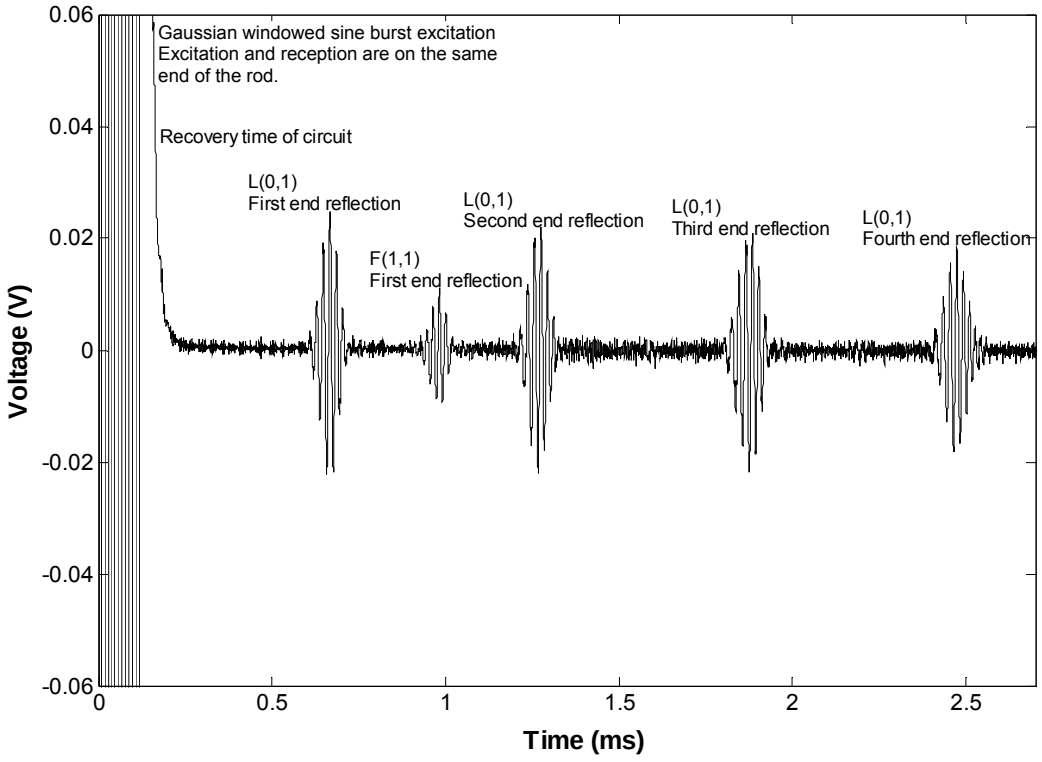

Figure 3.5: Time trace for a 50 kHz pulse in a 1.5 m free smooth bolt

In figure 3.5 the time trace for a 50 kHz pulse is shown. The time of arrival can be used to determine the speed of the waves in the bolt at this frequency. The time of arrival for the 1.5 m bolt, is approximately 0.6 ms, which gives a group velocity speed of 5000 m/s. The F(1,1) is also present in the 50 kHz time trace in figure 3.5.

At a frequency of 40 kHz the fourth L(0,1) end reflection has a slightly smaller amplitude than the first end reflection. It can be seen that the attenuation at these low frequencies is not very high. At 50 kHz the fourth end reflection is smaller but this is

mainly due to dispersion and not attenuation. At 40 kHz the waves are not dispersed to the same extent as at the higher frequencies. If the group velocity dispersion curve is examined in figure 2.11, one can see that the L(0,1) mode group velocity gradient between 30-60 kHz is small. However after 60 kHz the group speed is significantly reduced. The end reflections at the higher frequencies are much more stretched because of dispersion. This effect can be seen in the fourth end reflection of the 50 kHz time trace in figure 3.5.

3.5.2 Finite element models

A three-dimensional model as well as an axisymmetric model of a bolt in a vacuum was built in MSC.Patran and solved with MSC.Dytran (Explicit) as well as MSC.Nastran (Implicit).

To avoid round-off errors the three-dimensional model's dimensions were defined in millimetres instead of meters. A cylinder of 1500 mm and 20 mm diameter was generated. The solid was meshed with HEX 8 elements. Time-varying fields between 30 and 90 kHz were imported from a text file and associated to the 30 Pa pressure. The pressure was applied to the one face of the cylinder. The material definition was that of mild steel with a density, elastic modulus and Poisson's ratio of 7850 kg/m³, 206 GPa and 0.3 respectively.

The size of the elements was computed as discussed in chapter 2. For a 50 kHz pulse the required element size was calculated to be 5 mm. With MSC.Dytran the time step size is adjusted automatically. The starting time step was set to 0.1 μs, which is smaller than the compulsory time step required by MSC.Dytran. For more detail refer to section 2.2.3. The total analysis time was set to 0.78 ms, which is long enough to see the first end reflection.

From the group velocity curve a 50 kHz wave packet will travel at 4976 m/s. Thus for the 1.5 m bolt, the time of arrival of the first wave packet should be:

$$t = \frac{2 \text{ x } 1.5}{4976} = 0.6 \text{ ms}$$

The edge node displacement was plotted and can be seen in figure 3.6. The time of arrival agrees with the group velocity.

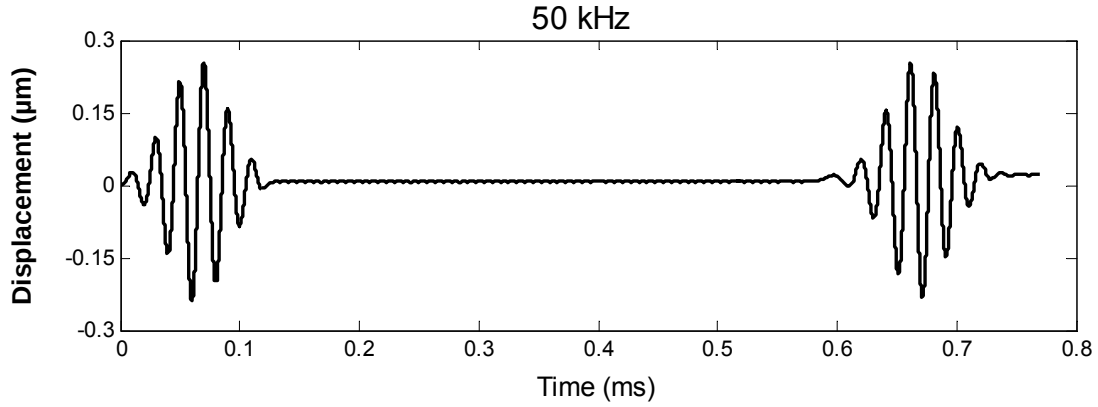

Figure 3.6: Time trace for a 3d model in MSC.Dytran of 1.5 m unbounded bolt

An axisymmetric model was also built for comparison to the three-dimensional model. A surface was generated with dimensions of 1500 mm x 10 mm which represented the axisymmetric surface of a 20 mm bolt with a length of 1.5 m. TRIA 6 elements were used with axisymmetric properties defined. The material properties were the same as in the three-dimensional model. A time-varying pressure with amplitude of 30 was applied on the one edge. The time step size was set to 1 μs and the total analysis time was set to 0.78 ms. The time trace for the axisymmetric and the three-dimensional models were identical.

The solution time for the two models was basically equal. Bearing in mind that the three-dimensional model had many more elements, the explicit solver already outperformed the implicit solver. For larger models this effect becomes even more apparent.

The three dimensional model showed the potential to model non-axisymmetric models with ease if an explicit solver is used. The experimental and finite element model results showed excellent agreement.

3.6 Embedded bolts

From the literature study the most promising frequency was around 50 kHz. The study by Beard (2002) showed that the group velocity speed was high and had a low attenuation at 50 kHz. Furthermore the Elastic Modulus and thickness of the rock and resin did not influence the group velocity and attenuation much at 50 kHz. The mode profile of the L(0,1) mode is predominantly axially and relatively easy to excite with the transducer (Beard, 2002). It was therefore decided to excite the L(0,1) mode in the bolts in a frequency range between 20 and 50 kHz.

Two cases for bolts embedded in rock were experimentally examined. The first is a bolt with a length of 1.5 m, protruding through the block. The second bolt was embedded 0.9 m in the rock/mortar.

The 1.5 m bolt protruding through the block

The results for the 1.5 m bolt are shown in figure 3.7.

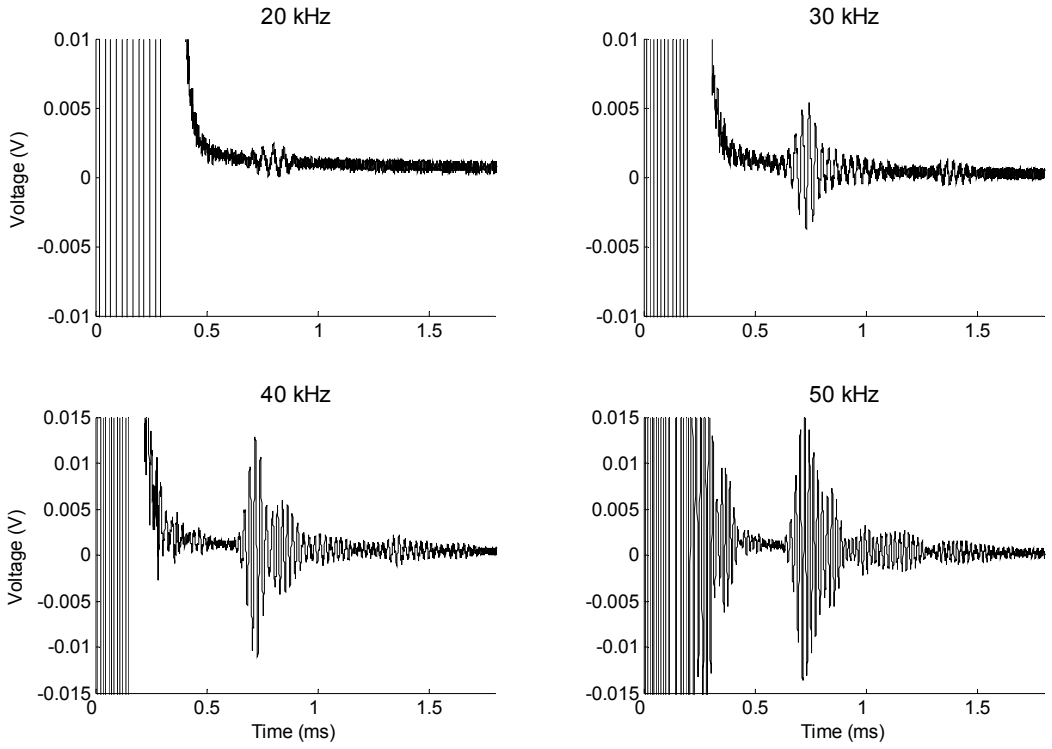

Figure 3.7: Time traces for a pulse-echo test on a 1.5 m experimental bolt embedded in mortar

At 20 kHz the first end reflection of L(0,1) can be seen. No other reflection is visible. At 30 kHz the second reflection can also be seen. It seems as if the L(0,1) first-end reflection is followed by some ringing. It is not the case if the 40 kHz and 50 kHz cases are examined. There it can be seen that it is another mode or reflection that is present. It is possible that it is the F(1,1). The attenuation is highest at 20 kHz and the lowest at 50 kHz.

The 0.9 m embedded bolt

The 0.9 m mild steel bolt with a diameter of 20 mm was installed in the testing block. The material properties for the rock, fibreglass and mortar are summarized in table 3.1. The fibreglass thickness was between 4 - 5 mm.

To compare the finite element model to the experimental 0.9 m bolt an axisymmetric model of the bolt, fibreglass and mortar was built. The size of the mortar core should be big enough, to ensure that no edge reflections of the mortar interfere with the end reflections of the bolt. If the mortar model is too big it will waste computational time. Therefore, a few calculations were done to determine the size of the embedding rock. The dimensions of the model are given in figure 3.8. 30-60 kHz time-varying fields were imported and applied as a pressure on the free edge of the bolt. The elements used were 5 mm TRIA 6 elements. The reason for the larger than recommended elements, is that the model becomes very large and time-consuming. Some accuracy will be lost, but it will only influence the exact values and not the trend. Some numerical experiments were done to observe the effect of bigger element and time step sizes. It appears that it doesn't have a significant effect. It will however influence the results if group velocity curves are generated. For all three cases the time step was set to 1 μs and the number of time steps was 650.

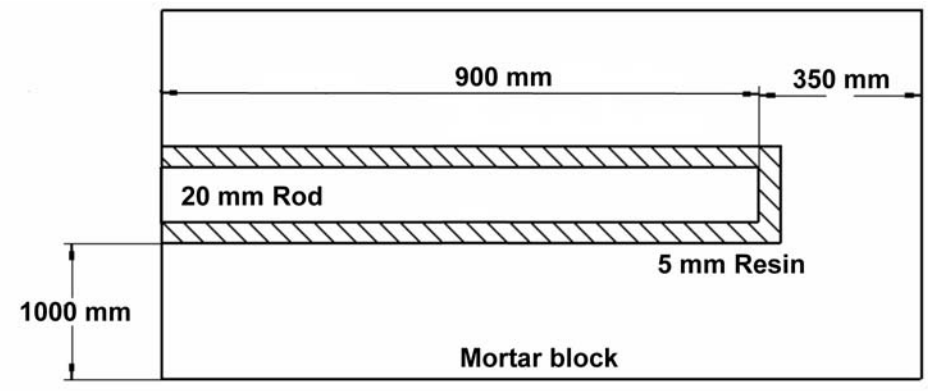

Figure 3.8: Axisymmetric model dimensions

The results for the finite element model as well as the experimental bolt for a 40 kHz pulse are shown in figure 3.9. The measurement units for the experimental bolt were in volts and for the finite element model in meters. It is difficult to find the relationship between voltage and displacement because the exact amplitude of the force transmitted on the experimental bolt could not be correlated to the excitation voltage. Modelling the piezoelectric transducer was beyond the scope of this project.

The first end reflection returns at 0.4 ms and it is notable that the experimental and finite element results show satisfactory agreement. It is noteworthy that the FEM model has more noise than the experimental result. A probable reason is that when the excitation signal passes an element, there are still vibrations due to the fact that the Gaussian windowed signal does not fade exactly to zero on the end. Neglecting the damping in the finite element models, which prohibits transients from fading away as time progresses, causes the element to vibrate freely. Investigating the effect of neglecting the damping in the finite element models is recommended for further research.

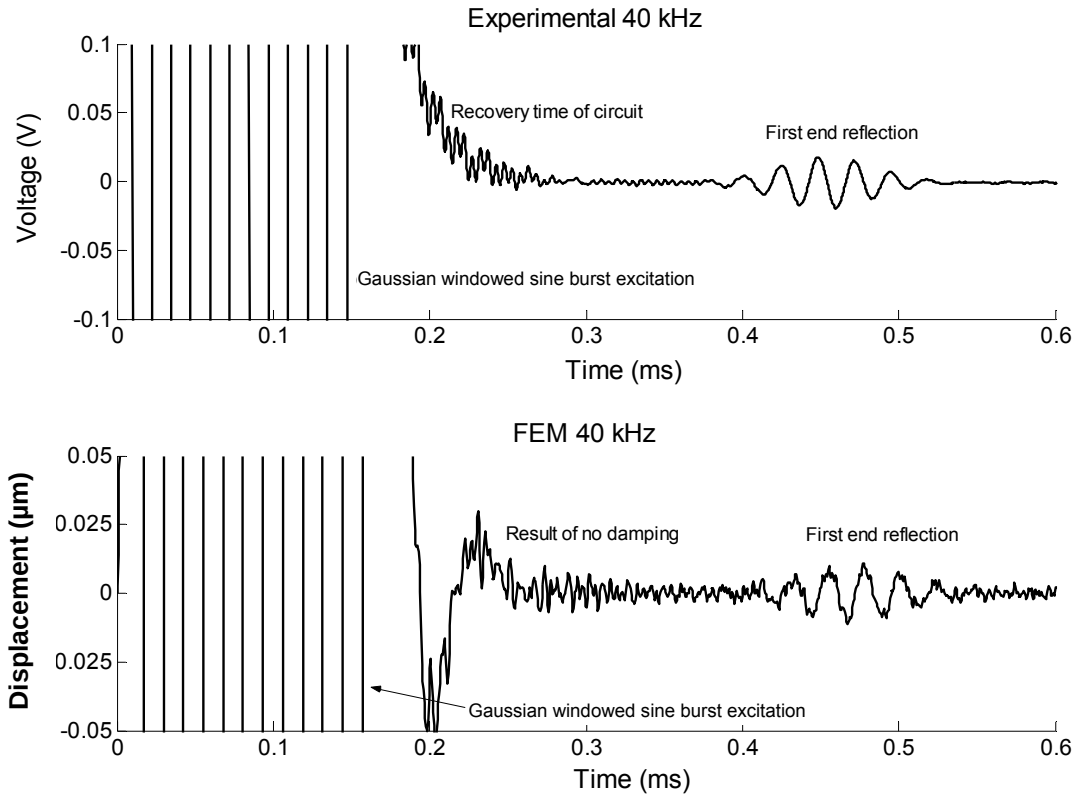

Figure 3.9: 0.9 m bolt embedded in mortar (40 kHz)

For the 50 kHz case, good agreement is found and is shown in figure 3.10. The attenuation of the signal is lower than in the 40 kHz case for both the measured and computed signals. The 60 kHz pulse displays larger reflecting amplitudes than the 50 kHz pulse. The attenuation is thus lower for the higher frequencies. The 60 kHz experimental bolt showed significant reverberation after the excitation and can be seen in figure 3.11. This is due to ringing of the transducer as the transducer is only lightly damped. The ringing was also found by Beard and Lowe (2003) in their study. The bandwidth of the higher frequency excitation is narrowed by the Gaussian windowed signal but it still have some frequency components near 140 kHz which is exciting the transducer, causing the ringing. 50 kHz seemed to be the most promising frequency to use when defect detection is done.

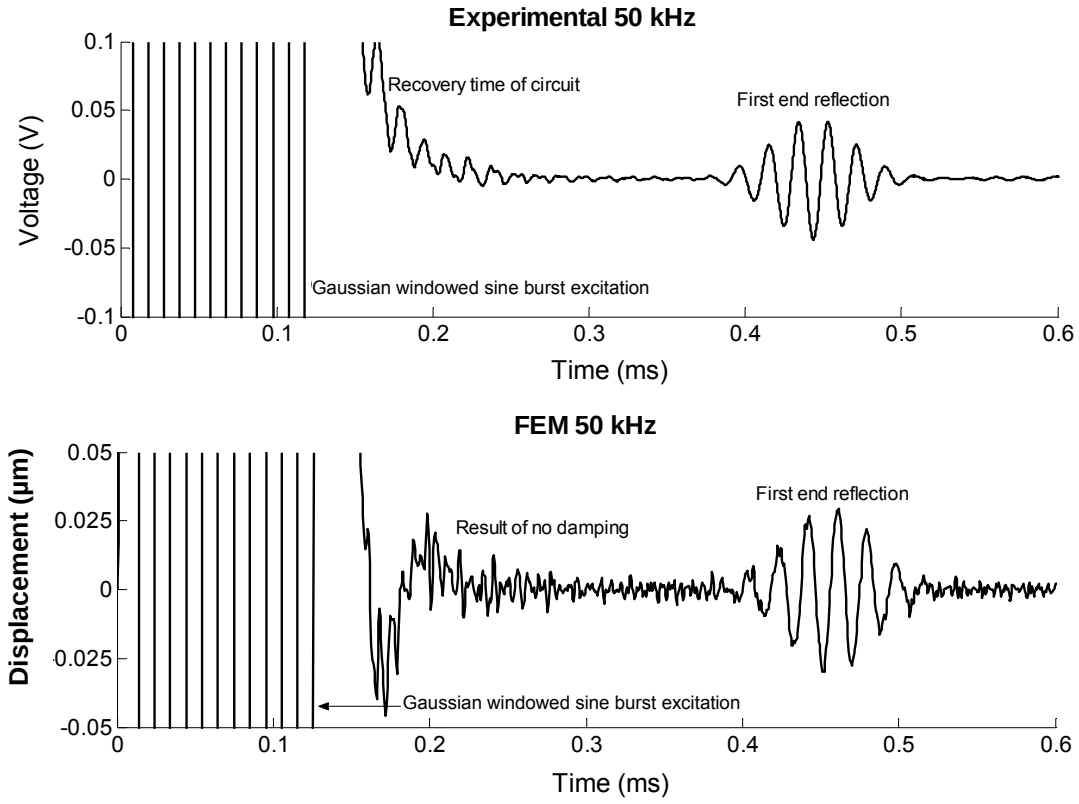

Figure 3.10: 0.9 m bolt embedded in mortar (50 kHz)

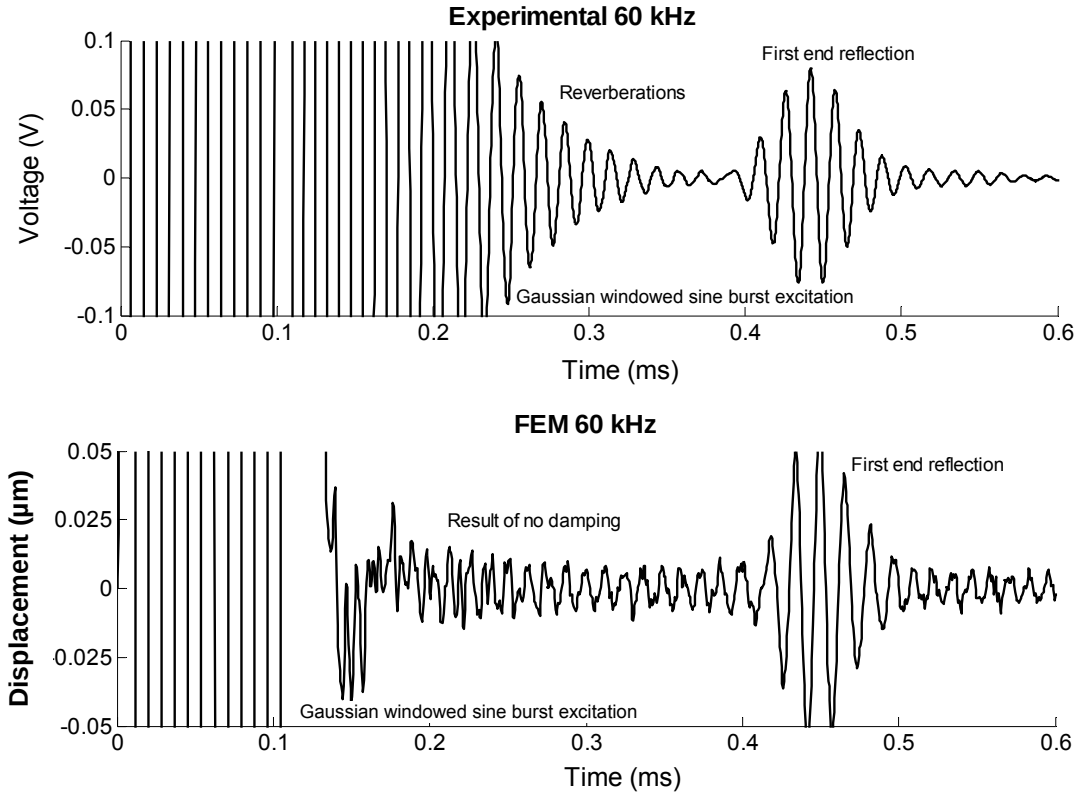

Figure 3.11: 0.9 m bolt embedded in mortar (60 kHz)

CHAPTER 4

INTERPRETATION OF FAULT SCENARIOS

4.1 Introduction

The finite element model results compared well with the experimental results for a 0.9 m bolt embedded in mortar. The group velocity plots of the 1.5 m embedded bolt for both the finite element model as well as the experimental setup compared well with the Pochhammer-Chree frequency equation plot. Thus the finite element models as well as the experimental setup will be capable to simulate different fault scenarios. As discussed in 1.3 of the literature study it appears that the unsatisfactory bond between the rock and the rock bolt are caused by weak rock, poor installation procedures and corrosion. The main causes for partially encapsulation bolts are firstly improper mixing where the required spin time is not followed and secondly, improper holes. In this study partially encapsulated bolts and bolts with local corrosion will be considered.

4.2 Partially encapsulated bolts

When the drilled hole is too deep or the drilled diameter is too large, the resin will not fully cover the bolt. An example of this is a bolt with the majority of the resin positioned at the end of the hole, anchoring only the end of the bolt. These scenarios will be investigated with finite elements as well as experimentally. An axisymmetric model of the bolt, resin and mortar was built and was compared to a simplified three-dimensional model. The measurement units for the experimental bolt were in volts and for the finite element model in meters. It was not attempted to find the relationship between voltage and displacement.

4.2.1 Finite element models and results

The finite element model of the partially encapsulated bolt is shown in figure 4.1. Note that the bolt is not anchored to the mortar for 1000 mm. This distance is long enough so that the reflection from the start of the encapsulation can be seen. The embedded part of the bolt is 375 mm, which is long enough to distinguish the start of the resin encapsulation and the end reflection. The embedded part of the finite element model was smaller than the experimental setup's embedded part. This was done to reduce the model size, improving the computational effectiveness. The resin thickness was 5 mm. An axisymmetric model as well as a three-dimensional model was built. The three-dimensional model was built to investigate the possibility for modelling non-axisymmetric defects.

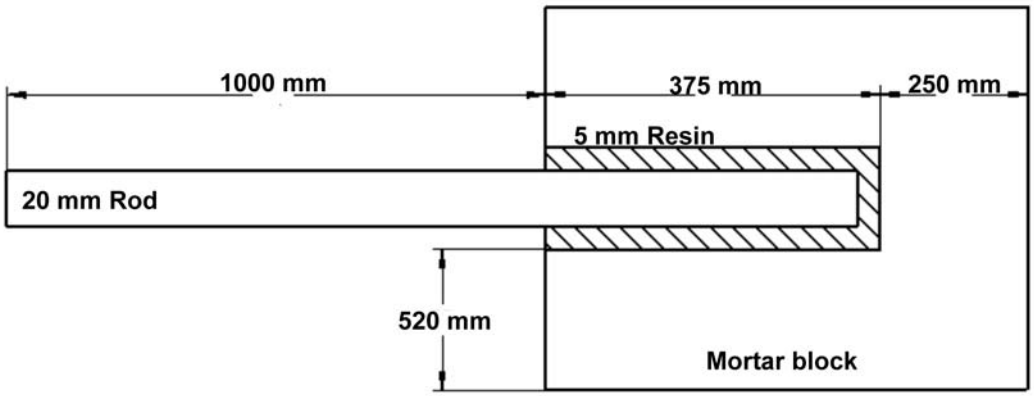

Figure 4.1: Finite element model details

- **Axisymmetric model**

For the axisymmetric model, the bolt, resin and mortar were all meshed with 5 mm TRIA 6 elements. The material properties and time-varying fields were applied as before. The time step size was set to 1 μs and the total number of steps to 800 steps. It took MSC.Nastran approximately half an hour to run the problem.

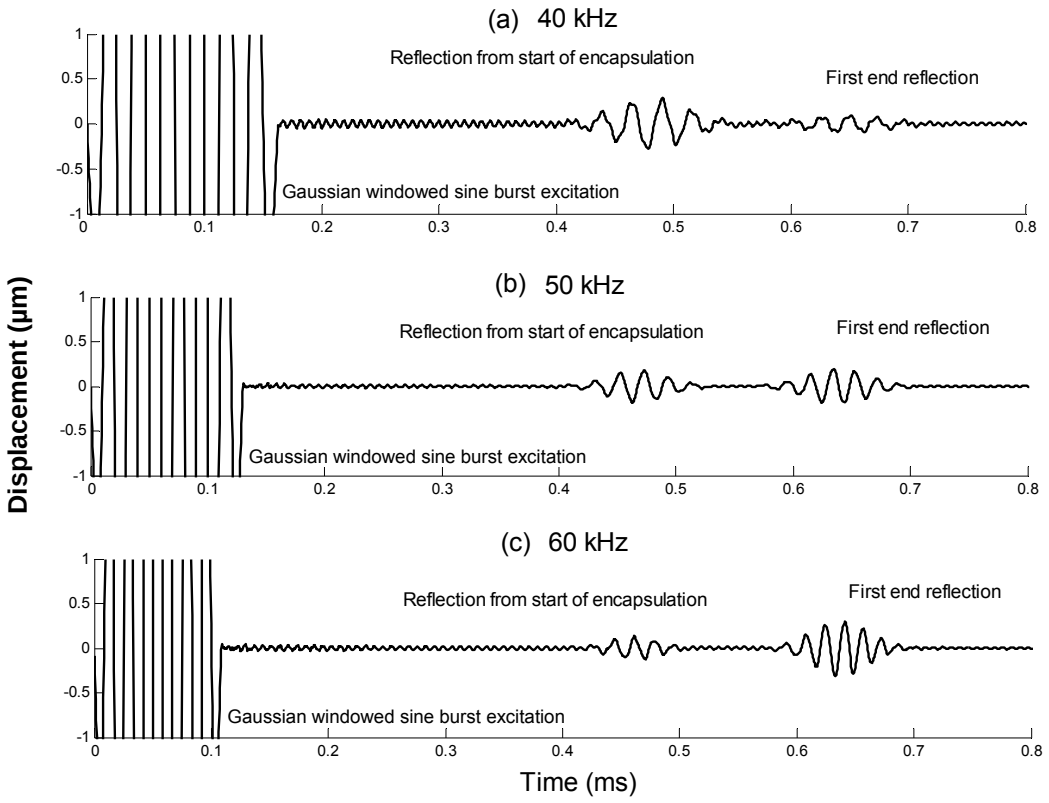

Figure 4.2 a, b, c: Results for the axisymmetric models, with 5 mm elements

The results for the axisymmetric models are shown in figure 4.2. The start of the resin encapsulation can clearly been seen. The amplitude of the reflection from the start of the encapsulation, of the 40 kHz signal, is larger than the reflection of the 50 and 60 kHz signals. The amplitude of the end-reflection, for the 40 kHz is smaller than the amplitude of the end-reflection of the 50 kHz and 60 kHz. It is apparent that the signal is not greatly influenced by resin defects when the frequency of the signal is high. The result confirms that the mode shape of the L(0,1) mode is changing as the frequency is swept. For the lower frequencies the L(0,1) mode is predominantly axial, but as the frequency is increased, radial motion becomes more significant and the mode shape becomes more complex. At the higher frequencies of the L(0,1) mode, the mode shape is such that the energy is travelling more in the centre of the bar and the waves will be less sensitive to resin defects.

- **Three-dimensional model**

The three-dimensional model of the bolt was built with 5 mm HEX 8 elements. The

resin was also modelled with 5 mm HEX 8 elements. The mortar was modelled with 10 mm HEX 8 elements. With this configuration the model had approximately 1.2 million elements. The larger elements utilized, were necessary to reduce the model size so that it could be solved. The materials properties and time-varying fields were applied as before. The time step size was set to 0.1 μs and the total analysis time was 0.75 ms. The problem was built in MSC.Patran and solved with MSC.Dytran, an explicit solver. It took MSC.Dytran approximately 4 hours to run this problem. The result for the three-dimensional model is presented in figure 4.3.

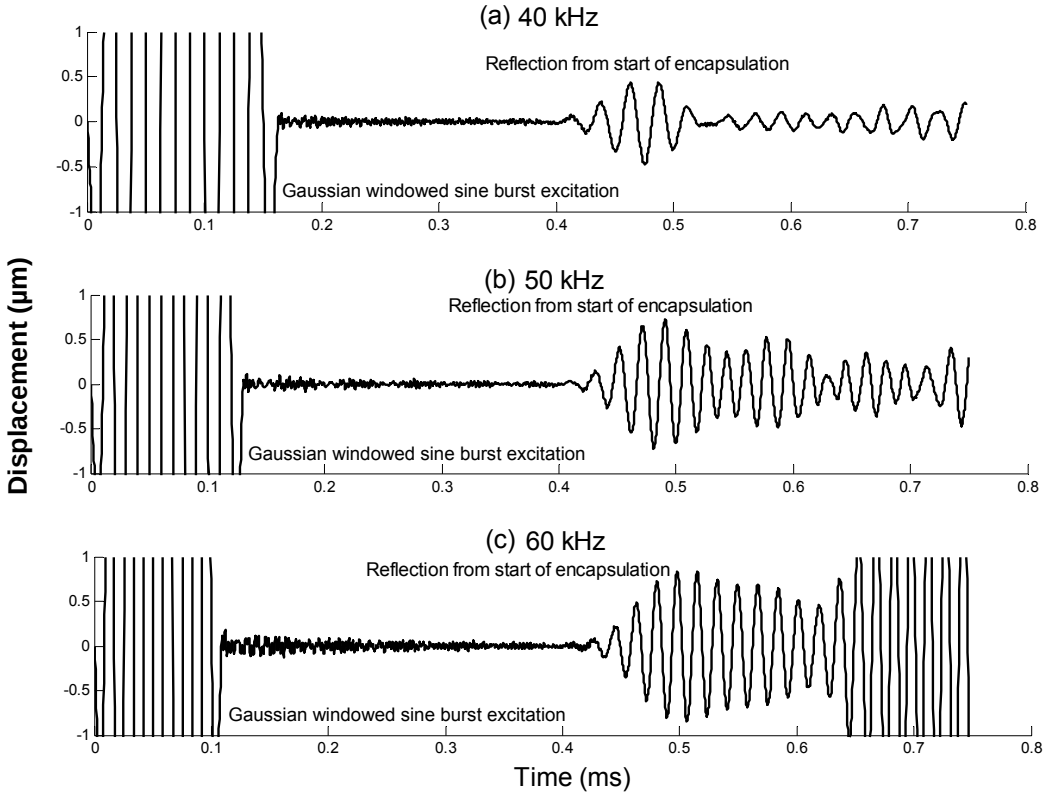

Figure 4.3 a, b, c: Three-dimensional model results with 10 mm elements

The reflection from the start of the resin encapsulation for the 40 kHz signal can be seen in figure 4.3a. The end reflection cannot clearly be distinguished. The reflection from the start of the resin encapsulation for the 50 kHz and 60 kHz, can be seen in figures 4.3 b, c. The reflections for both signals were stretched. The end reflections for the 50 and 60 kHz can also been seen in figures 4.3 b and c. It is clear that the three-dimensional model is not accurate. The modelling of the mortar with bigger elements causes early reflections and interference. It was not possible to solve larger

three-dimensional models with the software and the computer resources available. It is recommended that software with energy absorbing elements should be utilized. The three-dimensional model will then be an excellent opportunity to model non-axisymmetrical defects.

4.2.2 The experimental setup

This study focussed on far field defects. The wave velocity in a 20 mm unbounded bolt is approximately 5000 m/s. The duration of a 6 cycle, 30 kHz signal, is more or less 0.2 ms. The distance the wave will travel in this period is calculated as 1 m. As a result the defect should be located further than 0.5 m from the excitation end of the bolt. This is without considering the recovering time of the electronic equipment. Thus, maximum time of excitation plus recovering time for six cycle, 40 to 60 kHz signals, were measured as 0.4 ms.

The nearest defect that can be detected for the experimental setup is calculated as:

$$d = \frac{1}{2} x \left[\frac{0.4 \text{ x } 10^{-3}}{5000} \right] = 1 \text{m}$$

The partially encapsulated experimental bolt is shown in figure 4.4. Note that the bolt is not anchored to the mortar for 1000 mm. This distance is long enough so that the reflection from the start of the encapsulation can be seen. The embedded part of the bolt is 500 mm, which is long enough to distinguish the start of resin encapsulation and the end reflection. The resin thickness was approximately 4 mm. The installation procedure described in section 3.3 was followed. This causes the angle of the resin, as seen in figure 4.4.

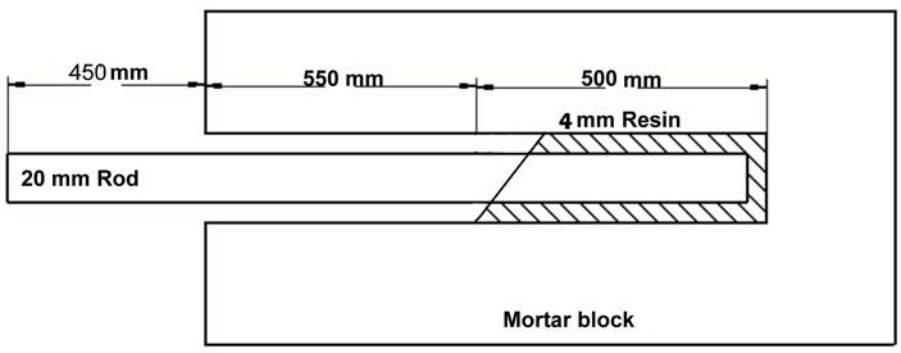

Figure 4.4: Experimental partially encapsulated bolt

The frequencies of the input signals were stepped in increments of 10 kHz from 40 kHz to 60 kHz. The results are shown in figure 4.5. The speed of the L(0,1) mode wave packet for the unbounded bolt, at 40 kHz, is 5033 m/s (according to the group velocity curve in figure 2.9). The predicted time of arrival of the reflection from the start of the resin encapsulation, is calculated as follows:

$$t = \frac{2}{5033} = 0.397 \text{ ms}$$

If the time trace of the 40 kHz signal in figure 4.5a is examined, no reflection of the resin encapsulation in the region of 0.397 ms could be seen.

To calculate the time of arrival of the end-reflection of the bolt, the velocity of the wave packet in an embedded bar, is needed. From figure 2.9, the speed of the wave packet, at a frequency of 40 kHz, was more or less 4500 m/s.

The predicted time of arrival of the end-reflection, for the partially encapsulated bolt, can be calculated as:

$$t = \frac{2}{5033} + \frac{1}{4500} = 0.62 \text{ ms}$$

This predicted value agrees with the reflection seen at 0.64 ms for the experimental result in figure 4.5a.

Similar calculations were done for the 50 kHz signal. The velocity of L(0,1) mode for a unbounded bolt, is 4976 m/s. The velocity in the embedded part of the bolt, is 4500 m/s. Therefore, the reflection from the start of the resin encapsulation should arrive at 0.4 ms. The bolt's end reflection will arrive approximately at 0.625 ms. If this is compared to the results for the 50 kHz case in figure 4.5b, the reflection from the start of the resin encapsulation can be seen, albeit weakly at 0.5 ms. The end reflection for both the predicted and the experimental signal is more or less 0.625 ms.

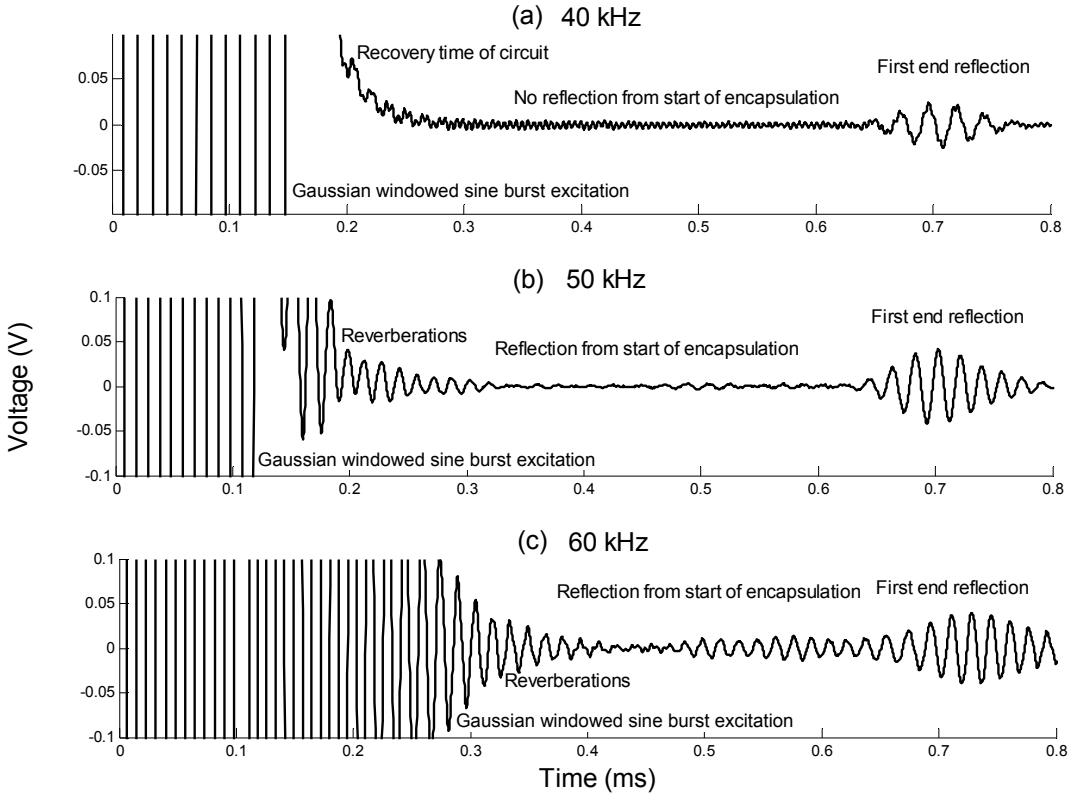

Figure 4.5 a, b, c: Experimental results for a partially encapsulated bolt

Similar calculations for the 60 kHz signal, showed that the time of arrival of the reflection from the start of the resin encapsulation, should be at 0.41 ms. This is not the case if one examines the time trace of the experimental test in figure 4.5c. A reflection could not clearly be distinguished, but it seems as if there was an end-reflection at 0.45 ms. The predicted end-reflection agrees with the measured experimental end-reflection. The measured end-reflection was stretched and is a result of the input force from the transducer that is very long due to the ringing at 60 kHz.

4.3 Local corrosion cracking

From the literature study in section 1.3 another source of failure that is attracting more and more attention, is the phenomenon of corrosion of rock bolts in an underground environment.

The process of recirculation of water, often gathers corrosive ions and renders the water more aggressive towards steel components. If a crack or void in the rock and resin develops, the water seeps through and the exposed surface of the bolt starts corroding. Cracks will start to develop, eventually leading to failure of the bolt.

Different fault scenarios were investigated to investigate the different type of cracks that can exist. An experimental bolt with a cut in the bolt was installed. Finite element models were built to simulate the different scenarios that could exist. The first model was a perfectly embedded bolt without any cracking. The second model was a bolt with a cut, to compare it to the experimental cracked bolt. The third bolt was simulating the first stage where only the rock and the resin had a crack. The last model was the scenario where the bolt started to corrode and the rock, resin and bolt had a crack.

4.3.1 Experimental cracked bolt

An experimental cracked bolt was installed to verify the finite element models. The dimensions of the model are shown in figure 4.6. Note that the defect is located in the far field, 900 mm from the exciting end. The size of the crack was 5 mm deep and 5 mm long. The 400 mm of the bolt protruding from the block was specifically chosen so that the reflection from the start of the encapsulation will return, while the end of the bolt is still being excited.

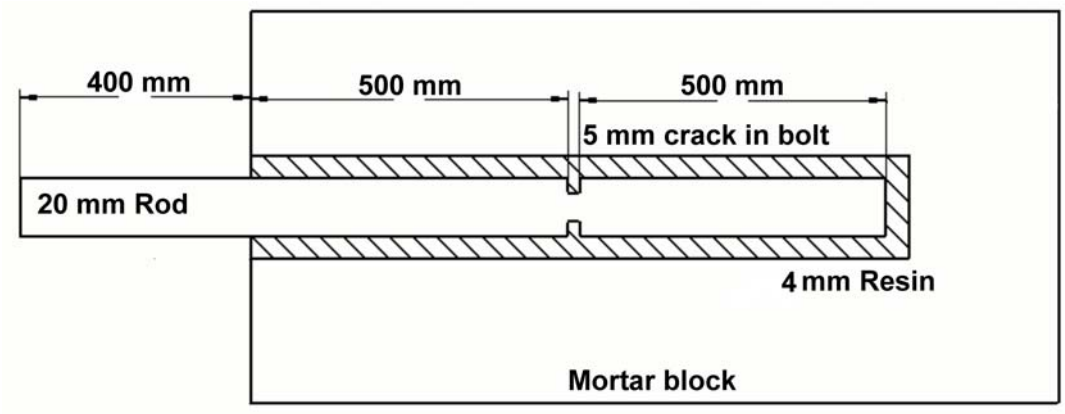

Figure 4.6: Experimental setup for a representation of a local corrosion crack

The time of arrival of the reflection from the crack is calculated as follows:

$$t = \frac{0.8}{5000} + \frac{1}{4500} = 0.38 \text{ ms}$$

The time of arrival of the reflections from the crack in figure 4.7 is more or less 0.4 ms.

The second reflection from the start of the resin is at:

$$t = \frac{2 \text{ x } 0.8}{5000} = 0.32 \text{ ms}$$

The second reflection from the start of the resin encapsulation can be seen in figures 4.7a, b and c. In figure 4.7a the second reflection from the start of the resin and the reflection from the crack in the bolt overlaps slightly. In figure 4.7c it appears as if the transducer is ringing and that there is a second reflection from the start of the encapsulation superimposed.

The predicted time of arrival of the end-reflection, can be calculated as:

$$t = \frac{0.8}{5000} + \frac{2}{4400} = 0.615 \text{ ms}$$

From figure 4.7 the first end reflection can be seen at 6.2 ms, which agrees with the predicted end-reflection.

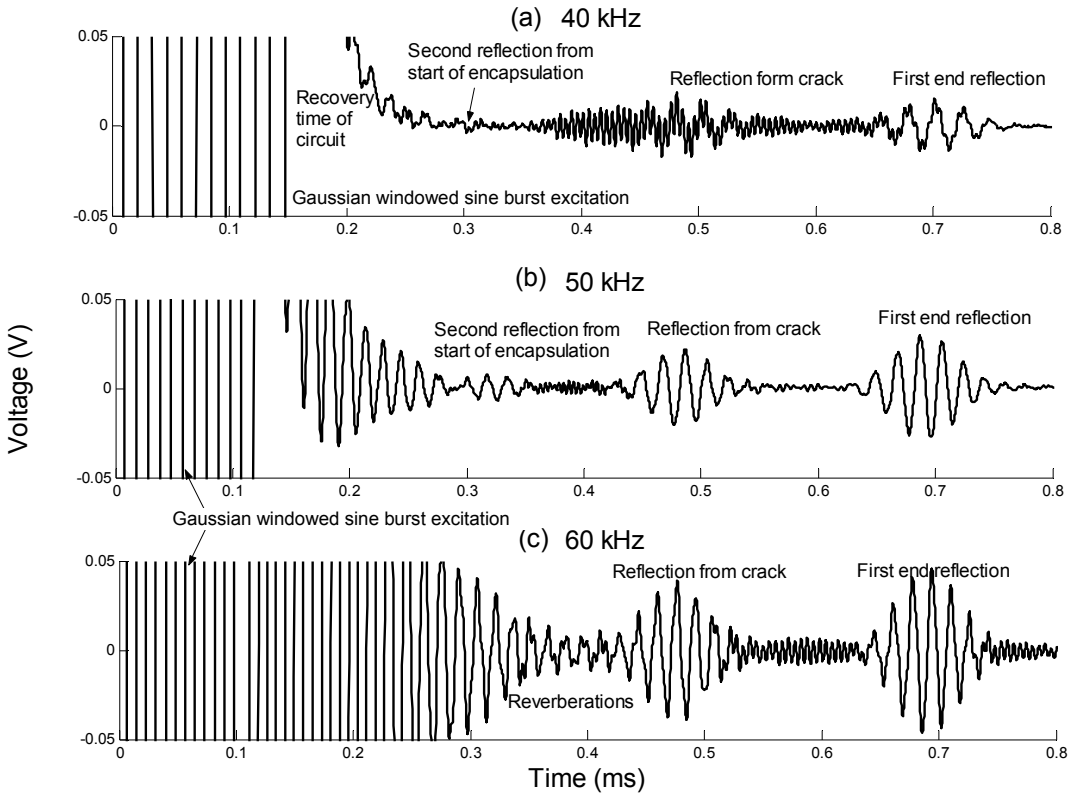

Figure 4.7 a, b, c : Experimental result for a bolt with a crack

4.3.2 Finite element models and discussion

Different models were built to simulate the scenarios that can exist. The models were the following:

- No defect
- Cracked bolt
- Crack of the resin and mortar
- Crack of the bolt, resin and mortar.

The three-dimensional model in the previous section showed its incapability for big models. Therefore only axisymmetric models were built and only axisymmetrical local corrosion cracks, could be considered.

A) No defect

The first model was an embedded bolt without any defects to use it as a reference. The model's dimensions can be seen in figure 4.8. The only difference is that the model does not have any cracks.

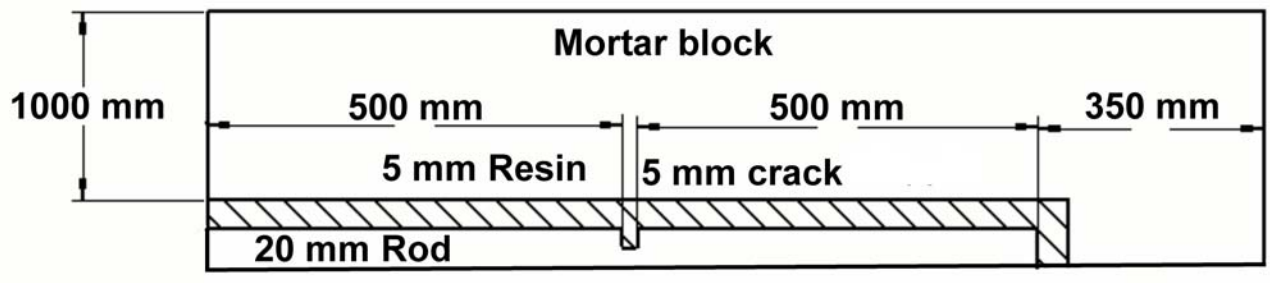

Figure 4.8: Finite element model details

The bolt, resin and mortar were meshed with 5mm TRIA 6 elements. The model consists of approximately 55000 elements. The material properties and time-varying fields were applied as before. The time step was set to 1 μs. The number of time steps was 650 steps. The model was built in MSC.Patran and solved with MSC.Nastran, an implicit solver. It took MSC.Nastran approximately 1 hour to run the problem.

The time traces for the undamaged 1 m bolt can be seen in figure 4.9.The results for 0.9 m embedded bolt in section 3.6 is compared to the 1 m embedded bolt. The time of arrival of all three time traces in figure 4.9 is more or less the same. It is similar to the results in section 3.6. The amplitude of the end-reflection of the 1 m embedded bolt is smaller than that of the 0.9 m embedded bolt. This demonstrates the attenuation caused by energy leaking into the surrounding rock.

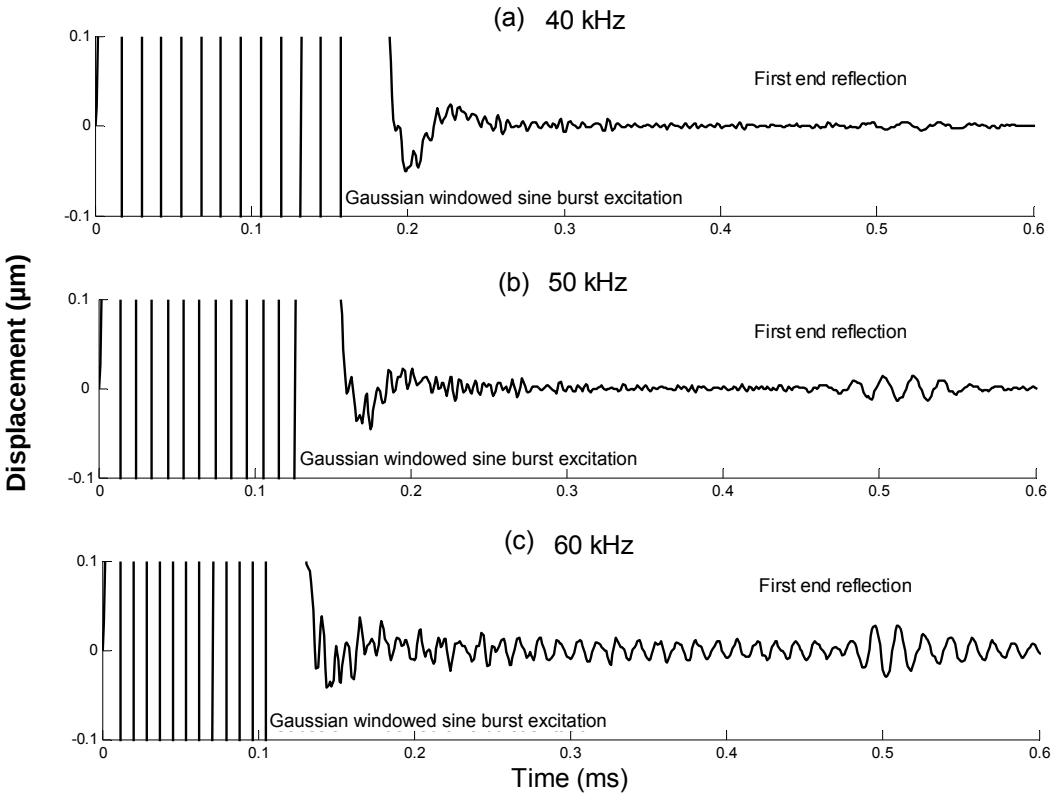

Figure 4.9 a, b, c: Finite element model results for a 1 m embedded bolt with no defects

B) Cracked bolt

A model of a bolt with a crack was built to compare it to the cracked experimental bolt. The details and dimensions of the model are presented in figure 4.8.

The predicted time of arrival of the reflection from the crack in the bolt can be calculated as follows:

$$t = \frac{1}{4500} = 0.22\,\text{ms}$$

This agrees with the time of arrival in figure 4.10. The amplitude of the reflections from the crack is notable. It is concluded that for a cracked bolt the amplitude of the reflection of the crack will be high because the cracks covers a gross area of the cross section.

The time of arrival for the end reflection of the 1m perfectly embedded bolt in figure 4.4 was between 0.44-0.48 ms. The time traces of the cracked bolt is shown in figure 4.10. No end reflection near 0.44 to 0.48 ms could be seen for the 40 kHz signal in figure 4.10a. The small end reflection of the 50 kHz signal in figure 4.10 b is visible at 0.48 ms. For the 60 kHz signal in figure 4.10c the end reflection could not clearly be distinguished from the other vibrations.

Both the experimental and finite element model for the cracked bolt showed the reflection from the crack. The experimental bolt showed clearer end-reflections than the finite element models reflections.

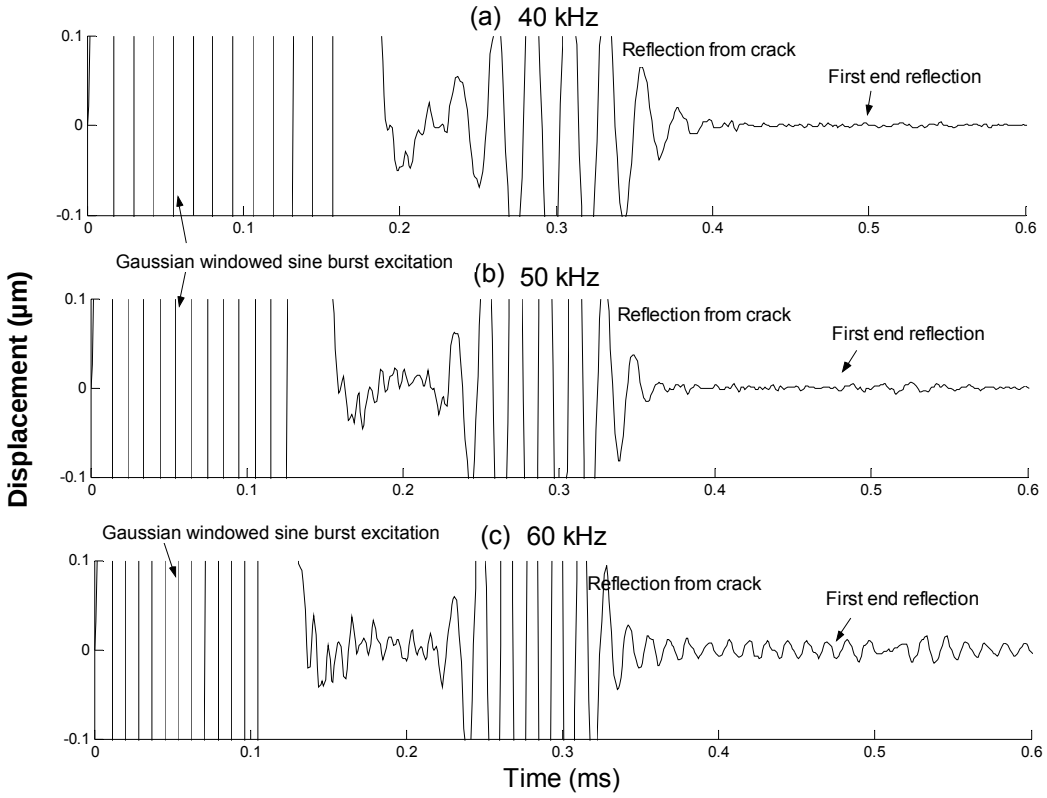

Figure 4.10 a, b, c: FEM model with a crack in the bolt only

C) Mortar and resin crack

A model of a resin crack and a rock crack was built according to figure 4.8. The only difference is that the bolt had no crack, but the rock and resin had cracks. The crack in the rock was chosen to be 0.1 m deep into the rock perpendicular to the bolt's axis.

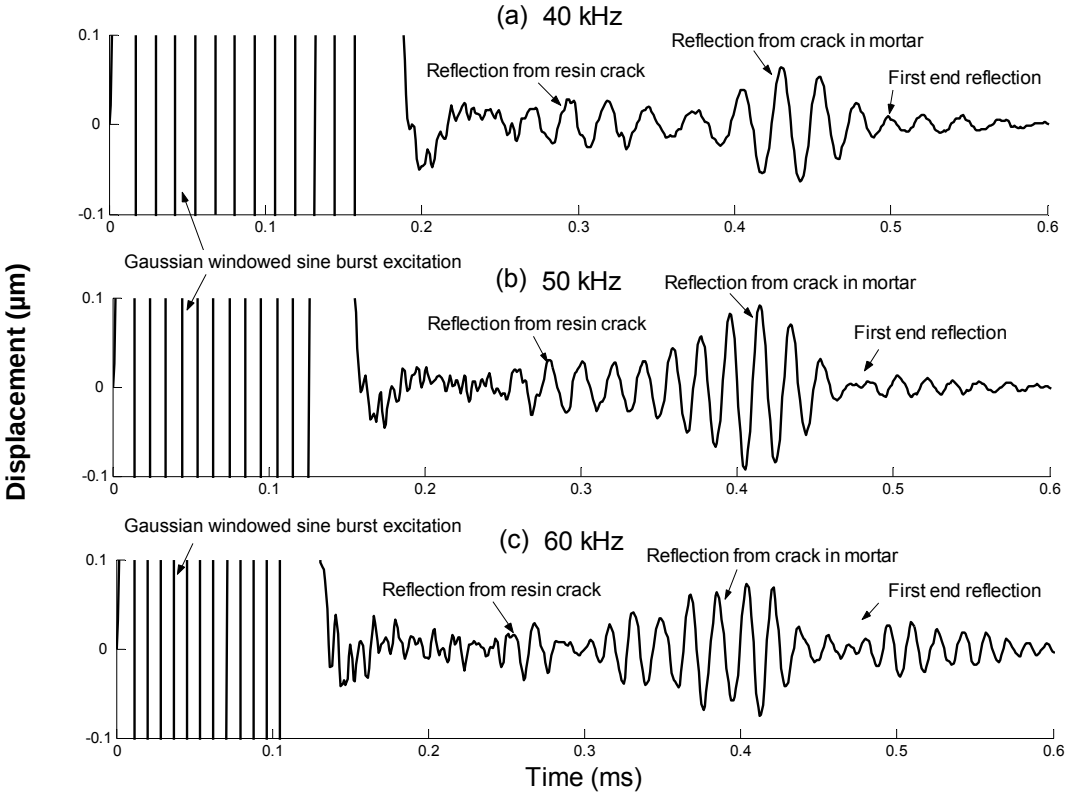

Figure 4.11 a, b, c: FEM model with a rock and resin crack

It is notable that the amplitude of the first reflection is smaller than the reflection of a bolt with a crack. The first reflection is likely to be the reflection from the crack in the resin. A second reflection could be seen just after the reflection of the resin crack. This reflection could be the reflection from the crack in the mortar. In all three cases the end reflection of the bolt, could be noticed. In figure 4.11a the reflections could clearly be distinguished from each other, but for the 50 and 60 kHz signals in figures 4.11 b and c it is more overlapping.

D) Bolt, resin and rock crack

To investigate the worse case scenario a model of the bolt, resin and mortar crack was simulated analogous as before. The results is shown in figure 4.12

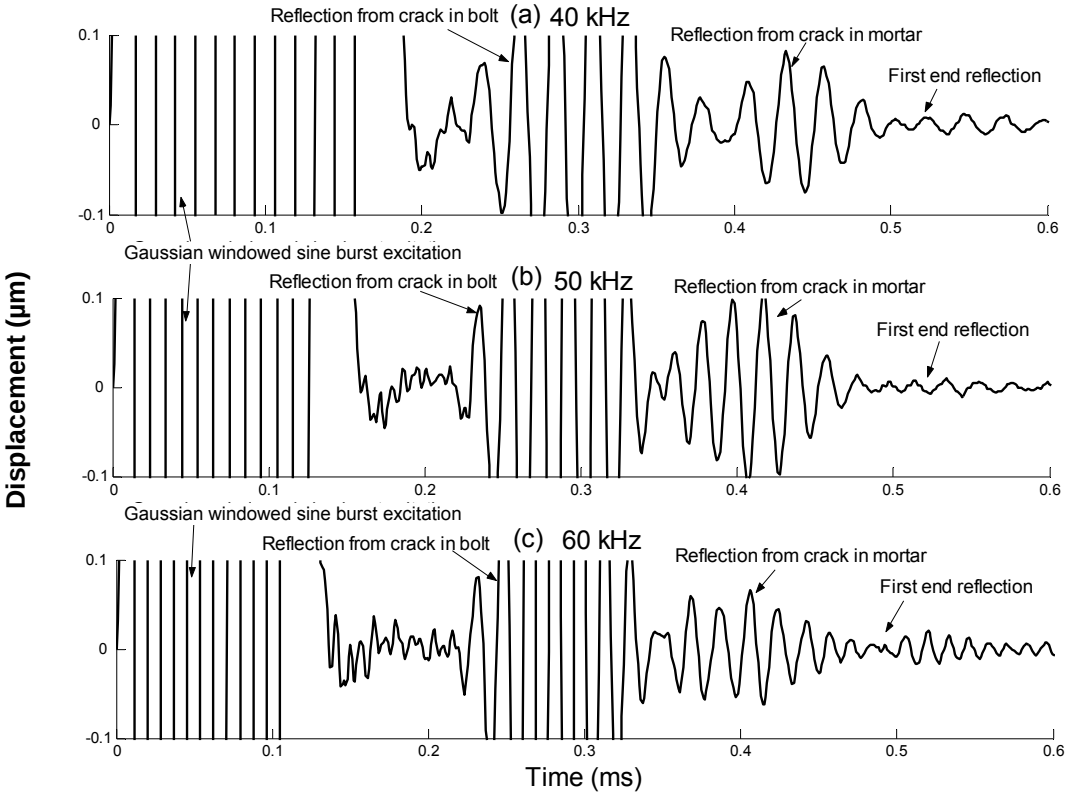

Figure 4.12 a, b, c: FEM model with the rock, resin and a bolt crack

The first reflection is the reflection from the crack in the bolt, and compare well to the results for crack in the bolt in figure 4.10. The second reflection could be the reflection from the crack in the mortar. The reflection from the resin could not been seen, because the reflection of the bolt is overlapping the reflection. The end reflection could be seen, but as before, the time of arrival is much later than expected. It is possible that this is not the end reflection but the second reflection from the bolt crack.

A noteworthy difference between the experimental setup and the FEA model is that the FEA model did not have the 400 mm protruding end. See Figure 4.6 and 4.8. This is one reason why the reflected signals of the FE model do not match the

signals of the experiments. Secondly, the material properties of the resin and mortar in the FEA model can cause a delayed response as can be seen in the FEA model's results. It is recommended for further study to investigate the effect of the protruding end and different material properties.

This chapter illustrated that guided waves can be an effective technique to detect certain defects. The finite element models showed the potential to simulate certain defect scenarios. Only far field defects were considered and all the defects were placed in the far field. For the finite element model the amplitudes of the reflections from the start of the encapsulation were smaller for the higher frequency signals than for the lower frequency signals. It is concluded that at higher frequencies the energy is travelling more in the centre of the bolt; consequently it will be less sensitive for partially embedded bolts. It is recommended to use lower frequencies when defects such as partially encapsulated bolts are tested.

In future research, a neural network could be trained on various defect scenarios modelled with finite elements. The amplitude of the reflecting signal may be an indication of the location of the defect. As the theoretical attenuation curves are available the amplitude of the reflecting signal can with the group velocity curves used to obtain the location of the defect. Furthermore the amplitude can also be used as an indication of the nature and severity of the defect. It will be of value to investigate the relationship between the amplitude and the location and amplitude and severity of the defect.

CHAPTER 5

CONCLUSIONS AND RECOMMENDATIONS

In the mining industry different types of roof support elements are in use. One of these support elements is the resin anchored rock bolt. There are different defects associated with a resin anchored rock bolt. These defects reduce the integrity of the roof, and thereby have an effect on the safety and productivity of the mines. A study on the different defects of the resin-anchored bolt was conducted. It was found that partially encapsulated bolts, over-spinning, incomplete mixing and corrosion were some of the major problems encountered. This research focused on partially encapsulated and locally corroded bolts.

Currently, South African mines have no non-destructive test to determine the condition of a rock bolt. The most promising technique found in the literature study was based on guided ultrasonic waves that embrace the following:

A short duration Gaussian windowed sine burst is used to excite a guided wave mode in the bolt from the free end. The wave is then reflected from the other end and from any major defects. With guided waves the quality of the grouting and the location of the defect can be determined. From the reflection arrival time and knowledge of the wave velocity dispersion curves, the positions of the defects or the bolt's length can be calculated. The maximum test range is limited by the extent of the attenuation that the wave experiences as it propagates. (Beard and Lowe, 2003)

Beard and Lowe (2003) investigated the effect of specific guided wave modes, frequencies and excitation periods to identify the optimal guided wave mode for defect detection.

The findings of Beard and Lowe (2003) was to use a six cycle sinusoidal Gaussian windowed signal. They further establish that embedded bolts should be tested by exciting the first axially symmetric longitudinal mode known as the L(0,1) mode, in its low frequency range (30 – 70 kHz) to detect grouting defects.

This study was conducted applying a six cycle Gaussian windowed sine burst with frequencies between 30 - 70 kHz to the total surface of the free end of the bolt. Thus exciting the first axially symmetric longitudinal mode (L0,1) in the bolt to investigate different defects scenarios such as partial bolt encapsulation and possibly corrosion patches near the bolt surface.

To mathematically simulate the different scenarios, the finite element (FE) method was selected due to the fact that it can handle more complicated defects and geometries. Furthermore, the advantage of the FE method is that there are numerous commercial FE codes available, thus eliminating any need to develop a specialized code.

To obtain a basic understanding of wave propagation modelling with the FE method, some modelling issues were investigated.

Different solver option was available in the FE package. After some preliminary studies it was clear that the explicit solver will be the most promising solver for large wave propagation problems. Furthermore, it was found that the time step is the critical factor when accurate answers are needed.

Material damping was neglected in the study, because damping influence the attenuation and therefore primarily the amplitude of the signal. In addition, the response of the embedded rock bolt is dominated by leakage rather than by material damping.

Another investigation showed that the boundary of the mortar has a huge influence on the results. This is because early reflections from the finite rock boundary interfere with the reflections from the bolt. From the literature a possible solution to this is to

use energy absorbing elements at the boundaries. A second approach is to move the boundaries far enough to prevent interference. As the software available for the study did not have energy absorbing elements, the latter approach was followed. However the latter approach increases the model size and thereby the computer resources required. It is recommended for further study to investigate the use of energy absorbing elements at the finite boundaries as this will reduce the size of the model and thereby the computer resources needed.

Another approach to reduce the problem size, is to model the bolt using axisymmetrical elements. However, only axisymmetrical defects can be modelled with this approach. For simulating non-axisymmetric defects a three-dimensional finite element model need to be utilized.

To compare the results of the axisymmetrical and three dimensional approaches an unbounded bolt and secondly an embedded bolt was investigated. For the unbounded bolt the three dimensional model gave comparable results to the experimental and axisymmetrical unbounded bolts. In addition, the group velocity curves of these models compared well with the Pochammer-Chree frequency equation group velocity curve for an unbounded bolt. The axisymmetrical defects modelled with axisymmetrical elements in this study gave comparable results to the experimental bolts. However, the three-dimensional finite element model of the embedded bolt was very large due to the fact that the surrounding rock need to be simulated. It was concluded that it will be a promising approach if the size of the model can be reduced or higher computer resources can be utilized. Over against that the axisymmetrical embedded bolts showed good agreement to the experimental bolt.

Simulating different defects was one of the objectives of the study. Two types of defects were considered, bolts with local corrosion cracks and partially encapsulated bolts. Due to the lower frequency limitation only far field defects were considered in this study. All the defects were located in the far field and could be detected.

It was possible to detect simulated local corrosion cracks with the finite element

models. Clear reflections for the crack in the bolt could be seen. If the bolt, resin and rock are cracked, different reflections will be detected. These different reflections complicated the interpretation of the results. Overlapping of returning signals can also add to complicate the interpretation of the results. It is therefore recommended that signal processing techniques be utilized for future studies. For instance, knowing the shape of exciting signal can help to separate two overlapping reflections.

Furthermore, the local corrosion defects simulated, only included one crack that was perpendicular to the travelling wave direction. It will be of much value to further investigate different crack scenarios with the finite elements such as inclined and multiple cracks.

For the partially encapsulated bolts, the FEA model compares well to the experimental bolts. However a certain time delay was observed in the returning signals of the FE model results. The reason for it can be the geometrical difference between the encapsulated experimental bolt and the FE bolt. The experimental bolt have a protruding end of 400 mm which was selected to overcome excitation reflections. Secondly, the difference of material properties of the resin and mortar in the FEA model compared to the experimental bolts can be another reason for the delayed response. It is recommended for further study to investigate the effect of the protruding end and different material properties.

The amplitudes of the FE encapsulated bolts were compared for different frequency signals. It was found that the signals from the start of the encapsulation were smaller for the higher frequency signals than for the lower frequency signals. This establish previous findings that at higher frequencies the energy travels more in the centre of the bolt for the L(0,1) mode. Thus fewer energy is lost due leakage at the higher frequencies. Consequently, the higher frequency tests will be less sensitive for partially embedded bolts. It is recommended to use lower frequencies when defects such as partially encapsulated bolt are tested.

It is apparent that chosing the correct frequency for optimized reflection, is critical. Scanning through the frequencies until a reflection from the end of the bolt could be

obtained, can be one approach for selecting the best frequency for detecting partially encapsulated bolts. However this needs to be further investigated.

This study did not fully investigate the amplitude of the returning signals as only the time of arrival was used to locate the different defects simulated. However, the amplitude of the reflecting signal may also be an indication of the location of the defect. As the theoretical attenuation curves are available the amplitude of the reflecting signal can with the group velocity curves be used to obtain the location of the defect. Furthermore the amplitude can also be used as an indication of the nature and severity of the defect. It will be of value to investigate the relationship between the amplitude and the location of the defect and amplitude and severity of the defect. The effect of material damping should also be investigated if the amplitudes of the reflecting signals are investigated. Further research on the transducer and the coupling of the transducer to the bolt will contribute in the repeatability of the experimental results which also effect the amplitude of the signals.

Basic principles and modelling issues were addressed and it may be expected that these principles could soon be extended to higher frequencies with a new generation of computers or apply absorbing boundaries. The benefits of also considering higher frequencies is that the higher frequency modes are less sensitive to material properties, epoxy thickness and surface defects. Furthermore the higher frequency modes can be used to obtain a reliable indication of the bolt's length. Knowing the bolt's length, the end reflections can be separated from the other reflections, simplifying the interpretation of the complicated reflections of the lower frequency tests. Once the integrity of models such as these has been established, the models could in principle be used to train neural networks for use in commercial equipment.

REFERENCES

Auld, B.A. (1973). *Acoustic fields and waves in solids*. New York: Wiley

Beard, M.D., Lowe, M.J.S. (2003). Non-destructive testing of rock bolts using guided ultrasonic waves. *International Journal of Rock Mechanics & Mining Sciences*, 40

Beard, M.D. (2002). *Guided wave inspection of cylindrical structures.* Doctoral Dissertation. London: University of London

Bornman, H. (25 April 2005). *South Africa rock bolts consumption.* Unpublished email to Buys B.J.

Charrette, F. (2004). *Rock bolt Corrosion in Mining and Tunnelling*, Atlas Copco.

Clifford, B. (2000). Ultrasonics for integrity testing of rockbolts In mines. Report prepared by Rock Mechanics Technology Ltd for the Health and Safety Executive, report no. 3792/R31.069

Gamboa, E., Atrens A. (2003). Environmental influence on the stress corrosion cracking of rock bolts. *Engineering Failure Analysis*, 10

Haarhoff, J. (2003*). In Situ Bolt Integrity Tester*. Unpublished thesis. Rand Afrikaans University.

Harper, G.S., Basson, E. (January 1998). *Develop a new methodology of determining the effectiveness of grouted support*. Report submitted to SIMRAC, report no. GAP412.

Hill, R., Forsyth, S.A. & Macey, P. (2004). Finite element modelling of ultrasound, with reference to transducers and AE waves. *Ultrasonics*, 42

Hoek, E., Kaiser, P.K. & Bawden, W.F. (1995). Support of underground excavations in hard rock. Rotterdam: Balkema.

Djordjevic, N. (1999). JK Rock Bolt Tester. JKMRC

Kelly, A.M., Jager, A.J. *et al.* (October 1996). Critically evaluate techniques for the in situ testing of steel tendon grouting effectiveness as a basis for reducing fall of ground injuries and fatalities. Report submitted to SIMRAC, report no. GAP205.

Kishore, N.N., Sridhar, I. & Iyengar N.G.R. (2000). Finite element modelling of the scattering of ultrasonic waves by isolated flaws. *NDT& E International*, 33

Krautkramer (Spring and Summer, 1998). Emerging technology - Guided wave ultrasonics. NDTimes 20(2)

Mark, C., Compton C.S., Oyler D.C., Dolinar D.R. (2002). *Anchorage pull testing for fully grouted roof bolts*. 21st International Conference on Ground Control in Mining.

MSC Document library, (2005).

Moser, F., Jacobs L.J. & Qu J. (1999). Modeling elastic wave propagation in waveguides with the finite element method. *NDT&E International*, 32

NDT Resource Center. (2001). http://www.ndt-ed.org/ (Accessed 5 July 2005).

Pavlakovic, B.N., Lowe M.J.S. & Cawley P. (2001). High-frequency low-loss ultrasonic modes in imbedded bars. *Journal of Applied Mechanics*, 68

Roberts, D.P. (1995). Testing of mining tunnel support elements and systems for hard rock mines. Masters dissertation. Natal: University of Natal.

RMT. (2003). Rock bolt pull test equipment. Rock Mechanics Technologies (RMT). Available at http://www.rmtltd.com/products.htm (Accessed 22 February 2005).

Rose, J.L. (2004). Ultrasonic guided waves in structural health monitoring. *Key Engineering Materials*

Rose, J.L. (1999). Ultrasonic waves in solid media. Cambridge: Cambridge University Press.

Rose, J.L. (2003). Dispersion curves in guided wave testing. *Materials Evaluation.*

Rose, J.L., Avioli M.J. *et al.*, (2003). Guided wave inspection potential of defects in rail. *NDT&E International*, 37

Ross, M. (2004). Modeling methods for silent boundaries in infinite media. Fluid-structure interaction aerospace engineering sciences- University of Colorado at Boulder

SAISC, South African Institute of Steel Construction, (1987). South African Steel Construction Handbook. Johannesburg

Seco, F., Martín, J.M., Jiménez, A., Pons, J.L., Calderón, L., Ceres, R., (2002). PCdisp: A tool for the simulation of wave propagation in cylindrical waveguides. 9th International Congress on Sound and Vibration. Orlando, Florida

Silk, M., Bainton, K., (1979). The propagation in metal tubing of ultrasonic wave modes equivalent to lamb waves. *Ultrasonics*.

Simmons, J.A., Drescher-Krasicka, E.D., Wadley, H.N.G, (1992). Leaky axisymmetric modes in infinite clad rods I. *Acoustical Society of America, 92 (2)*

South African Department of Minerals and Energy - Mine Health and Safety. Accidents, deaths and injuries - All mines. Annual Report 2005.

Starkey, A., Ivanovic A. *et al.* (2003). Using a lumped parameter dynamic model of a rock bolt to produce training data for a neural network for diagnosis of real data. *Meccanica*, 38

Staszewski, W.J., Boller C. & Tomlinson G.R. (2004). Health monitoring of aerospace structures. Wiley.

Technical info about and how to use the Boltometer. Available at : http://www.geodynamik.com/english/se26.htm. (Accessed 15 March 2005).

Thurner, H.F. (1996). *Rock Bolting – Reference Bank*, AMFO 84-0847 Final Report, Translated from the Swedish by BC Baur and Associates, Courtesy of CSIR. Johannesburg (Appendix of Kelly A.M., Jager A.J. *et al.*, Critically evaluate techniques for the in situ testing of steel tendon grouting effectiveness as a basis for reducing fall of ground injuries and fatalities.

Yassien, A.M. (2003). 2-D Numerical simulation and design of fully grouted bolts for underground coal mines. Doctoral dissertation. Morgantown: West Virginia University

APPENDIX A

Different types of tendons exist and the selection is based on the roof conditions. (Yassien, 2003:4) classifies the different types under five categories. These types are:

- Mechanical anchor bolts
- Resin-assisted mechanical anchor bolts
- Fully grouted resin rebar
- Torque-tension bolts
- Combination bolts

Yassien (2003:10) also discussed some guidelines for choosing the bolt type:

Mechanical bolts are mostly used in the following conditions:

- Hard and strong rock as it can resist bit biting and keep the anchor force.
- Temporary reinforcement system.
- Where bolt tension can be checked regularly.
- Rocks that will not undergo high shear force.
- Areas away from blast sites where bolt tension may be lost.

The fully grouted bolts are used in the following conditions:

- Areas and conditions where mechanical bolts are not recommended.
- Rock without wide fractures or voids that will cause lost of grout.
- Long-term support of thinly bedded roof strata.

The resin-assisted mechanical anchor, torque-tension and combination bolts are recommended for use in areas and conditions where large pretension is required.

- **Mechanically anchored rock bolt**

These types of bolts are usually actively tensioned upon installation, thus immediately bearing load (Kelly *et al.*, 1996). This type of bolt is shown in figure A1.

Different types of problems are encountered with this type of bolt, for instance it is not very effective in closely jointed rocks and in soft rocks, because of the deformation and failure of the rock in contact with the wedge grips (Hoek, *et al.*, 1995). A second problem is that it is easily subject by corrosion damage (Kelly et al., 1996).

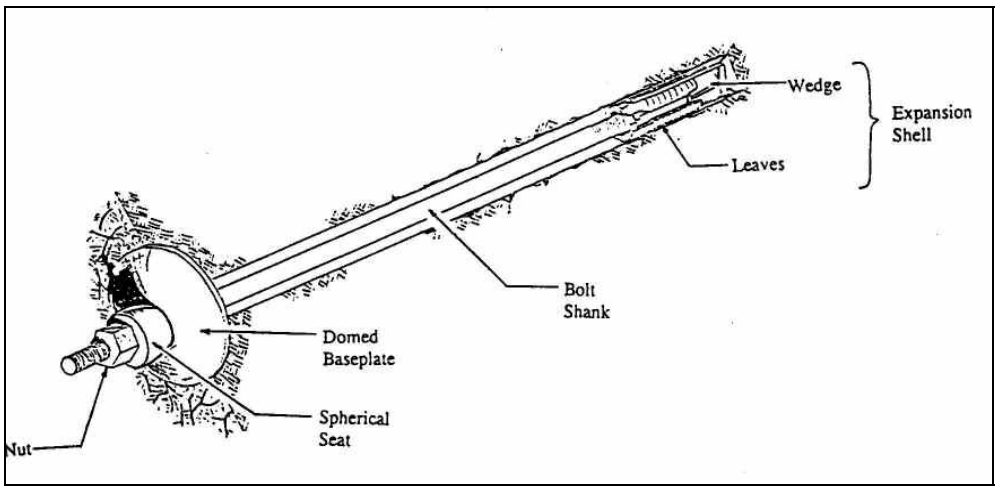

Figure A1: A typical mechanically end anchored rock bolt (Roberts, 1995).

- **Resin-Assisted anchored rock bolt**

To prevent corrosion the mechanically anchored bolts are filled with grout or resin and these types of bolts can be seen in figure A2 (Kelly *et al.*, 1996).

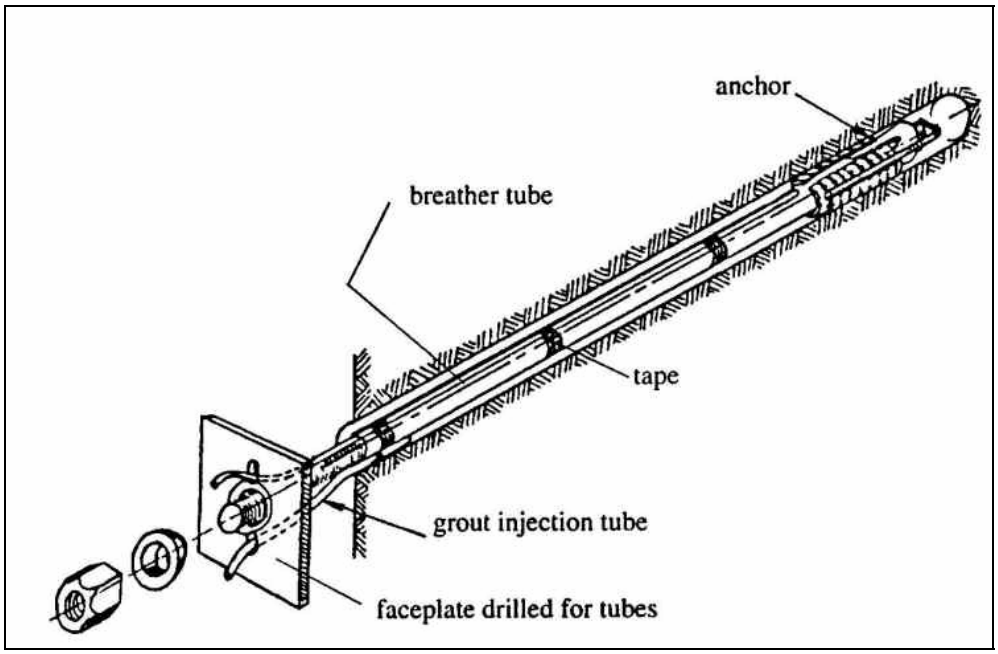

Figure A2: Grout injection arrangements for a mechanically anchored rock bolt (Hoek, *et al.*, 1995)

- **Cementitious anchored rock bolt**

This bolt is classified under fully grouted bolts. One of the installation procedures is to take a dry cementitious capsule, soak in water and push it up into the hole. The bolt is then spun or hammered into the hole. A second approach is to pump grout in the hole after the bolt was inserted. These bolts may be divided into straight bars as in figure A3 or shepherd's crooks as in figure A4 (Kelly *et al.*, 1996).

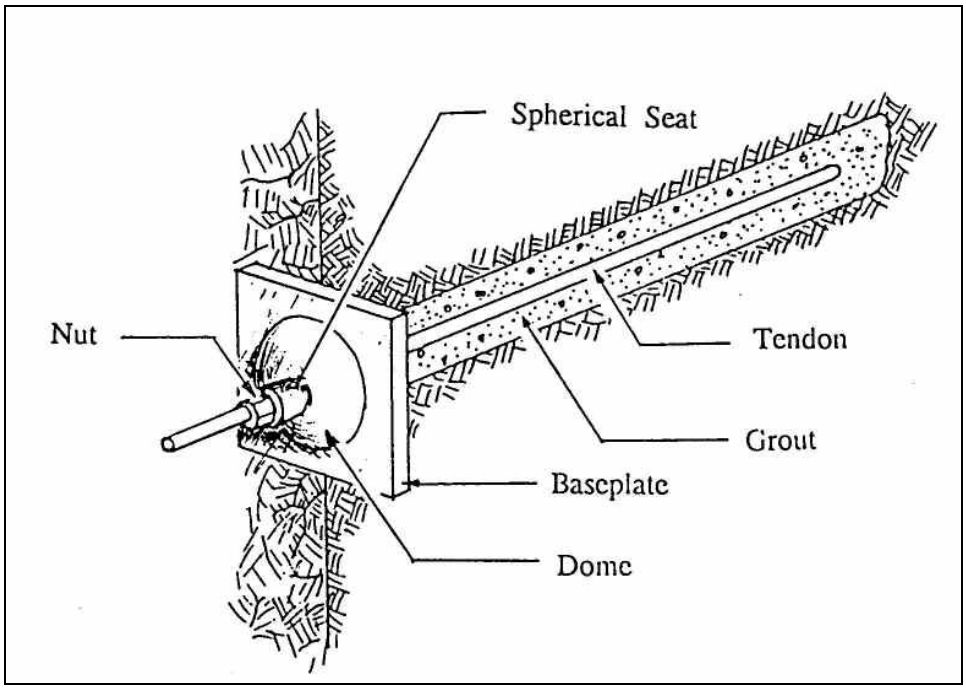

Figure A3: A typical straight bar grouted tendon with base plate and nut (Roberts, 1995)

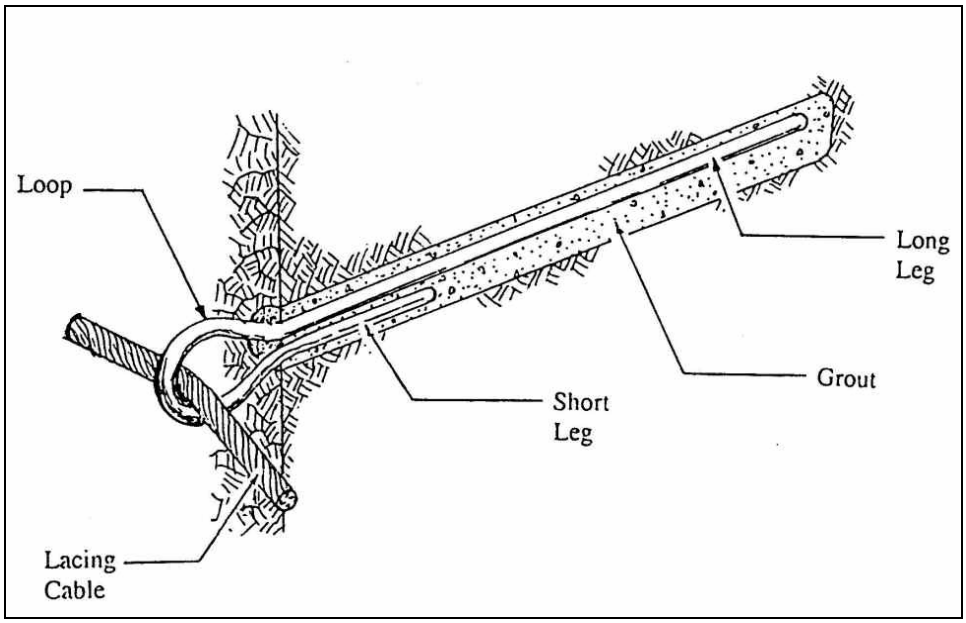

Figure A4: A typical shepherd's crook grouted tendon (Roberts, 1995)

- **Torque tensioned and combination bolts**

The torque-tension bolt is a resin-rebar system that is pretensioned during installation. It is basically the same as the resin anchored bolt, except that two different speeds of resin are used; a fast setting resin in the upper part of the hole and a slower setting resin in the lower part. A nut with a torque-delay mechanism is used to torque and tension the bolt. During installation the bolt is inserted and rotated, as the upper fast resin sets first, tension is built up in the lower portion before the lower slow resin cures up.

The combination bolt consists of a rebar anchor 0.9 to 1.2 meter long connected to a smooth headed bar through a special coupler. This type of bolt make up only 1 % of the U.S total bolt consumption (Yassien, 2003).

APPENDIX B

- **Instrumentation**

The conversion of electrical pulses to mechanical vibrations and the conversion of returned mechanical vibrations back into electrical energy is the basis of a piezoelectric transducer.

Piezoelectric transducers exist of an active element. This active element is basically a piece polarized material (i.e. some parts of the molecule are negatively charged, while other parts of the molecule are positively charged) with electrodes attached to two of its opposite faces. When an electric field is applied across the material, the polarized molecules will align themselves with the electric field, resulting in induced dipoles within the molecular or crystal structure of the material. This alignment of molecules will cause the material to change dimensions. The reverse effect can also take place, a permanently polarized material such as quartz or barium titanate will produce an electric field when the material changes dimensions as a result of an imposed mechanical force.

In figure B1 the piezoelectric effect can be seen.

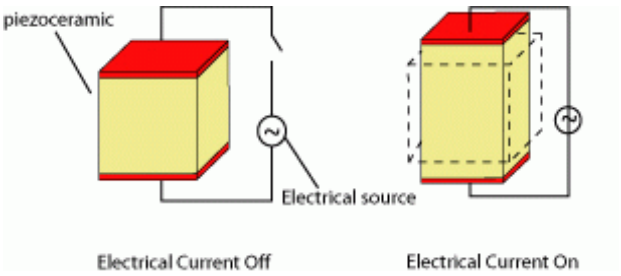

Figure B1: Piezoelectric effect

The piezo-ceramic transducer is connected to a circuit that is built to utilize the transducer as a sender and receiver. Secondly, the circuit was designed to reduce any unwanted noise.

The circuit for the pulse echo configuration can be seen in figure B2.

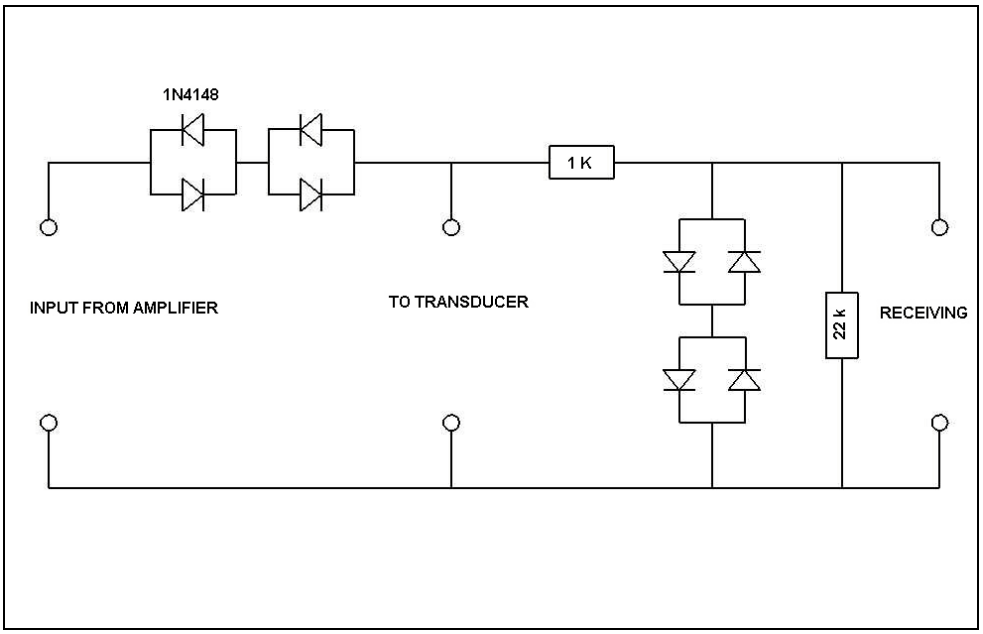

Figure B2: Circuit for pulse-echo tests

APPENDIX C

- **MATLAB Programs**

```
% DATA ACQUISITION PROGRAM TO DRIVE THE NATIONAL INSTRUMENTS CARD

%% SIGNAL AND USER DEFINED PROPERTIES=======================
tf=2.8e-3;                                  % end time
f=F(ii);                                    %frequency of pulse
SampleRate_ao=4e6;                          % samplerate for output channel
SampleRate_ai=5e6;                          % samplerate for input channel
SamplesPerTrigger_ai=tf*SampleRate_ai;      % number of samples for input channel

% Gausspulse
tc=gauspuls('cutoff',f,0.35,[],-40);        % 6 cycle gauspulse
ts=-tc:1/SampleRate_ao:tc;
dataout=10*gauspuls(ts,f,0.3);
ts=ts+tc;
dataout(1)=0;dataout(length(dataout))=0;
%% ============================================================

%% OUTPUT=====================================================
%% Create the analog output_1, add a channel, set sample rate, number of samples
ao=analogoutput('nidaq');
ch0_out=addchannel(ao,0,'ao1_0');
SampleRate_ao_act=setverify(ao,'SampleRate',SampleRate_ao);
set(ao,'TriggerType','Immediate');
set(ch0_out,'UnitsRange',[-10 10]);
OutputRange_act=setverify(ch0_out,'OutputRange',[-10 10]);
%% Put the data in the buffer, start the device
putdata(ao,dataout');
% ============================================================

%% INPUT ======================================================
%% Create the analog input_1, add a channel, set sample rate, number of samples
ai=analoginput('nidaq');
ch_in=addchannel(ai,[0,1],{'ai_0','ai_1'});
```

```
SampleRate_ai_act=setverify(ai,'SampleRate',SampleRate_ai);
set(ai,'SamplesPerTrigger',SamplesPerTrigger_ai);
set(ai,'TriggerType','HwAnalogChannel');
set(ai,'TriggerCondition','AboveHighLevel');
set(ai,'TriggerConditionValue',0);
set(ch_in(2),'SensorRange',[-10 10]);
set(ch_in(2),'UnitsRange',[-10 10]);
InputRange_act=setverify(ch_in(2),'InputRange',[-0.2 0.2]);
start(ai);
%% ================================================================

%% Start triggering output and input=====================================
start(ao);waittilstop(ao,length(ts));
delete(ao);
clear ao
%% ================================================================

%% Capture data from input device========================================
[datain,time]=getdata(ai);
waittilstop(ai,SamplesPerTrigger_ai);
delete(ai);
clear ai;
```

```
% PROGRAM TO PLOT THE GROUP VELOCITY CURVE FOR A 20 MM DIAMETER STEEL BOLT IN AIR

clear all;clc;close all;

F=30000:10000:90000;                    % frequencies (Hz)

%% RUNNING THE DAQ DEVICE, CAPTURE THE DATA AND MODIFYING THE DATA====
% For loop to run different frequency pulses on the DAQ device
for ii=1:1:length(F)
   clear i t b r s y I k a;
   a=0;
% For loop to run numerous daq to averaging the noise
for cc=1:500;
waittime=timer('TimerFcn','disp(F(ii))','StartDelay',100e-3);          % delay between the different daq
start(waittime);
wait(waittime);
f=F(ii);
sampling;% DAQ program to open channels,send the signal to transducer and capture the data
a=a+datain(:,2);                                % amplitude data
end
a=a/500;                                        % averaging of the daq to improve the signal/noise ratio
a(1:2800)=0;                                    % delete the output signal data from the captured data
y=max(a);                                       % determine the peak of the signal
fact=[1.5 3 3 3 3 3 3 3];
I=find(a>y/fact(ii));       % find the indexes of all the data that is fact times smaller than the peak
t=time(I);                  % find the time vector of the above data
b=a(I);                     % amplitude value of above data

% PROCESSING DATA=====================================================
% For loop to determine the index of the different wave packets(reflecting waves)
for i=1:length(t)-1;
   r=t(i+1)-t(i);
  if r>15*(1/f);
     s(i)=t(i);
  end
end
k=find(s);                                      % find the indexes for the start and end of the wave
```

```
packets
w=b(1:k(1));[mw,jw]=max(w);t1=t(1:k(1));ta1=t1(jw);          % determine the maximum and the time for the maximum of the first wavepacket
x=b(k(1)+1:k(2));[mx,jx]=max(x);t2=t(k(1)+1:k(2));ta2=t2(jx); % determine the maximum and the time for the maximum of the second wavepacket
z=b(k(2)+1:k(3));[mz,jz]=max(z);t3=t(k(2)+1:k(3));ta3=t3(jz); % determine the maximum and the time for the maximum of the third wavepacket
za=b(k(3)+1:k(4));[mza,jza]=max(za);t4=t(k(3)+1:k(4));ta4=t4(jza); % determine the maximum and the time for the maximum of the fourth wavepacket

% PLOTTING THE DATA=====================================================
figure(F(ii))
plot(time,datain(:,2),'k');hold on;grid on;    % plot of original data
plot(t,b,'b.');;                % plot all the data 0-3.1 times smaller than the peak
plot(t1,w,'c',t2,x,'m',t3,z,'g',t4,za,'y')     % plot the determined wave packet data
plot(ta1,mw,'r+',ta2,mx,'r+',ta3,mz,'r+',ta4,mza,'r+'); % plot the maximum of each reflecting wave packet

%% CALCULATION OF THE GROUP VELOCITIES===================================
tg(ii)=((ta2-ta1)+(ta3-ta2)+(ta4-ta3))/3;    % determine the average time between the end reflections
v_group(ii)=3/tg(ii);                        % calculate the group velocity
end
end

% PLOTTING OF THE DISPERSION CURVES ====================================
figure(10)
h=20:10:120;
vv=(-4.5661e-6.*h.^4)-(2.2572e-4.*h.^3)-(6.0767e-3.*h.^2)-(1.6196.*h)+(5.1344e+3); % equation for the theoritical curve
plot((F/1e3),v_group,'r.-',h,vv,'k.-');grid on;hold on;
xlabel('Frequency (kHz)');ylabel('Group velocity (m/s)');title('Group Velocity of a 20mm bolt');
figure(F(ii))
plot(time,datain(:,2));grid on;
xlabel('Time (s)');ylabel('Voltage (V)');title(['Time trace for a ',num2str(F(ii)/1000),' kHz pulse']);
```